

**FACULTY
OF MATHEMATICS
AND PHYSICS**
Charles University

MASTER THESIS

Bc. Jan Střeleček

**Geometric approach to externally
driven quantum systems**

Supervisor of the master thesis: prof. RNDr. Pavel Cejnar, Dr., DSc.

Study programme: Physics

Study branch: Theoretical physics

Prague 2022

I declare that I carried out this master thesis independently, and only with the cited sources, literature and other professional sources. It has not been used to obtain another or the same degree.

I understand that my work relates to the rights and obligations under the Act No. 121/2000 Sb., the Copyright Act, as amended, in particular the fact that the Charles University has the right to conclude a license agreement on the use of this work as a school work pursuant to Section 60 subsection 1 of the Copyright Act.

In date
Author's signature

Huge thanks go to my supervisor, prof. Pavel Cejnar, who was willing to discuss the results and theory anytime my mind needed some guidance. It is also worth mentioning the lengthy consultations with friends concerning quantum mechanics or differential geometry in general. I hereby thank Michal Grňo, Jakub Novotný, and Martin Zika for allowing me to sort thoughts in this way.

Title: Geometric approach to externally driven quantum systems

Author: Bc. Jan Střeleček

Institute: Institute of Particle & Nuclear Physics

Supervisor: prof. RNDr. Pavel Cejnar, Dr., DSc.

Abstract: The theory of quantum driving is presented and reformulated using the language of differential geometry. The general fidelity driving in a two-level Hamiltonian system is then analyzed with the particular importance of the fidelity time dependence. For the Lipkin-Meshkov-Glick model, the geometrical structure of its energy state manifolds is calculated with an aim to analyze adiabatic and close adiabatic drivings.

Keywords: adiabaticity driving fidelity Lipkin-Meshkov-Glick quench

Contents

Some notes to the notation	3
Introduction	5
1 Mathematical introduction	7
1.1 Essentials	7
1.2 Fiber bundle	9
1.3 Riemannian geometry	10
1.4 Geometry in 2 dimensions	11
2 Introduction to quantum geometry	13
2.1 Space of all states	13
2.2 Rays and bare states	14
2.3 Sectioning the space	15
2.4 Transporting states on state manifolds	16
2.5 Fidelity	19
2.6 Metric and geometric tensor	20
3 Quantum state driving	24
3.1 Counter-diabatic driving	25
3.1.1 Classical gauge potential	26
3.1.2 Quantum gauge potential	26
3.2 Driving on the ground state manifold	28
3.2.1 Minimizing the distance on state manifolds	28
3.2.2 Minimizing the energy variance	29
3.2.3 Transport using quenches	30
3.3 Adiabatic perturbation theory	30
4 Two level system	33
4.1 Hamiltonian	33
4.2 Harmonic oscillator correspondence	34
4.3 Energy variance for two-level system	35
4.4 Geodesic driving	35
4.4.1 Derivation of the fidelity	36
4.4.2 Analysis of the infidelity formula	38
4.4.3 Energy variance	39
4.5 Linear driving	41
4.5.1 Dependence on time	42
4.5.2 Final fidelity	43
4.5.3 Energy variance	47
4.5.4 Linear driving summary	47
5 Lipkin-Meshkov-Glick model	50
5.1 Hamiltonian	50
5.2 Geometry for fixed dimension	51
5.2.1 3-dimensional Hamiltonian	51

5.2.2	5-dimensional Hamiltonian	58
5.2.3	Infinite dimension limit	61
5.3	General spectrum behavior	62
5.4	Transport using quenches	65
Conclusion		67
Bibliography		68
List of Figures		70
A Geometrization of quantum mechanics		73
A.1	From the projective Hilbert space to state manifolds	73
A.2	Restriction to eigenstate manifolds	74
B Eigenvalues for Lipkin-Meshkov Glick model		76

Some notes to the notation

Symbol	Meaning	Characterizing formula
\mathcal{A}_μ	Calibrational (gauge) potential	$\mathcal{A}_\mu := i\hbar\partial_\mu$
A_μ	Berry connection	$A_\mu := \langle o \mathcal{A}_\mu o\rangle$
\mathcal{C}	closed driving curve in parametric space	
\mathcal{C}^k	k -times continuously differentiable function	
\mathbb{C}	complex numbers	
γ_s	geometrical phase induced by s^{th} energy level	
D_μ	covariant derivative	
E_s	s^{th} energy level of Hamiltonian	
F	fidelity	$F(\psi\rangle, \phi\rangle) = \langle\psi \phi\rangle ^2$
F^*	infidelity	$F^* := 1 - F$
f	fidelity amplitude	$ f ^2 := F$
$g_{\mu\nu}$	metric tensor	$g_{\mu\nu} = \text{Re}\chi_{\mu\nu}$
$\hat{H}(\boldsymbol{\lambda})$	parameter controlled Hamiltonian	
\mathcal{H}	Hilbert space	
$\mathcal{H}(\boldsymbol{\lambda})$	Hilbert space for $\hat{H}(\boldsymbol{\lambda})$	
Ind_a	winding number around point a	
$\hat{\mathbf{J}}$	angular momentum operator	
\mathcal{J}	driving curve in parametric space	
$\boldsymbol{\lambda}$	n -dimensional real parameter of Hamiltonian	$\boldsymbol{\lambda} \in \mathcal{U} \subset \mathbb{R}^n$
\mathcal{M}	manifold	
\mathcal{M}_s	s^{th} energy state manifold	$\mathcal{M}_s := \cup_{\boldsymbol{\lambda} \in \mathcal{U}, \varphi \in [0, 2\pi)} e^{i\varphi} s(\boldsymbol{\lambda})\rangle$
n	dimension of the parametric space	
N	dimension of the Hamiltonian	
\mathbb{N}	natural numbers (excluding zero)	
$ o(\boldsymbol{\lambda})\rangle$	ground state of Hamiltonian $\hat{H}(\boldsymbol{\lambda})$	
\mathcal{O}	order of the function (Big O notation)	
\mathcal{PM}_s	s^{th} energy projective state manifold	$\mathcal{PM}_s := \cup_{\boldsymbol{\lambda} \in \mathcal{U}} s(\boldsymbol{\lambda})\rangle$
φ_B	Berry phase	$\varphi_B := -\oint_{\mathcal{C}} A_j(\boldsymbol{\lambda}) d\boldsymbol{\lambda}^j$
\mathbb{R}	Real numbers	
$R_{\mu\nu}^\alpha$	Riemann tensor	
$R_{\mu\nu}$	Ricci tensor	$R_{\mu\nu} := R_{\mu\nu}^\alpha$
$R \equiv \text{Ric}$	Ricci scalar, or Ricci curvature	$R := R^\mu_\mu$
$\nu_{\mu\nu}$	Berry curvature	$\nu_{\mu\nu} = \text{Im}\chi_{\mu\nu}$
$ s\rangle$	eigenstate corresponding to energy E_s	$\hat{H} s\rangle = E_s s\rangle$
t	time	
T	final time of driving	
$\mathbb{T}_a \mathcal{M}$	tangent vector field of \mathcal{M} in $a \in \mathcal{M}$	
$\mathbb{T}_a^* \mathcal{M}$	cotangent vector field of \mathcal{M} in $a \in \mathcal{M}$	
$\mathbb{T}_q^p \mathcal{M}$	q -times covariant and p -times contravariant tensor field of \mathcal{M}	
\mathcal{U}	parametric space, open subset of \mathbb{R}^n	
$U(k)$	k -parametric unitary transformation group	
$\chi_{\mu\nu}$	geometric tensor	$\chi_{jk} := \langle \partial_j o \partial_k o \rangle_c$
$(\chi; \lambda)$	LMG model parameters	$(\chi, \lambda) \equiv \boldsymbol{\lambda} \in \mathbb{R}^2$

Operation	Notation
commutator	$[A, B]$
connected bra-ket	$\langle \partial_j o \partial_k o \rangle_c \equiv \langle \partial_j o \partial_k o \rangle - \langle \partial_j o o \rangle \langle o \partial_k o \rangle$
fiber space	$(\mathcal{E}, \mathcal{U}, \pi, \mathcal{F}) \equiv (\text{total space}, \text{base space}, \text{surjection}, \text{fiber})$
Poisson bracket	$\{A, B\}$
quantum bra-ket	$\langle \psi \phi \rangle$
Shortcut	Full name
APT	adiabatic perturbation theory
LZS	Landau-Zener-Stueckelberg
LMG	Lipkin-Meshkov-Glick

- Quantum operators are denoted with *hat*,
- abstract indices are written in *Greek*, pointer indices in *Latin*.
- If the object is defined by the formula on the right, “:=” is used. If the equality holds by definition, “≡” is used.
- Coordinate derivative can be denoted using a comma before index and covariant derivative using a semicolon.
- The colored text is sometimes used. The text can be understood without the colors; their goal is strictly pedagogical and helps the reader see some underlying connections.

Introduction

One of the big unsolved problems of modern physics is constructing the quantum computer. The implications here are mainly to so-called *adiabatic quantum computers*, where the solution to some mathematical problem is substituted for finding the wavefunction corresponding to the global energy minima of some system. This system usually consists of coupled qubits¹. The energy minimum can be found by numerous measurements of the specific superposition of qubits. The preparation of such a state in superposition is a complicated process, and one method of achieving it is so-called *quantum annealing*². Annealing is the process of changing the state from some simple *initial state* to the required state in superposition (*final state*). The initial state is typically chosen to be the ground state of some easily preparable configuration, such as *all spins up*. The change in states is called *quantum state transport* or *quantum state driving*.

The point of interest of this thesis is the quantum state driving. This driving usually needs to be performed *adiabatically*, i.e., without excitation of the system. The probability that the state will remain in a ground state during such transport is called *fidelity*. For an illustration of this problem, see Fig. 1, where two scenarios are drawn. In the first case, the state moves adiabatically (fidelity is one). In the second, the state excites in the small energy gap area, which in the case of quantum computers devalues the experiment.

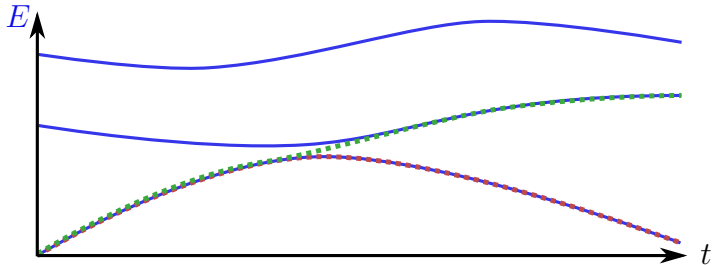


Figure 1: Visualization of the **state adiabatic transport** compared to **transport with excitation** in a system with time varying **energy eigenstates**.

The whole problem of state preparation can be formulated more generally. From the mathematical point of view, the example above is described by *parameter driven Hamiltonian* $\hat{H}(\lambda)$, which depends on some vector λ from *parametric space*. Change in the driving parameter (for example, the orientation of a magnetic field or strength of qubit coupling) influences the qubits and *drives* them to some final state in superposition.

The question of interest is: “How to achieve the better *final fidelity*, meaning *how to prepare the final ground state with the higher probability?*” During the driving, one might add some energy to the qubit, which leads to its excitation and possibly destroys the superposition. Many methods can improve this. From the theory of *quantum state driving* three methods are emphasized here — *adiabatic driving*, *counter-diabatic driving*, or *choosing better driving path*. Adiabatic

¹As qubits one might use for example quantum dots [1] or Josephson junctions [2].

²The name comes from the resemblance to annealing in metallurgy.

driving can be performed by infinitely slow drivings, making it unsuitable for practical applications. Counter-diabatic driving requires adding another element to the Hamiltonian, which leads to *unit fidelity protocols* (the system does not excite), making it a good candidate for practical applications. Finding a better driving path can be combined with all other methods and means that different paths in parameter space lead to different fidelity. Because energy spectra influence these trajectories, one might be interested in the *quantum state manifolds*. These are especially important for some drivings, such as driving using small *quenches* (quick, but small changes in driving parameter), or close-adiabatic driving, where the fidelity is almost one.

Before moving to the theory of quantum state driving, the basics of differential geometry are presented in Chapter 1. It does not serve the full theory, only some basic intuition and notation is presented. In addition, some useful definitions and theorems are provided here. The theory of quantum driving itself is described in Chapter 2. First the geometrical space is constructed, then the concept of *quantum state driving*, *fidelity* and *metric tensor* are introduced. The driving methods are described in Chapter 3. Especially *counter-diabatic*, *adiabatic* and *close-adiabatic* drivings are introduced, along with reformulation of theorems about fidelity. Special importance is played by the *ground state manifold* and geodesics, for which some applications are proposed.

The basic phenomena of quantum state driving are demonstrated on a simple two-level system in Chapter 4. Driving fidelity and energy variance are calculated for two special drivings — *linear* and *geodesic*. Finally, the more convoluted Lipkin-Meshkov-Glick model is analyzed in Chapter 5. The analysis is first performed in specific dimensions, from which some general formulas in arbitrary dimensions are derived. The focus is mainly on the ground state manifold and its geometrical structures. This can help to understand drivings with a unit or almost unit fidelity.

1. Mathematical introduction

The modern approach to the closed system dynamics is using *differential geometry* formalism. Before we get to the quantum mechanics itself, let's introduce this formalism and recapitulate some definitions of this branch of mathematics. This chapter does not serve the full introduction to differential geometry, but reminds the essential realizations which should lead the reader to a better understanding of physical theory in the following chapters. Full introduction to differential geometry can be found for example in notes by Krtouš [3], Loring [4], or Fecko [5].

1.1 Essentials

Consider manifold \mathcal{M} over the field of complex numbers \mathbb{C} . Curves on this manifold are parametrized by some real interval:

$$\mathcal{J} : \mathbb{R} \supset (P_i, P_f) \rightarrow \mathcal{M}, \quad \xi \mapsto \mathcal{J}(\xi) \text{ for } \xi \in (P_i, P_f).$$

The space of functions is $\mathcal{FM} \equiv \{f : \mathcal{M} \rightarrow \mathbb{C}\}$.

To define *vectors* on \mathcal{M} , it is important to have some meaning of the *direction*. The direction is defined using curves \mathcal{J}_i satisfying

$$\mathcal{J}_1(0) = \mathcal{J}_2(0) \equiv P$$

$$\frac{d}{dt}x^i(\mathcal{J}_1(t))\Big|_{t=0} = \frac{d}{dt}x^i(\mathcal{J}_2(t))\Big|_{t=0}.$$

Taking the equivalence class created by these two rules, sometimes noted as $[\mathcal{J}]$, we have an element of the tangent space to \mathcal{M} . We use standard notation for the *tangent space of \mathcal{M}* in some point $P \in \mathcal{M}$ as $\mathbb{T}_P\mathcal{M}$. Cotangent space is denoted as $\mathbb{T}_P^*\mathcal{M}$. Unifying all *tangent* and cotangent spaces over all x we get tangent $\mathcal{T}\mathcal{M}$ and cotangent $\mathcal{T}^*\mathcal{M}$ bundle respective. To generalize this notation to higher tensors, we denote $\mathcal{T}\mathcal{M} \equiv \mathcal{T}^1\mathcal{M}$, $\mathcal{T}^*\mathcal{M} \equiv \mathcal{T}_1\mathcal{M}$. This gives us the possibility to increase the order, leading to p -times *contravariant* and q -times *covariant* tensors. These are denoted $\mathcal{T}_q^p\mathcal{M}$. Tensor space in point $P \in \mathcal{M}$ is denoted $\mathcal{T}_P^p\mathcal{M}$. Using the congruence of curves on \mathcal{M} , the expression

$$\frac{d}{d\xi} f \circ \mathcal{J}(\xi)\Big|_{\xi=0} \tag{1.1}$$

has a good meaning, and we can define the *vector* in some $P \in \mathcal{M}$ as

$$\mathbf{v} : \mathcal{FM} \rightarrow \mathbb{C} \quad f \mapsto \mathbf{v}[f] \equiv \frac{df(\mathcal{J}(\xi))}{d\xi}\Big|_P \equiv \partial_\xi\Big|_P f. \tag{1.2}$$

It holds that $\mathbf{v} \in \mathbb{T}_P\mathcal{M}$ and can be expressed as the *derivative in direction*, which can be understood in coordinates as

$$\mathbf{v}[f] = \frac{d}{d\mathbf{v}} f \circ \mathcal{J}(\xi)\Big|_{\xi=0} = v^k \frac{d}{dx^k} f(x)\Big|_P. \tag{1.3}$$

The directional derivative is denoted ∇_v and in basis $\mathbf{e}_i \equiv \partial/\partial x^i$ it becomes

$$\nabla = (\mathbf{e}_1, \mathbf{e}_2, \mathbf{e}_3).$$

If needed, the *abstract indices* (written by Greek letters) and *pointer indices* (written using Latin letters) are differentiated. Abstract indices show the rank of the tensor, meaning *how many empty slots for contraction the tensor has*. Pointer indices extract specific number from the tensor. For example

$$t_{\nu\kappa}^\mu \in \mathcal{T}_2^1 \mathcal{M}, \quad \text{whilst for some } i, j, k \in \mathbb{N} : t_{jk}^i \in \mathbb{C}.$$

The summation over abstract and Latin indices has the same meaning. For *Tensor contraction*, the index notation is used. When it is clear what type of tensors we are operating with, the Object notation can be used, for example $t(\mathbf{u}, \mathbf{v}) \equiv t_{\mu\nu} \mathbf{u}^\mu \mathbf{v}^\nu$. The contraction can also be noted using the contraction operator \mathbf{C} when it is clear which indices are contracted or when it does not matter which of them are.

Now we have the notation to define one strong structure on manifolds — *metric tensor*.

Definition 1 (Metric tensor). *If the 2-form $g_{\mu\nu} \in \mathcal{T}_2^0 \mathcal{M}$ is*

- *linear in second argument*: $\forall \alpha, \beta \in \mathbb{C}; \mathbf{u}, \mathbf{v}, \mathbf{w} \in \mathcal{T}^1 \mathcal{M} : g(\mathbf{u}, \alpha \mathbf{v} + \beta \mathbf{w}) = \alpha g(\mathbf{u}, \mathbf{v}) + \beta g(\mathbf{u}, \mathbf{w})$,
- *hermitian*: $\forall \mathbf{v}, \mathbf{w} \in \mathcal{T}^1 \mathcal{M} : g(\mathbf{v}, \mathbf{w}) = g(\mathbf{w}, \mathbf{v})^*$,
- *non-degenerate*: $\forall \mathbf{v} \in \mathcal{T}^1 \mathcal{M}$ the function $\mathbf{w} \mapsto g(\mathbf{v}, \mathbf{w})$ is not identically zero,

we call $g_{\mu\nu}$ a metric tensor. The star $$ marks complex conjugation.*

We often require *differentiable metric tensor*, or at least almost everywhere¹. That assures that *covariant derivatives* and *parallel transport* are well-defined almost everywhere differentiable.

Vectors of tangent space to some manifold can be compared only within one such space, and for that, they need to be transported to some common tangent space. The transport can be done using *parallel transport* which is connected to the notion of *covariant derivative*.

Definition 2 (Covariant derivative). *$D_{\mathbf{v}}$ is called the covariant derivative in a direction $\mathbf{v} \in \mathbb{T}_P \mathcal{M}$, if $\forall f \in \mathcal{F} \mathcal{M}$, $\mathbf{A}, \mathbf{B} \in \mathcal{T}_q^p \mathcal{M}$, $\alpha \in \mathbb{C}$:*

- $D_{\mathbf{v}} : \mathcal{T}_P^p \mathcal{M} \rightarrow \mathcal{T}_q^p \mathcal{M}$
- $D_{f\mathbf{v}} \mathbf{A} = f D_{\mathbf{v}} \mathbf{A}$ (*ultralocality in a direction*)
- $D_{\mathbf{v}}(\mathbf{A} + \alpha \mathbf{B}) = D_{\mathbf{v}} \mathbf{A} + \alpha D_{\mathbf{v}} \mathbf{B}$ (*linearity in argument*)
- $D_{\mathbf{v}}(\mathbf{AB}) = (D_{\mathbf{v}} \mathbf{A}) \mathbf{B} + \mathbf{A} (D_{\mathbf{v}} \mathbf{B})$ (*Leibniz rule*)
- $D_{\mathbf{v}}(\mathbf{CA}) = \mathbf{C} D_{\mathbf{v}}(\mathbf{A})$ (*commutation with contraction*)

¹Almost everywhere means *with an exception to the submanifold of zero measure*.

- $\mathbf{D}_v f = v[f] \equiv v^\beta \mathbf{d}_\beta f$ (*operation on functions*)

Definition 3 (Parallel transport). *Parallel transport of tensors in tensor field $\mathbf{A} \in \mathcal{T}_q^p \mathcal{M}$ along some path \mathcal{J} going from $P_i \in \mathcal{M}$ to $P_f \in \mathcal{M}$ is denoted*

$$\begin{aligned} par_{\mathcal{J}} : \mathcal{T}_{P_i} \mathcal{T}_q^p \mathcal{M} &\rightarrow \mathcal{T}_{P_f} \mathcal{T}_q^p \mathcal{M} \\ \mathbf{A}|_{P_i} &\mapsto (par_{\mathcal{J}} \mathbf{A})|_{P_f}. \end{aligned}$$

This means that the parallel transport takes a tensor at some $\mathcal{T}_{P_i} \mathcal{T}_q^p \mathcal{M}$ and transports it to $\mathcal{T}_{P_f} \mathcal{T}_q^p \mathcal{M}$. Those two tensors belong to the same tensor field, but are essentially different. One cannot simply add or subtract them. For that they need to be parallel transported into the same tensor space $\mathcal{T}_q^p \mathcal{M}$.

Another object needed for calculating the covariant derivative is *affine connection*. It is generally defined as the difference between covariant and coordinate derivative $\Gamma := \mathbf{D} - \partial$. Because this definition requires some additional theory, only the *connection on metric spaces* is provided here.

Definition 4 (Connection and Christoffel symbols). *The Affine connection on metric spaces can be defined as*

$$\Gamma_{\mu\nu}^\alpha := \frac{1}{2} g^{\alpha\beta} (g_{\beta\mu,\nu} + g_{\nu\beta,\mu} - g_{\mu\nu,\beta}), \quad (1.4)$$

where comma notation for coordinate derivative is used. Its elements are called the Christoffel symbols.

The covariant derivative of a vector $\mathbf{a} \in \mathbb{T}_P \mathcal{M}$ for manifold with coordinates x^μ can be expressed as

$$\frac{D\mathbf{a}^\mu}{dx^\nu} = \mathbf{a}_{,\nu}^\mu - \Gamma_{\alpha\beta}^\mu x^\alpha \mathbf{a}^\beta \quad (1.5)$$

and for $\alpha \in \mathbb{T}_P^* \mathcal{M}$ it is

$$\frac{D\alpha_\mu}{dx^\nu} = \alpha_{\mu,\nu} - \Gamma_{\mu\beta}^\alpha x^\beta \alpha_\alpha. \quad (1.6)$$

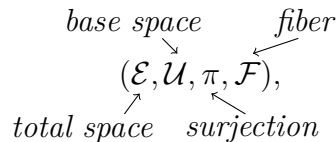
The vector $v \in \mathbb{T}_P \mathcal{M}$ is said to be parallel transported along curve $\mathcal{J}(\lambda)$, if its covariant derivative vanishes along $\mathcal{J}(\xi)$, meaning

$$\frac{Dv^\mu}{d\xi} = 0. \quad (1.7)$$

1.2 Fiber bundle

Sometimes one needs to add additional structure to every point on the manifold. At every point of the manifold we introduced a tensor space. This structure can be described by so-called *fiber bundles*.

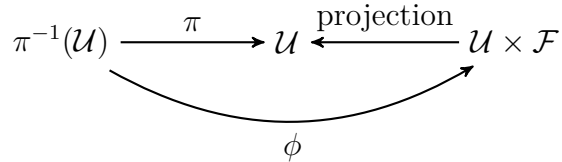
Definition 5 (Fiber bundle). *Structure*



for topological spaces \mathcal{E} , \mathcal{U} , \mathcal{F} and continuous surjection $\pi : \mathcal{E} \rightarrow \mathcal{U}$ satisfying a local triviality, is called a Fiber bundle. The local triviality means that \mathcal{U} is connected² and for every $x \in \mathcal{U}$, there is an open neighborhood $\mathcal{N} \subset \mathcal{U}$ (trivializing neighborhood) such that there exists a homeomorphism from \mathcal{N} to so-called product space

$$\phi : \pi^{-1}(\mathcal{N}) \rightarrow \mathcal{N} \times \mathcal{F},$$

such that $\pi^{-1} \circ \pi(\mathcal{N}) = \mathcal{N}$. Plus there exist natural projection from $\mathcal{N} \times \mathcal{F}$ to \mathcal{N} , setting the coordinate in fibers to zero. The structure can be visualized as follows:



Because the projections of products are open maps, $\pi : \mathcal{E} \rightarrow \mathcal{N}$ must be an open map. The manifolds at every point $x \in \mathcal{F}$ are all locally diffeomorphic to each other.

These structures are usually imagined like fibers from the manifold, similar to your head's hair. One can imagine the \mathcal{N} as head, \mathcal{F} the hair, π applied on any point on hair returns the point on the head, and \mathcal{E} is the head with all the hairs. This analogy holds only if all hairs are the same.

1.3 Riemannian geometry

Some Riemannian geometry theorems have implications in the theory of quantum driving. First, some basic definitions are needed.

Definition 6 (Riemannian manifold). *Manifold is called Riemannian if it is equipped with a positive definite metric tensor.*

Definition 7 (Connected manifold). *A manifold is connected if the distance between two points is the infimum of the lengths of curves joining the two points.*

Definition 8 (Compact manifold). *A manifold is said to be compact if its every open cover has a finite subcover.*

Definition 9 (Geodesical completeness). *A manifold is said to be geodesically complete if every geodesic on it can be extended to infinite values of their affine parameter.*

The geodesical completeness is a coordinate-independent notion.

Definition 10 (Geodesic maximality). *A manifold is said to be geodesically maximal if it is either geodesically complete or every non-complete geodesic (such that cannot be extended to infinite values of their affine parameter) ends in a singularity.*

²Connected mean, it can't be represented as a union of two and more disjoint sets

Geodesic maximality is a coordinate-dependent notion only if the manifold is geodesically complete.

Theorem 1 (Von Neumann-Wigner). Landau and Lifshitz [6, page 305]

This, sometimes called the Non-Crossing Theorem, states that the eigenvalues of the Hermitian matrix driven by N continuous real parameters forms at a maximum $(N - 2)$ -dimensional submanifold.

Theorem 2 (Hopf-Rinow Theorem). Petersen [7, page 125]

For connected Riemannian manifold \mathcal{M} with the metric g , following are equivalent:

- (\mathcal{M}, g) is geodesically complete, i.e., all geodesics are infinite,
- (\mathcal{M}, g) is geodesically complete at some point P , meaning the geodesics going through P are infinite,
- (\mathcal{M}, g) satisfies the Heine-Borel property, i.e., every closed bounded set is compact,
- (\mathcal{M}, g) is complete as a metric space.

Theorem 3 (Modified Hopf-Rinow Theorem). Gorodski [8, Chapter 3]

For connected Riemannian manifold \mathcal{M} with the metric g , any two points on \mathcal{M} can be joined with a minimizing geodesic.

This generally means that in a space with singularity exists such points, which cannot be connected with the rest of the manifold using geodesics. In General relativity, this area is, for example, below the event horizon of black holes.

Theorem 4. Gorodski [8, Chapter 3]

A compact Riemannian manifold is geodesically complete.

An important tensor in differential geometry is the *Riemann tensor*

$$R^\alpha_{\beta\gamma\delta} := \Gamma^\alpha_{\beta\delta,\gamma} - \Gamma^\alpha_{\beta\gamma,\delta} + \Gamma^\mu_{\beta\delta}\Gamma^\alpha_{\mu\gamma} - \Gamma^\mu_{\beta\gamma}\Gamma^\alpha_{\mu\delta}. \quad (1.8)$$

Ricci tensor can be defined as its contraction

$$R_{\alpha\gamma} := R^\mu_{\alpha\mu\gamma}, \quad (1.9)$$

which is second order symmetric tensor. *Ricci scalar*, describing the curvature on manifold, is defined as contraction of the Ricci tensor

$$R := R^\mu_\mu. \quad (1.10)$$

1.4 Geometry in 2 dimensions

Ricci scalar can be simplified for 2-dimensional manifold as

$$R = \frac{2}{g_{22}} \left(\Gamma^1_{22,1} - \Gamma^1_{12,2} + \Gamma^1_{11}\Gamma^1_{22} + \Gamma^1_{12}\Gamma^2_{22} - \Gamma^1_{21}\Gamma^1_{12} - \Gamma^1_{22}\Gamma^2_{12} \right). \quad (1.11)$$

Another possibility to express the Ricci tensor in two dimensions, see Gutiérrez-Ruiz et al. [9, eq. 6,7], is

$$R = \frac{1}{\sqrt{|g|}}(\mathcal{S} + \mathcal{T}), \quad (1.12)$$

for

$$\mathcal{S} := \left(\frac{g_{12}}{g_{11}\sqrt{|g|}}g_{11,2} - \frac{1}{\sqrt{|g|}}g_{22,1} \right)_{,1} \quad (1.13)$$

$$\mathcal{T} := \left(\frac{2}{\sqrt{|g|}}g_{12,1} - \frac{1}{\sqrt{|g|}}g_{11,2} - \frac{g_{12}}{g_{11}\sqrt{|g|}}g_{11,1} \right)_{,2}. \quad (1.14)$$

2. Introduction to quantum geometry

This chapter depends on the mathematical formalism developed in Chapter 1, and some basic knowledge of quantum mechanics is required. Most parts are inspired by notes from Kolodrubetz et al. [10] and original notes by Berry [11](1984), [12](1989), [13](2009) with attempt to give them more rigorous meaning in the language of differential geometry.

The aim of this chapter is the construction of space on which the *driving of quantum states* (changing the states by controlling the Hamiltonian parameter) is performed and introducing some basic concepts needed. There may be many geometrical constructions of the space because usually, only some sections of the full space are used. Different constructions require different mathematical formalism. One might choose the way of *vector bundles*, or *fiber bundles* (our case), or just sectioning one Hilbert space in different ways, constructing the needed physical spaces. The reason for choosing the way of fiber bundles is that from the Hamiltonian with free parameter $\hat{H}(\lambda)$, we get one Hilbert space for every parameter value. The fiber structure then gives the natural formalism for connecting these spaces and embeds the space with natural geometry due to changing eigenbasis during the driving. Another reason is purely formal, that is, that one might look at the quantum system, construct Hilbert space and some Hamiltonian on it. The approach leading to fiber spaces is that one has a Hamiltonian, for which the Hilbert space is constructed as linear span of all its eigenvectors.

Even though the theory below depends on differential geometry, it does not reformulate the whole quantum mechanics into this language. This kind of reformulation is a rather complicated task and for an introduction to this approach, see Appendix A.

From now on, we use natural units, so $\hbar = 1$.

2.1 Space of all states

Assume parameter $\boldsymbol{\lambda} \in \mathcal{U} \subset \mathbb{R}^n$ for \mathcal{U} open set. This parameter controls some finite-dimensional Hamiltonian $\hat{H}(\boldsymbol{\lambda})$, which is bounded from below and has discrete spectrum. From this we can construct the fiber bundle, such that at every point of the base manifold $\boldsymbol{\lambda} \in \mathcal{U}$, we construct fiber as a Hilbert space $\mathcal{H}(\boldsymbol{\lambda})$. The fiber structure can be according to Def. 5 written as

$$\left(\mathcal{H}_{full} := \bigcup_{\boldsymbol{\lambda} \in \mathcal{U}} \mathcal{H}(\boldsymbol{\lambda}), \quad \mathcal{U} \subset \mathbb{R}^n, \quad \pi, \quad \mathcal{H}(\boldsymbol{\lambda}) := \bigcup_{states} |\psi(\boldsymbol{\lambda})\rangle \right).$$

The projection is defined as $\pi(\boldsymbol{\lambda}) : |\psi(\boldsymbol{\lambda})\rangle \mapsto \boldsymbol{\lambda}$ and $\mathcal{H}(\boldsymbol{\lambda})$ is a Hilbert space containing all pure states of $\hat{H}(\boldsymbol{\lambda})$. Geometric intuition is displayed in Fig. 2.1.

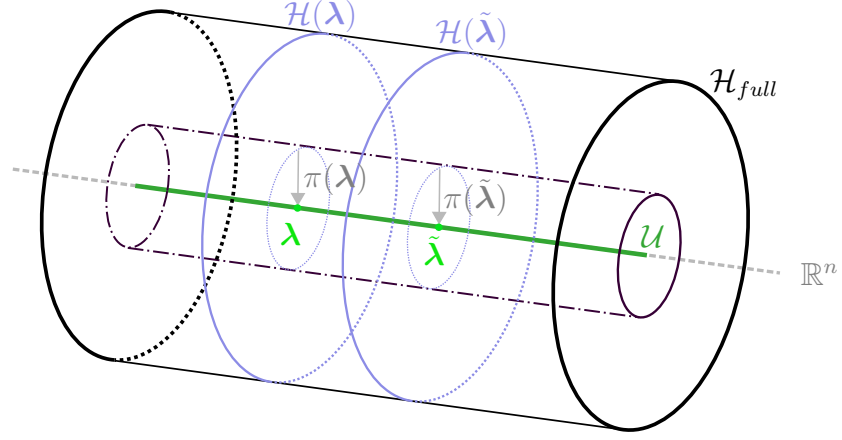


Figure 2.1: Base manifold $\mathcal{U} \subset \mathbb{R}^n$ is visualized as a line. For every point $\lambda \in \mathcal{U}$ one Hilbert space $\mathcal{H}(\lambda)$ (blue disk) is constructed as a fiber. The union of all these fibers creates the full Hilbert space \mathcal{H}_{full} (hollow cylinder) and from every Hilbert space there exist projection π onto the base manifold.

2.2 Rays and bare states

Physical observables in quantum mechanics are related to the *space of rays* or *projective Hilbert space*, defined as $\mathcal{PH} := \mathcal{H}/U(1)$, where elements of $U(1)$ are unitary transformations $e^{i\varphi}$ for $\varphi \in [0, 2\pi]$. This defines the global gauge symmetry between quantum states. The phase φ is chosen the same for every vector and can be chosen arbitrarily. We cannot alter the phase of individual vectors, meaning there is no local gauge symmetry.

This resembles the fiber structure

$$(\mathcal{H}, \mathcal{PH}, \pi_{rays}, \{e^{i\varphi} | \varphi \in [0, 2\pi]\}),$$

where π_{rays} is just rule setting phase φ to arbitrary value. The geometrical intuition is drawn in Fig. 2.2.

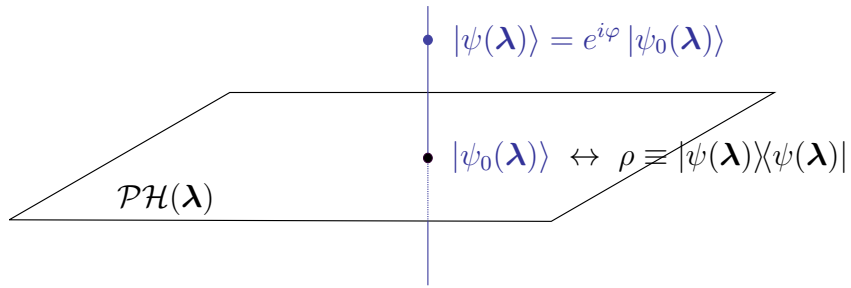


Figure 2.2: For every λ we have the projective Hilbert space $\mathcal{PH}(\lambda)$ containing physical states $|\psi(\lambda)\rangle$ corresponding to density matrix $\rho \equiv |\psi(\lambda)\rangle\langle\psi(\lambda)|$. Every state can be multiplied by phase factor $e^{i\varphi}$, extending it to Hilbert space $\mathcal{H}(\lambda)$.

2.3 Sectioning the space

Consider initial state $|\psi_0\rangle \in \mathcal{H}(\boldsymbol{\lambda}_0)$. The state then evolves along some path

$$\mathcal{J} := \{\boldsymbol{\lambda}(t) | t \in [0, T], \boldsymbol{\lambda} \in \mathcal{U}\} \subset \mathbb{R}^n, \quad \boldsymbol{\lambda}(0) = \boldsymbol{\lambda}_0 \quad (2.1)$$

parametrized by time t , according to the Schrödinger equation

$$i\hbar \frac{d}{dt} |\psi(\boldsymbol{\lambda}(t))\rangle = \hat{H}(\boldsymbol{\lambda}(t)) |\psi(\boldsymbol{\lambda}(t))\rangle. \quad (2.2)$$

For eigenstates $\{|s\rangle\}_{s=0}^{N-1}$ of instantaneous Hamiltonian it reads as a Schrödinger energy equation

$$\hat{H}(\boldsymbol{\lambda}) |s(\boldsymbol{\lambda})\rangle = E_s(\boldsymbol{\lambda}) |s(\boldsymbol{\lambda})\rangle. \quad (2.3)$$

Notice that these states are independent on the trajectory \mathcal{J}_t . For every $\hat{H}(\boldsymbol{\lambda})$ its energies can be sorted from the smallest, defining the *Hamiltonian spectrum*

$$\sigma(\hat{H}(\boldsymbol{\lambda})) := \{E_0, \dots, E_{N-1}\}. \quad (2.4)$$

In this set degeneracies are not unified into one element, therefore every $\sigma(\boldsymbol{\lambda})$ has N elements. From this there exists an isomorphism between all σ -sets, and we can define *section*

$$\sec_s : |s(\boldsymbol{\lambda})\rangle \mapsto \mathcal{U} \subset \mathbb{R}^n, \quad \text{for } s \in \{0, \dots, N-1\}.$$

This maps eigenstates corresponding to energy E_s to the base manifold. This mapping is similar to previously introduced π , except it is an isomorphism, not a projection. The isomorphism is showed later on, when introducing the metric structure on these spaces.

Now we have constructed N sections of the full Hilbert space, which are isomorphic to the base manifold. Because \mathcal{U} is a Riemannian manifold, these so-called *projective state manifolds*

$$\mathcal{PM}_s := \left\{ \bigcup_{\boldsymbol{\lambda} \in \mathcal{U}} |s(\boldsymbol{\lambda})\rangle \right\}, \quad (2.5)$$

must be also Riemannian. Of special importance is the *projective ground state manifold* \mathcal{PM}_0 , which is used later on for adiabatic transports of ground states. Geometrical intuition for state manifolds is drawn in Fig. 2.3.

The reason for calling the manifolds *projective* is the gauge symmetry of the Schrödinger equation. We can change the phase of vector $|s\rangle \mapsto e^{i\varphi} |s\rangle$ by any $\varphi \in \mathbb{R}$. If all the possible \mathcal{PM} are unified over all phases (only interval $(0, 2\pi]$ is used to avoid degeneracy), we get *state manifolds*

$$\mathcal{M}_s := \left\{ \bigcup_{\varphi \in [0, 2\pi)} \bigcup_{\boldsymbol{\lambda} \in \mathcal{U}} e^{i\varphi} |s(\boldsymbol{\lambda})\rangle \right\}. \quad (2.6)$$

Because these manifolds were created by sectioning, they are considered vector spaces in a geometrical sense. This was expected because they contain quantum states, which themselves are vectors.

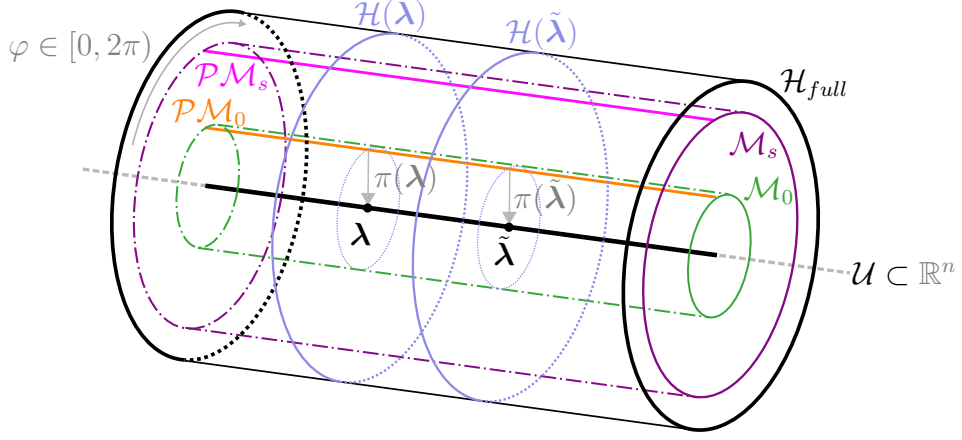


Figure 2.3: From the full Hilbert space \mathcal{H}_{full} (the biggest hollow cylinder) we identified eigenstates and unified them into state manifolds \mathcal{M}_s . These are drawn as inner cylinders of \mathcal{H}_{full} , especially see the ground state manifold \mathcal{M}_0 as the inner cylinder. The phase φ introduces gauge symmetry $e^{i\varphi}$. If it is fixed, we get projective state manifolds \mathcal{PM}_s , especially see \mathcal{PM}_0 . Projective state manifolds are isomorphic to the base manifold \mathcal{U} .

The Hilbert spaces in different points λ have the same finite dimension, so the natural question is if we need the fiber structure at all and if we could understand the projection π as a surjection from one Hilbert space to the base manifold $\pi : \mathcal{H} \rightarrow \mathcal{M}$. This can indeed be done, but we would lose some generality in description. For example, the natural choice for basis in the Hilbert space is the eigenbasis, which is different for every $\mathcal{H}(\lambda)$. In addition, dependent on the space structure, two different interpretations of a wavefunction collapse can be considered.

1. In the fiber structure, we can imagine changing the parameter λ as moving between $\mathcal{H}(\lambda)$ subspaces of \mathcal{H}_{full} , in which the eigenbasis can be embedded geometrically. The space coordinate then holds information about λ and position in Hilbert space.
2. If we imagine only one Hilbert space, the eigenbasis varies in time, and the driving is performed in a time-varying space.

2.4 Transporting states on state manifolds

This chapter is inspired by Berry [11]. The decomposition of \mathcal{H}_{full} to different state manifolds \mathcal{M}_s is imagined as sheets above the parametric space.

Changing the state from eigenstate $|s(\lambda)\rangle$ to $|s(\tilde{\lambda})\rangle$ on \mathcal{M}_s during some time period is unitary transformation and can be thought of as *parallel transport on fiber bundle* between two states. Assuming the transport goes along \mathcal{J} defined by Eq. 2.1, the transported state is the solution to the Schrödinger equation 2.2 and can be written at any time as

$$|s(\lambda(t))\rangle = \text{par}_{\gamma_s(t)} |s(\lambda(0))\rangle = \exp\left(-i \int_0^t E_s(\tau) d\tau\right) \exp(i\gamma_s(t)) |s(\lambda(0))\rangle. \quad (2.7)$$

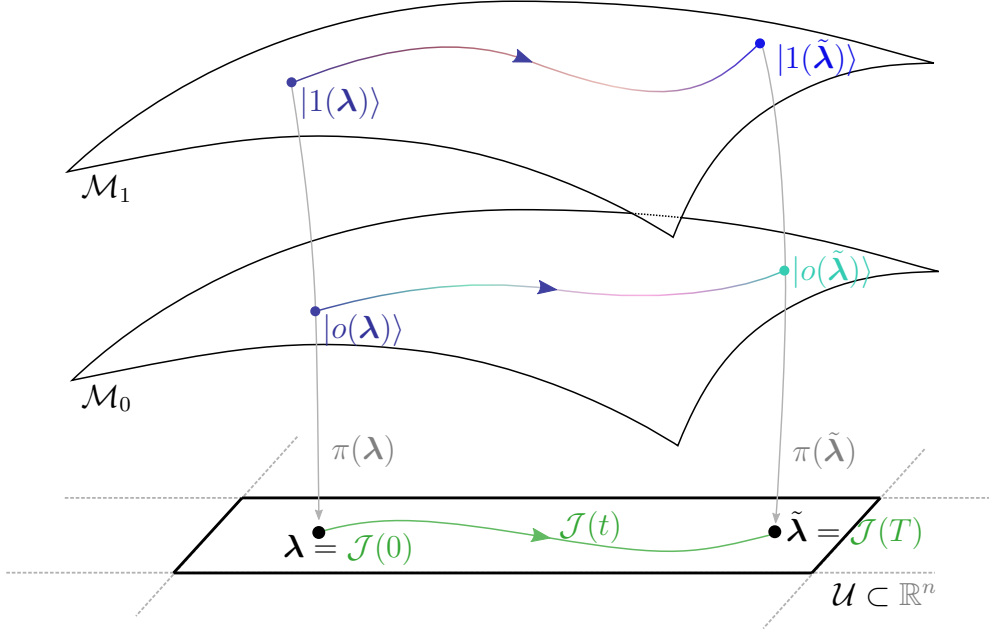


Figure 2.4: The cylinders from Fig. 2.3 are now displayed as two-dimensional sheets. The [transport of states](#) is performed on state manifolds \mathcal{M}_s along the [path](#) $\mathcal{J}(t)$, defined in parametric space. The information about gauge phase φ is represented by color (see the changing color on the paths in \mathcal{M}_s).

Two exponentials in parallel transport in Eq. 2.7 have separate meaning and are called *dynamical* and *geometrical* phase. The geometric intuition on driving can be seen in Fig. 2.4.

Dynamical phase

The first exponential in Eq. 2.7, the *dynamical phase* depends only on time and Hamiltonian spectrum during the transport. This dynamical phase changes the states only within the projective state manifold \mathcal{PM}_s .

Geometrical phase

The complication arises with the fact that our playground is a state manifold \mathcal{M}_s and some element $\varphi = \gamma_s(t)$, called *geometrical phase*, needs to be included. This phase is generally non-integrable, meaning it depends on the whole path and cannot be written simply as $\gamma_s(\lambda)$. For a closed curve

$$C = \{\lambda(t) | t \in [0, T], \text{ such that } \lambda(0) = \lambda(T)\} \subset \mathcal{U} \quad (2.8)$$

we generally get $\text{par}_C |\psi(\lambda)\rangle \neq |\psi(\lambda)\rangle$. This property is sometimes called an *anholonomy* and can be imagined in Fig. 2.4 as change of the path color during the driving. Without anholonomy the path color would not change. In Fig. 2.3, the change of phase means the curve goes around the inner cylinder \mathcal{M}_s and without anholonomy it gets restricted to \mathcal{PM}_s line. Substituting general solution

2.7 to Eq. 2.2 yields¹

$$\hat{H}(\boldsymbol{\lambda}(t)) |\psi(t)\rangle = i \frac{d}{dt} |\psi(t)\rangle \quad (2.9)$$

$$E_s(\boldsymbol{\lambda}(t)) |s(\boldsymbol{\lambda}(t))\rangle = E_s(\boldsymbol{\lambda}(t)) |s(\boldsymbol{\lambda}(t))\rangle - \frac{d\gamma_s(t)}{dt} |s(\boldsymbol{\lambda}(t))\rangle + \frac{d}{dt} |s(\boldsymbol{\lambda}(t))\rangle \quad (2.10)$$

$$\frac{d\gamma_s(t)}{dt} = i \langle s(\boldsymbol{\lambda}(t)) | \frac{d}{dt} |s(\boldsymbol{\lambda}(t))\rangle. \quad (2.11)$$

Separating the dependence of vectors on driving parameter and time, we get

$$\frac{d\gamma_s(\boldsymbol{\lambda}(t))}{dt} = i \langle s(\boldsymbol{\lambda}(t)) | \partial_j s(\boldsymbol{\lambda}) \rangle \dot{\boldsymbol{\lambda}}^j(\lambda), \quad (2.12)$$

for partial derivative along \mathcal{U} coordinates ∂_j and dot as time derivative. Integrating this equation around some closed curve C , we get

$$\gamma_s(C) = i \oint_C \langle s(\boldsymbol{\lambda}) | \partial_j s(\boldsymbol{\lambda}) \rangle d\boldsymbol{\lambda}^j. \quad (2.13)$$

This equation implies that the geometrical phase does not depend on energy or time, only on the sequence of Hamiltonians, which means it depends only on the path \mathcal{J} and spectrum $\sigma(\hat{H}(\boldsymbol{\lambda}))$.

Restriction to 3-dimensional parametric space

The problem with integration in Eq. 2.13 lies in the derivative $\partial_{\boldsymbol{\lambda}} s(\boldsymbol{\lambda})$, which locally requires knowledge of single-valued basis $\{|0\rangle, \dots, |N-1\rangle\}$. This can be avoided in 3-dimensions using Stokes's theorem for S as the surface with boundary $\partial S = C$, for coordinate gradient ∇

$$\begin{aligned} \gamma_s(C) &= -\text{Im} \iint_C \mathbf{d}S \cdot \nabla \times \langle s(\boldsymbol{\lambda}) | \nabla n(\boldsymbol{\lambda}) \rangle \\ &= -\text{Im} \iint_C \mathbf{d}S \cdot \langle \nabla s(\boldsymbol{\lambda}) | \times | \nabla s(\boldsymbol{\lambda}) \rangle \\ &= -\text{Im} \iint_C \mathbf{d}S \cdot \sum_{m \neq s} \langle \nabla s(\boldsymbol{\lambda}) | m(\boldsymbol{\lambda}) \rangle \times \langle m(\boldsymbol{\lambda}) | \nabla s(\boldsymbol{\lambda}) \rangle \\ &= - \iint_C \mathbf{d}S \cdot \mathbf{V}_s(\boldsymbol{\lambda}), \end{aligned} \quad (2.14)$$

for the *vector potential*

$$\mathbf{V}_s(\boldsymbol{\lambda}) = \sum_{m \neq s} \text{Im} \frac{\langle s(\boldsymbol{\lambda}) | \nabla \hat{H}(\boldsymbol{\lambda}) | m(\boldsymbol{\lambda}) \rangle \times \langle m(\boldsymbol{\lambda}) | \nabla \hat{H}(\boldsymbol{\lambda}) | s(\boldsymbol{\lambda}) \rangle}{(E_m(\boldsymbol{\lambda}) - E_s(\boldsymbol{\lambda}))^2}. \quad (2.15)$$

The element of summation $m = s$ in the third step of derivation 2.14 is real, therefore has no influence on γ_s and can be omitted, and $| \nabla s(\boldsymbol{\lambda}) \rangle := \nabla | s(\boldsymbol{\lambda}) \rangle$.

Comparing the first expression in Eq. 2.14 with its last one and extending it to real numbers, we get

$$\mathbf{V}_s(\boldsymbol{\lambda}) = \nabla \times \langle s(\boldsymbol{\lambda}) | \nabla m(\boldsymbol{\lambda}) \rangle. \quad (2.16)$$

¹Here the derivation along upper bound $F(x) := \int_0^{g(x)} f(t) dt \Rightarrow F'(x) = f(g(x))g'(x)$ for $f(t) \in L^1(0, g(x))$ and differentiable function g , is used.

Proof of Eq. 2.14. All steps are simple algebraic operations, except for the last equivalence. This can be shown by differentiating the Schrödinger equation 2.3. For any $|s(\boldsymbol{\lambda})\rangle \in \mathcal{M}_s$, $|m(\boldsymbol{\lambda})\rangle \in \mathcal{M}_m$ (the dependence on $\boldsymbol{\lambda}$ in notation is omitted), we get

$$\begin{aligned} \nabla(\underbrace{\hat{H}|s\rangle}_{E_s|s\rangle}) &= (\nabla \hat{H})|s\rangle + \hat{H}|\nabla s\rangle \\ \langle m|E_s|s\rangle &= \langle m|\nabla \hat{H}|s\rangle + \underbrace{\langle m|\hat{H}}_{\langle m|E_m}|\nabla s\rangle \\ \langle m|\nabla s\rangle &= \frac{\langle m|\nabla \hat{H}|s\rangle}{E_s - E_m}, \quad s \neq m. \end{aligned} \quad (2.17)$$

□

As was mentioned, the above procedure from Eq. 2.13 was performed only for three-dimensional space. Proper generalization to k-dimensional space would yield

$$\gamma_s(C) = - \iint_C (\mathbf{d}S)^{\alpha\beta} \cdot \text{Im} \overbrace{\frac{\langle s(\boldsymbol{\lambda})|\mathbf{d}_\alpha \hat{H}(\boldsymbol{\lambda})|m(\boldsymbol{\lambda})\rangle \wedge \langle m(\boldsymbol{\lambda})|\mathbf{d}_\beta \hat{H}(\boldsymbol{\lambda})|s(\boldsymbol{\lambda})\rangle}{(E_m(\boldsymbol{\lambda}) - E_s(\boldsymbol{\lambda}))^2}}^{\in \mathcal{T}_1 \mathcal{M}}, \quad (2.18)$$

for exterior derivative \mathbf{d} .

2.5 Fidelity

The *fidelity* measures “closeness” of two quantum states. It is generally defined for two density operators $\hat{\rho}, \hat{\sigma}$ as

$$\begin{aligned} \mathcal{F} : \text{End}(\mathcal{H}) \times \text{End}(\mathcal{H}) &\mapsto \mathbb{R}, \\ \mathcal{F}(\hat{\rho}, \hat{\sigma}) &:= \left(\text{Tr} \sqrt{\sqrt{\rho}\sigma\sqrt{\rho}} \right)^2 = (\text{Tr} \sqrt[4]{\rho\sigma\sigma\rho})^2 = \left(\text{Tr} \sqrt[4]{\rho\sigma(\rho\sigma)^+} \right)^2, \end{aligned} \quad (2.19)$$

where last equality holds due to hermiticity of density matrices. The usefulness of this definition can be shown in three special cases.

- If both states are pure, $\hat{\rho} =: |\rho\rangle\langle\rho|$, $\hat{\sigma} =: |\sigma\rangle\langle\sigma|$, the fidelity formula reduces to

$$\begin{aligned} F : \mathcal{H} \times \mathcal{H} &\mapsto \mathbb{R}, \\ \mathcal{F}(\hat{\rho}, \hat{\sigma}) &=: F(|\rho\rangle, |\sigma\rangle) = |\langle\rho|\sigma\rangle|^2. \end{aligned} \quad (2.20)$$

- For pure state $\hat{\rho} = |\rho\rangle\langle\rho|$, the fidelity is

$$\mathcal{F}(\hat{\rho}, \hat{\sigma}) = \langle\rho|\hat{\sigma}|\rho\rangle \left(\text{Tr} \sqrt{|\rho\rangle\langle\rho|} \right)^2 = \langle\rho|\hat{\sigma}|\rho\rangle. \quad (2.21)$$

- Commuting density matrices have a meaning of probability distributions. The commutativity implies that $\hat{\rho}, \hat{\sigma}$ can be diagonalized in the same eigenbasis. For $\hat{\rho} = \sum_i p_i |i\rangle\langle i|$, $\hat{\sigma} = \sum_i s_i |i\rangle\langle i|$ we get

$$\sqrt{\hat{\rho}\hat{\sigma}} = \text{Tr} \left(\sum_k \sqrt{p_k s_k} |i\rangle\langle i| \right) = \sum_k \sqrt{p_k s_k} \quad (2.22)$$

and inserting into the definition 2.19 gives

$$F(\hat{\rho}, \hat{\sigma}) = \left(\sum_k \sqrt{p_k s_k} \right)^2. \quad (2.23)$$

The physical meaning of fidelity can also be seen on the state manifolds, imagining *quantum quench between two states* (rapid change of some Hamiltonian parameters). In this case, F is the probability that the system prepared in some initial ground state $|\rho\rangle$ is found in the new ground state $|\sigma\rangle$. $1 - F$ is then the probability of exciting the system during this quench.

Before moving to the practical usage of fidelity, let's look at some general properties.

Theorem 5 (The fidelity properties). *For any two density matrices $\hat{\rho}, \hat{\sigma}$*

- $\mathcal{F}(\hat{\rho}, \hat{\sigma}) \in [0, 1]$ (*normalization*),
- $\mathcal{F}(\hat{\rho}, \hat{\sigma}) = \mathcal{F}(\hat{\sigma}, \hat{\rho})$ (*symmetry*),
- $\mathcal{F}(\hat{\rho}, \hat{\sigma}) = 1 \Leftrightarrow \hat{\rho} = \hat{\sigma}$.

Proof. The first statement is a consequence of Cauchy-Schwarz inequality. The second and third go from Uhlmann's theorem, see publication from Uhlmann [14]. \square

2.6 Metric and geometric tensor

As a playground for this chapter, we choose the projective ground state manifold \mathcal{PM}_0 , but it can be easily generalized to any \mathcal{PM}_s . This means the geometrical phase is neglected, because the states are considered to be the physical states from the projective Hilbert space.

To obtain restriction on metric tensor definition, the local gauge dependence needs to be suppressed. This means the distance on \mathcal{PM}_0 cannot depend on coordinate dependent gauge phase $\varphi(\lambda)$. This phase induces the change in a ground state $|o(\lambda)\rangle$ of the Hamiltonian $\hat{H}(\lambda)$ ²

$$|o(\lambda)\rangle \mapsto e^{i\varphi(\lambda)} |o(\lambda)\rangle, \quad (2.24)$$

which implies

$$\langle o(\lambda) | \nabla o(\lambda) \rangle \mapsto \langle o(\lambda) | \nabla o(\lambda) \rangle + i \nabla \varphi(\lambda). \quad (2.25)$$

²Note that we can also write $|o(\lambda)\rangle \in \mathcal{PM}_0 \cap \mathcal{H}(\lambda)$, which is the set containing exactly one vector — the ground state of $\hat{H}(\lambda)$.

For twice differentiable function $\varphi(\boldsymbol{\lambda}) \in \mathcal{C}^2$, the gauge independent³ function f , would be for infinitesimal change for example

$$f := \langle o(\boldsymbol{\lambda} + \delta\boldsymbol{\lambda}) | o(\boldsymbol{\lambda}) \rangle. \quad (2.26)$$

This is called the *fidelity amplitude of a ground state*, because for pure states we get the fidelity $F = |f|^2$. The meaning of fidelity as a probability transition between the states during some quench, leads to the definition of *distance on \mathcal{M}_0*

$$ds^2 \equiv 1 - F(|o(\boldsymbol{\lambda} + \delta\boldsymbol{\lambda})\rangle, |o(\boldsymbol{\lambda})\rangle) = 1 - |\langle o(\boldsymbol{\lambda} + \delta\boldsymbol{\lambda}) | o(\boldsymbol{\lambda}) \rangle|^2. \quad (2.27)$$

We can easily check, that the axioms for metric distance holds:

- identity of indiscernibles $s(|\psi\rangle, e^{i\alpha}|\phi\rangle) = 0 \Leftrightarrow |\psi\rangle = |\phi\rangle, \alpha \in \mathbb{R}$,
- symmetry for any two states $|\psi\rangle, |\phi\rangle$ is implied by $|\langle \psi | \varphi \rangle| = |\langle \varphi | \psi \rangle|$,
- triangle inequality is implied by bra-ket properties:
 $s(|\psi\rangle, |\psi_2\rangle) < s(|\psi\rangle, |\psi_1\rangle) + s(|\psi_1\rangle, |\psi_2\rangle)$ for any $|\psi\rangle, |\psi_1\rangle, |\psi_2\rangle$.

If we take the fidelity between two parameter-dependent states, the infidelity $1 - F(|\psi(\boldsymbol{\lambda})\rangle, |\psi(\boldsymbol{\lambda} + \Delta)\rangle) > 0$ and the first term of Taylor expansion in Δ is zero, implying it can be used for the metric tensor definition.

Definition 11 (Metric tensor on projective state manifolds). *Because the projective state manifolds \mathcal{PM}_s are isomorphic to the base manifold \mathbb{R}^n , we can define*

$$\begin{aligned} g_{\mu\nu} : \textcolor{red}{T}\mathcal{U} \times \textcolor{red}{T}\mathcal{U} &\rightarrow \mathbb{R} \\ g_{jk} d\boldsymbol{\lambda}^j d\boldsymbol{\lambda}^k + \mathcal{O}(\lambda^3) &\equiv ds^2 := 1 - |\langle o(\boldsymbol{\lambda} + \delta\boldsymbol{\lambda}) | o(\boldsymbol{\lambda}) \rangle|^2. \end{aligned} \quad (2.28)$$

Even though we call $g_{\mu\nu}$ the metric tensor *on projective state manifolds*, it takes forms from $\textcolor{red}{T}\mathcal{U}$. Using abstract indices this means

$$g^{\mu\nu} d_{\mu} \boldsymbol{\lambda} d_{\nu} \boldsymbol{\lambda}. \quad (2.29)$$

This whole procedure can be made more rigorous using so-called *vector bundles*, see the book by Loring [4][Chap. 7]. In our case we can use the isomorphism of $\textcolor{red}{T}\mathcal{U} \times \textcolor{red}{T}\mathcal{U}$ and $\textcolor{blue}{T}\mathcal{M} \times \textcolor{blue}{T}\mathcal{M}$ and simply write

$$g_{jk} d\boldsymbol{\lambda}^j d\boldsymbol{\lambda}^k = g_{jk} \frac{\partial \boldsymbol{\lambda}^j}{\partial \mathbf{v}^l} \frac{\partial \boldsymbol{\lambda}^k}{\partial \mathbf{v}^m} d\mathbf{v}^l d\mathbf{v}^m =: G_{lm} d\mathbf{v}^l d\mathbf{v}^m. \quad (2.30)$$

Practically only g_{jk} is used; thus, what should have been called *the metric tensor on state manifolds* $G_{\mu\nu}$ leaves forgotten. “And some things that should not have been forgotten were lost.” Tolkien [15].

Because the metric tensor is a real analytical function of coordinates, its analytical continuation into complex numbers can be performed. For the motivation behind the following definition, see the book by Cheng [16].

³Here the gauge independence means that the function does not depend on phase φ .

Definition 12 (Geometric tensor). *On the ground state manifold \mathcal{M}_0 , the geometric tensor can be defined as*

$$\chi_{jk} := \langle \partial_j o | \partial_k o \rangle_c \equiv \langle \partial_j o | \partial_k o \rangle - \langle \partial_j o | o \rangle \langle o | \partial_k o \rangle, \quad (2.31)$$

where shortened notation $\partial_k := \frac{\partial}{\partial \lambda^k}$ is used. The subscript c means connected and is defined by the formula.

This definition is in fact gauge independent and can be extended onto any state manifold.

Real part of geometric tensor is symmetric, and it is the metric tensor from Def. 11. The imaginary part is antisymmetric and is called the *curvature tensor*, or *Berry curvature*. The metric tensor can then be expressed as

$$g_{jk} = \text{Re}\chi = \frac{1}{2}(\chi_{jk} + \chi_{kj}) = \text{Re} \sum_{o \neq s} \frac{\langle o | \frac{\partial \mathcal{H}}{\partial \lambda^j} | s \rangle \langle s | \frac{\partial \mathcal{H}}{\partial \lambda^k} | o \rangle}{(E_o - E_s)^2}. \quad (2.32)$$

The Berry curvature is

$$\nu_{jk} = \text{Im}\chi = \frac{i}{2}(\chi_{jk} - \chi_{kj}) = -\text{Im} \sum_{o \neq s} \frac{\langle o | \frac{\partial \mathcal{H}}{\partial \lambda^j} | s \rangle \langle s | \frac{\partial \mathcal{H}}{\partial \lambda^k} | o \rangle}{(E_o - E_s)^2}. \quad (2.33)$$

Derivation of formulas 2.32 and 2.33 is rather technical and is postponed to Appendix A.2. Here we only proof that both definitions of metric distance above have the same physical meaning.

Proof of the metric tensor definitions correspondence.

To prove the correspondence of geometric tensor, defined by Eq. 2.31, to distance on \mathcal{M}_0 in Eq. 2.27, we start with the state $|o(\lambda)\rangle \in \mathcal{M}_s \cap \mathcal{H}(\lambda)$ — the ground state of $\hat{H}(\lambda)$. Changing parameter λ to $\lambda + \delta\lambda$ results in a state, which is a linear combination of eigenstates $|s(\lambda + \delta\lambda)\rangle \in \mathcal{M}_s \cap \mathcal{H}(\lambda + \delta\lambda)$, meaning the state is no longer eigenstate of an instantaneous Hamiltonian. Its collapse to any new eigenstate has a probability amplitude

$$\begin{aligned} a_s &= \langle s(\lambda + \delta\lambda) | o(\lambda) \rangle \approx \delta\lambda^j \langle \partial_j s(\lambda) | o(\lambda) \rangle \\ &= -\delta\lambda^j \langle s(\lambda) | \partial_j | o(\lambda) \rangle. \end{aligned} \quad (2.34)$$

If we introduce the *gauge potential*, sometimes called the *calibration potential*, as⁴

$$\hat{\mathcal{A}}_j := i\partial_j, \quad (2.35)$$

the probability amplitude can be expressed as

$$a_s = i \langle s(\lambda) | \hat{\mathcal{A}}_j | o(\lambda) \rangle \delta\lambda^j, \quad (2.36)$$

which has a meaning of gauge potential matrix elements. Probability of the excitation, i.e., the transition to any state $s > 0$ from ground state is then (omitting the λ dependence in notation)

$$\begin{aligned} \sum_{s \neq 0} |a_s|^2 &= \sum_{s \neq 0} \delta\lambda^j \delta\lambda^k \langle o | \hat{\mathcal{A}}_j | s \rangle \langle s | \hat{\mathcal{A}}_k | o \rangle + \mathcal{O}(|\delta\lambda^3|) \\ &= \delta\lambda^j \delta\lambda^k \langle o | \hat{\mathcal{A}}_j \hat{\mathcal{A}}_k | o \rangle_c + \mathcal{O}(|\delta\lambda^3|) =: \delta\lambda^j \delta\lambda^k \chi_{jk} + \mathcal{O}(|\delta\lambda^3|), \end{aligned} \quad (2.37)$$

where last term defines the geometric tensor. □

⁴In SI units, the gauge potential is $\hat{\mathcal{A}}_j := i\hbar\partial_j$

The calibration invariance of the gauge potential can be explained using the Berry connection.

Definition 13 (Berry connection). *On the ground state manifold \mathcal{M}_0 , the Berry connection is defined as the mean value of gauge potential*

$$A_j(\boldsymbol{\lambda}) := \langle o(\boldsymbol{\lambda}) | \hat{\mathcal{A}}_j | o(\boldsymbol{\lambda}) \rangle = -i \langle o(\boldsymbol{\lambda}) | \partial_j | o(\boldsymbol{\lambda}) \rangle. \quad (2.38)$$

This empowers us to take derivatives in any direction and the expression for geometric tensor on \mathcal{M}_0

$$\chi_{jk}(\boldsymbol{\lambda}) = \partial_j A_k(\boldsymbol{\lambda}) - \partial_k A_j(\boldsymbol{\lambda}). \quad (2.39)$$

This formula can be directly proven by comparing with 2.31. Here we see that the calibration invariance is

$$A_j \mapsto A_j + \partial_j \alpha(\boldsymbol{\lambda}), \quad \alpha \in \mathcal{C}^2, \quad (2.40)$$

meaning any twice differentiable function can be added to the gauge potential, leaving the geometric tensor unchanged.

Definition 14 (Berry phase). *The Berry phase, as an integral of the Berry connection along some closed curve \mathcal{C}* ⁵

$$\varphi_B := - \oint_{\mathcal{C}} A_j(\boldsymbol{\lambda}) d\boldsymbol{\lambda}^j = \int_{\mathcal{S}} \chi_{jk}(\boldsymbol{\lambda}) d\boldsymbol{\lambda}^j \wedge d\boldsymbol{\lambda}^k, \quad (2.43)$$

where we used the Stokes theorem for some area \mathcal{S} with boundary $\partial\mathcal{S} = \mathcal{C}$.

The Berry phase can be imagined on models with *one degeneracy* as an angle, under which the *closed* driving curve is seen from the point of degeneracy. This is demonstrated on spin model in [11].

The energy spectrum degeneracies $E_s - E_{s-1} = 0$ are sometimes referred to as *singularities*, because they cause the metric tensor divergence, or *diabolic* because of the energy spectrum shape in the parametric space.⁶

⁵The reasonability of this definition can be seen, if we assume the ground state of a free particle $\langle \mathbf{x} | i(\boldsymbol{\lambda}) \rangle \equiv i(\mathbf{x}, \boldsymbol{\lambda}) = |i(\mathbf{x})| e^{i\phi(\boldsymbol{\lambda})}$, then the Berry connection is

$$A_j = - \int d\mathbf{x} |i(\mathbf{x}, \boldsymbol{\lambda})|^2 \partial_j \phi(\boldsymbol{\lambda}) = - \partial_j \phi(\boldsymbol{\lambda}) \quad (2.41)$$

and Berry phase

$$\varphi_B = \oint_{\mathcal{C}} \partial_j \phi d\boldsymbol{\lambda}^j, \quad (2.42)$$

which represents total phase accumulated by the wavefunction. It is really the analogy for Berry phase in classical mechanics, which for example in the case Foucault pendulum on one trip around the Sun makes $\varphi_B = 2\pi$

⁶<https://en.wikipedia.org/wiki/Diabolo>

3. Quantum state driving

The concept of quantum state driving was introduced in the previous chapter. In this chapter the initial state is chosen as eigenstate $|s(\boldsymbol{\lambda})\rangle$. The driving parameter $\boldsymbol{\lambda}$ is changed along path parametrized by time t

$$\mathcal{J} := \{\boldsymbol{\lambda}(t) | t \in [0, T], \boldsymbol{\lambda} \in \mathcal{U}\} \subset \mathbb{R}^n, \quad \boldsymbol{\lambda}(0) = \boldsymbol{\lambda}, \quad \boldsymbol{\lambda}(T) = \tilde{\boldsymbol{\lambda}}, \quad (3.1)$$

inducing the change in Hamiltonian $\hat{H}(\boldsymbol{\lambda})$ of dim N , and consequently in $|\psi(\boldsymbol{\lambda})\rangle$, according to the Schrödinger equation. This leads to solving the system of N first order differential equations with initial condition $|\psi(\boldsymbol{\lambda}(0))\rangle = |o(0)\rangle$.

It is often needed to achieve as high fidelity as possible during the driving, meaning avoiding the state excitation. If $F = 1$, we speak about *unit fidelity driving* or *adiabatic driving* and \mathcal{J} is called the *unit fidelity protocol*. Higher fidelity can be achieved by many methods; three of them are

- close adiabatic driving — changing the driving parameters $\boldsymbol{\lambda}$ slowly, so the system has plenty of time to collapse into the ground state,
- path variation — varying the driving trajectory \mathcal{J} , avoiding the topological defects on manifolds, which would excite the system,
- counter-diabatic driving — countering the excitation by adding some element to the Hamiltonian, making the fidelity precisely 1.¹

Before going through individual methods, let's look at the adiabaticity itself.

Definition 15 (Adiabaticity). *The slow change of the driving parameters of the Hamiltonian $H(\boldsymbol{\lambda})$ in a sense that it does not excite the system and allows the system to return to the same energetic state after circulation around any closed path on the ground state manifold with fidelity $F = 1$.*

This means that adiabatic transport is an endomorphism of \mathcal{M}_s . The meaning of the word “slow” clears up the next theorem. It defines when the distance between two states can be considered zero.

Theorem 6 (Adiabatic theorem). *For slowly varying Hamiltonian \hat{H} in the time range $[0, T]$, the solution of the Schrödinger equation*

$$\hat{H}(\lambda) |\psi_s(\lambda)\rangle = E_s(\lambda) |\psi_s(\lambda)\rangle$$

with initial condition in x -representation $\langle x|\psi(t=0)\rangle = \psi(x, 0)$ can be approximated as

$$||\psi(\lambda) - \psi_{ad}(\lambda)|| \approx o\left(\frac{1}{T}\right) \quad (3.2)$$

for the adiabatic state evolved according to Eq. 2.7

$$|\psi_{ad}\rangle = e^{\omega_s(\lambda)} e^{\gamma_s(\lambda(t))} |\psi(\lambda)\rangle, \quad (3.3)$$

¹There is a nice analogy with driving a toy car (a quantum state) in a curved terrain (a Hilbert space). To avoid the car jumping on the hills (the state excitation), you can either drive slowly (close adiabatic driving), or you can go around the hills (vary the path), or you can alter the space for a specific driving (add a counter-diabatic element), such that it exactly copies the jumping trajectory, therefore the car does not leave the ground.

for dynamical phase

$$\omega_s(\lambda) \equiv - \int_0^t E_s(\tau) d\tau$$

and geometrical phase

$$\gamma_s(\lambda(t)) \equiv \int_0^t i \langle \psi_s(\tau) | \partial_t \psi_s(\tau) \rangle d\tau.$$

Proof. The proof can be found in Sakurai and Napolitano [17, Chap. 6]. \square

3.1 Counter-diabatic driving

Assume differentiable and non-singular Hamiltonian $\hat{H}(\boldsymbol{\lambda})$ with non-degenerate eigenbasis $\{|s, \boldsymbol{\lambda}\rangle\}_{s=0}^{N-1}$ called the *adiabatic basis*. This is generally the family of adiabatically connected eigenstates² The transition amplitude between states for adiabatic change is

$$0 = \langle m(\boldsymbol{\lambda}) | \hat{H} | s(\tilde{\boldsymbol{\lambda}}) \rangle \quad \text{for } s \neq m, \forall \boldsymbol{\lambda}, \forall \tilde{\boldsymbol{\lambda}}. \quad (3.4)$$

Differentiation by ∂_t yields

$$\begin{aligned} 0 &= \langle \partial_t m(\boldsymbol{\lambda}) | \hat{H}(\tilde{\boldsymbol{\lambda}}) | s(\tilde{\boldsymbol{\lambda}}) \rangle + \langle m(\boldsymbol{\lambda}) | \underbrace{\partial_t \hat{H}(\tilde{\boldsymbol{\lambda}})}_{\approx \partial_t \hat{H}(\boldsymbol{\lambda})} | s(\tilde{\boldsymbol{\lambda}}) \rangle + \langle m(\boldsymbol{\lambda}) | \hat{H}(\tilde{\boldsymbol{\lambda}}) | \partial_t s(\tilde{\boldsymbol{\lambda}}) \rangle \\ &= E_s(\boldsymbol{\lambda}) \langle \partial_t m(\boldsymbol{\lambda}) | s(\tilde{\boldsymbol{\lambda}}) \rangle + E_m(\boldsymbol{\lambda}) \langle m(\boldsymbol{\lambda}) | \partial_t s(\tilde{\boldsymbol{\lambda}}) \rangle + \langle m(\boldsymbol{\lambda}) | \partial_t \hat{H}(\tilde{\boldsymbol{\lambda}}) | s(\tilde{\boldsymbol{\lambda}}) \rangle \quad (3.5) \\ &= (E_m(\boldsymbol{\lambda}) - E_s(\boldsymbol{\lambda})) \underbrace{\langle m | \partial_t s(\tilde{\boldsymbol{\lambda}}) \rangle}_{-\frac{i}{\hbar} \langle m | \hat{\mathcal{A}}_t | s(\tilde{\boldsymbol{\lambda}}) \rangle} + \langle m | \partial_t \hat{H} | s(\tilde{\boldsymbol{\lambda}}) \rangle, \end{aligned}$$

which can be rewritten in matrix form as

$$i\hbar \partial_t \hat{H} = [\hat{\mathcal{A}}_t, \hat{H}] - i\hbar \hat{M}_t \quad \text{for } \hat{M}_t \equiv - \sum_s \frac{\partial E_s(\lambda)}{\partial t} |s(\lambda)\rangle \langle s(\lambda)|. \quad (3.6)$$

\hat{M} is diagonal in energy basis and its elements has meaning of *generalized force*. We can see that $[\hat{H}, \hat{M}] = 0$, implying

$$[\hat{H}, i\hbar \partial_t \hat{H} - [\hat{\mathcal{A}}_t, \hat{H}]] = 0. \quad (3.7)$$

This equation is essentially the system with constraint $\hat{\mathcal{A}}_t$. Its strength lies in the fact that it finds the counter-diabatic potential without Hamiltonian diagonalization. For more, see Kolodrubetz et al. [10, Chap. 2.3].

In section 2.6 we introduced the gauge potential and stated its correspondence to transition probability, see Eq. 2.36. *Gauge transformations*, in classical mechanics called *canonical*, can be defined such that they *preserve Lagrangian of the system under local transformations from some Lie group*. The implication is that Hamiltonian $\hat{H}(\boldsymbol{\lambda})$ commutes with its canonically transformed version.

To understand the meaning of gauge symmetries, let's first consider classical systems and then move to quantum mechanics.

²In the case of energy level crossing, the eigenstates are not unified, because transition between them is not adiabatic.

3.1.1 Classical gauge potential

This part is inspired by Kolodrubetz et al. [10, Chap. 2.1]. In the Hamiltonian classical mechanics, the manifold \mathcal{M} is assumed to be a subset of the phase space defined by Hamiltonian $H = H(q^i, p_i)$, where momentum p_i and position q^i are assumed to form the orthogonal basis of the phase space

$$\{q^i, p_j\} = \delta_j^i, \quad (3.8)$$

which also defines *calibrational freedom* in their choice. *Canonical transformations* then by definition preserve this formula. Using the *Poisson bracket*, defined on observables as

$$\{A, B\} := \frac{\partial A}{\partial q^j} \frac{\partial B}{\partial p_j} - \frac{\partial B}{\partial q^j} \frac{\partial A}{\partial p_j}, \quad (3.9)$$

we examine continuous canonical transformations generated by gauge potential \mathcal{A}_λ

$$q^j(\lambda + \delta\lambda) = q^j(\lambda) - \frac{\partial \mathcal{A}_\lambda(\mathbf{p}, \mathbf{q})}{\partial p_j} \delta\lambda \Rightarrow \frac{\partial q^j}{\partial \lambda} = -\frac{\partial \mathcal{A}_\lambda}{\partial p_j} = \{\mathcal{A}_\lambda, q^j\} \quad (3.10)$$

$$p_j(\lambda + \delta\lambda) = p_j(\lambda) - \frac{\partial \mathcal{A}_\lambda(\mathbf{p}, \mathbf{q})}{\partial q^j} \delta\lambda \Rightarrow \frac{\partial p_j}{\partial \lambda} = -\frac{\partial \mathcal{A}_\lambda}{\partial q^j} = \{\mathcal{A}_\lambda, p_j\}. \quad (3.11)$$

Substituting this to relations of orthogonality 3.8, we get

$$\{q^j(\lambda + \delta\lambda), p_j(\lambda + \delta\lambda)\} = \delta_j^i + \mathcal{O}(\delta\lambda^2). \quad (3.12)$$

If λ is time parameter and $\mathcal{A}_t = -H$, equations 3.10,3.11 are identical to the Hamilton equations

$$\begin{aligned} \dot{q}^j &= \{q^j, H\} = \frac{\partial H}{\partial p_j} \\ \dot{p}_j &= \{p_j, H\} = -\frac{\partial H}{\partial q^j}. \end{aligned} \quad (3.13)$$

Because the Hamiltonian is a generator of the movement in the phase space (\mathbf{q}, \mathbf{p}) , we can interpret \mathcal{A}_t as the generators of the movement on \mathcal{M} . Another specific choice might be $\lambda = q^i$, which gives us the momentum components $\mathcal{A}_{q^i} = p_i$.

3.1.2 Quantum gauge potential

This part is inspired by Kolodrubetz et al. [10, Chap. 2.2]. Now the aim is to find some special basis transformations \hat{U} between the initial system S and the transformed \tilde{S} . Both of them describe the system with Hamiltonian $\hat{H}(\boldsymbol{\lambda})$ with eigenstates $|s(\boldsymbol{\lambda})\rangle$ on state manifolds \mathcal{PM}_s .

Any state of $\mathcal{H}(\boldsymbol{\lambda})$ for $\forall \boldsymbol{\lambda} \in \mathcal{U}$ can be decomposed as

$$|\psi(\boldsymbol{\lambda})\rangle \equiv \sum_s \psi_s(\boldsymbol{\lambda}) |s\rangle \quad (3.14)$$

for some coordinate independent basis $\{|s\rangle\}_{s=0}^{N-1}$. Then there exist unitary transformation

$$\hat{U}(\boldsymbol{\lambda}) : \tilde{S} \rightarrow S, \quad \hat{U}(\boldsymbol{\lambda}) |m(\boldsymbol{\lambda})\rangle = |s\rangle. \quad (3.15)$$

where scalar parameter $\boldsymbol{\lambda}(t)$ is assumed to be changing along the path \mathcal{J} , therefore we can write the Hamiltonian and states only as functions of t . The unitary transformation then satisfies

$$i\hbar\partial_t \hat{U}(t) = \hat{H}(t)\hat{U}(t) \quad (3.16)$$

for \hat{H} the full Hamiltonian of the system and any point on \mathcal{J} , along which the partial derivative is taken.

The generators of unitary transformations are the adiabatic potentials, which can be defined on wavefunction $|\tilde{\psi}(\boldsymbol{\lambda})\rangle$ defined in system \tilde{S} , as

$$i\hbar\partial_\lambda |\tilde{\psi}(\boldsymbol{\lambda})\rangle = i\hbar\partial_\lambda \left(\hat{U}^+(\boldsymbol{\lambda}) |\psi\rangle \right) = \underbrace{i\hbar \left(\partial_\lambda \hat{U}^+(\boldsymbol{\lambda}) \right)}_{-\tilde{\mathcal{A}}_\lambda} \hat{U}(\boldsymbol{\lambda}) |\tilde{\psi}(\boldsymbol{\lambda})\rangle. \quad (3.17)$$

The adiabatic potential $\tilde{\mathcal{A}}_\lambda$ can be transformed to non-tilde system as

$$\begin{aligned} \hat{\mathcal{A}}_\lambda &= \hat{U}(\boldsymbol{\lambda}) \tilde{\mathcal{A}}_\lambda \hat{U}^+(\boldsymbol{\lambda}) = -i\hbar \hat{U}(\boldsymbol{\lambda}) \left(\partial_\lambda \hat{U}^+(\boldsymbol{\lambda}) \right) = \\ &= -i\hbar \partial_\lambda \left(\underbrace{\hat{U}^+(\boldsymbol{\lambda}) \hat{U}(\boldsymbol{\lambda})}_1 \right) - \left(\partial_\lambda \hat{U}(\boldsymbol{\lambda}) \right) \hat{U}^+(\boldsymbol{\lambda}) = i\hbar \left(\partial_\lambda \hat{U}(\boldsymbol{\lambda}) \right) \hat{U}^+(\boldsymbol{\lambda}). \end{aligned} \quad (3.18)$$

Now we have explicit formulas for adiabatic potential in two systems

$$\hat{\mathcal{A}}_\lambda = i\hbar \left(\partial_\lambda \hat{U}(\boldsymbol{\lambda}) \right) \hat{U}^+(\boldsymbol{\lambda}) \quad (3.19)$$

$$\tilde{\mathcal{A}}_\lambda = -i\hbar \left(\partial_\lambda \hat{U}^+(\boldsymbol{\lambda}) \right) \hat{U}(\boldsymbol{\lambda}). \quad (3.20)$$

The adiabatic potentials can be shown to be Hermitian

$$\tilde{\mathcal{A}}_\lambda^+ = i\hbar U(\boldsymbol{\lambda})^+ \left(\partial_\lambda \hat{U}(\boldsymbol{\lambda}) \right) = -i\hbar \left(\partial_\lambda \hat{U}(\boldsymbol{\lambda})^+ \right) \hat{U}(\boldsymbol{\lambda}) = \tilde{\mathcal{A}}_\lambda, \quad (3.21)$$

analogically for non-tilde potential.

Using the eigenbasis of \hat{H} , the matrix elements are

$$\langle s | \tilde{\mathcal{A}}_\lambda | m \rangle = i\hbar \langle s | \hat{U}(\boldsymbol{\lambda})^+ \partial_\lambda \hat{U}(\boldsymbol{\lambda}) | m \rangle = i\hbar \langle s(\boldsymbol{\lambda}) | \partial_\lambda | m(\boldsymbol{\lambda}) \rangle. \quad (3.22)$$

Because

$$\langle s(\boldsymbol{\lambda}) | \hat{\mathcal{A}}_\lambda | m(\boldsymbol{\lambda}) \rangle = \langle s | \tilde{\mathcal{A}}_\lambda | m \rangle, \quad (3.23)$$

we get

$$\hat{\mathcal{A}}_\lambda = i\hbar\partial_\lambda. \quad (3.24)$$

To see that the gauge potential performs transformation to non-exciting system, one can recall the general form of the adiabatic potential

$$\mathcal{A} = (\nabla U(t)) U^{-1}(t) + U(t) \mathcal{A} U^{-1}(t). \quad (3.25)$$

The fact that second element is missing in Eq. 3.24 implies the space has zero curvature. The curvature $\partial_j A_k(\boldsymbol{\lambda}) - \partial_k A_j(\boldsymbol{\lambda})$ equals, according to Eq. 2.31, χ_{jk} . This means that adiabatic gauge transformations are a class of gauge transformations with $g_{jk} = \text{Re}\chi_{jk} = 0$ and according to Eq. 2.27, fidelity $F = 1$. Therefore,

the system is driven by Hamiltonian $\hat{H}(\boldsymbol{\lambda})$ with fidelity $F < 1$, there exists such adiabatic potential \mathcal{A}_λ , that driving of the same system using $\hat{H} - \mathcal{A}_\lambda$ has unit fidelity.

The adiabatic gauge potentials can then be understood as affine connections defining the parallel transport on fiber bundle, if we define covariant derivative as

$$D_j := \partial_j + i\hat{\mathcal{A}}_j, \quad (3.26)$$

which yields $D_j |\psi_n\rangle = 0$ for every eigenstate, meaning the transport of eigenvalues on \mathcal{PM}_0 is parallel. $\hat{\mathcal{A}}_j$ is generally defined by Eq. 3.19, which gives non-zero covariant derivative for states not belonging to \mathcal{PM}_0 .

3.2 Driving on the ground state manifold

As was mentioned in the introduction of chapter 3, one method of achieving low driving fidelity is *path variation*. It means *finding the best possible driving path*. One might say that the ground state manifold geodesics are a good candidate for this path because they minimize the distance. The problem is that general fidelity driving does not happen on any state manifold, and this premise cannot be used. The natural question here is: “For which drivings do geodesics minimize the fidelity?”. The whole role of geodesics is not yet known, but there are a few known cases in which they have particular meaning and which are demonstrated here.

3.2.1 Minimizing the distance on state manifolds

Let’s have path \mathcal{J} with fixed boundary conditions $\boldsymbol{\lambda}(0) = \boldsymbol{\lambda}_i$, $\boldsymbol{\lambda}(T) = \boldsymbol{\lambda}_f$. The driving on projective ground state manifold \mathcal{PM}_0 then consists of infinitesimal quenches over the distance ds . By integration over this path we get the distance

$$s_{\mathcal{J}} = \int_{\mathcal{J}} ds = \int_0^T \sqrt{g_{jk} \dot{\boldsymbol{\lambda}}^j \dot{\boldsymbol{\lambda}}^k} dt \quad (3.27)$$

Let’s state and prove the theorem demonstrating the importance of geodesics.

Theorem 7. *The distance described by formula 3.27 is minimized if \mathcal{J} is a geodesic.*

Proof. Functional of distance is

$$s = \int_0^T \sqrt{g_{jk} d\boldsymbol{\lambda}^j d\boldsymbol{\lambda}^k} = \int_0^T \sqrt{g_{jk} \frac{d\boldsymbol{\lambda}^j}{dt} \frac{d\boldsymbol{\lambda}^k}{dt}} dt =: \int_0^T \mathcal{L}(t, \boldsymbol{\lambda}^j, \dot{\boldsymbol{\lambda}}^j) dt \quad (3.28)$$

for

$$\mathcal{L} = \sqrt{g_{jk} \dot{\boldsymbol{\lambda}}^j \dot{\boldsymbol{\lambda}}^k}. \quad (3.29)$$

Using Euler-Lagrange equations

$$\frac{d\mathcal{L}}{d\boldsymbol{\lambda}^j} - \frac{d}{dt} \frac{d\mathcal{L}}{d\dot{\boldsymbol{\lambda}}^j} = 0, \quad (3.30)$$

we get for $g_{jk} = g_{jk}(\boldsymbol{\lambda})$ second order differential equation

$$\ddot{\boldsymbol{\lambda}}^j + \Gamma_{ab}^j \dot{\boldsymbol{\lambda}}^a \dot{\boldsymbol{\lambda}}^b = 0 \quad \Gamma_{ab}^j = \frac{1}{2} g^{jk} (g_{ka,b} + g_{kb,a} - g_{ba,k}), \quad (3.31)$$

which is the Geodesic equation. \square

3.2.2 Minimizing the energy variance

The driving can be restricted to the ground state manifold only in approximation, such that the excited parts of the wavefunction can be neglected in every step. This fact is used for so-called *close adiabatic drivings*. The first theorem about geodesics is from Bukov et al. [18].

Theorem 8. *For any fast-forward Hamiltonian³ $\hat{H}(\lambda(t))$ driven along one dimensional path $\lambda : \mathbb{R} \mapsto \mathbb{R}$ using time t as parametrization, there exist driving speed, for which the fidelity is close to one, $F(t) \approx 1$, $\forall t \in [0, T]$, and the energy fluctuations δE^2 , averaged along the path, are larger than the geodesic length l_λ*

$$\int_0^T \sqrt{\delta E^2(t)} dt =: l_t \geq l_\lambda := \int_{\lambda_i}^{\lambda_f} \sqrt{g_{\lambda\lambda} d\lambda d\lambda} = \int_0^T \sqrt{g_{\lambda\lambda}} |\dot{\lambda}| dt. \quad (3.32)$$

The length l_λ is defined in parametric space. For energy variance it holds

$$\delta E^2 := \langle o(t) | \hat{H}(t)^2 | o(t) \rangle - \langle o(t) | \hat{H}(t) | o(t) \rangle^2 = \langle \partial_t o(t) | \partial_t o(t) \rangle_c = G_{tt}, \quad (3.33)$$

where in second equality the Schrödinger equation is used.

The Metric tensor in parametric space is defined as

$$g_{\lambda\lambda} := \langle \partial_\lambda o(t) | \partial_\lambda o(t) \rangle_c, \quad (3.34)$$

see Chapter 2.6.

Proof. The essential realization is

$$\delta E^2 \equiv \langle o(t) | \hat{H}(t)^2 | o(t) \rangle_c = \dot{\lambda}^2 G_{\lambda\lambda} + \mathcal{O}(\dot{\lambda}^4), \quad (3.35)$$

where $\mathcal{O}(\dot{\lambda}^4)$ needs to be positive for any real-valued Hamiltonian. The positivity comes from the fact, that the system has instantaneous time-reversal symmetry. For details see Bukov et al. [18]. \square

The conjecture can be extended to an arbitrary dimensional path. The main problem of this conjecture is the statement *close unit fidelity protocol*. It is not clear how good the approximation needs to be. This makes the statement much weaker because it only states that *for any driving, there exists nonzero driving speed for which the energy variance is minimized on geodesics*.

³The system is driven to the target state in some fixed final time T .

3.2.3 Transport using quenches

Unifying the ground states $|o(\boldsymbol{\lambda})\rangle$ over all points $\boldsymbol{\lambda} \in \mathcal{U}$ in parametric space, we get the ground state manifold. Here the fidelity F and distance s are

$$ds^2 = 1 - F(|\boldsymbol{\lambda} + \delta\boldsymbol{\lambda}\rangle, |\boldsymbol{\lambda}\rangle) = 1 - |\langle o(\boldsymbol{\lambda} + \delta\boldsymbol{\lambda})|o(\boldsymbol{\lambda})\rangle|^2. \quad (3.36)$$

The final fidelity of transport on \mathcal{M} is then

$$F = \iint_{\mathcal{J}} g_{jk} d\boldsymbol{\lambda}^j d\boldsymbol{\lambda}^k = \int_{t_i}^{t_f} \underbrace{\int_{t_i}^{\tau} g_{jk} \frac{d\boldsymbol{\lambda}^j}{dt} \frac{d\boldsymbol{\lambda}^k}{dt} dt d\tau}_{\mathcal{L}(\boldsymbol{\lambda}, \dot{\boldsymbol{\lambda}}, \tau)}. \quad (3.37)$$

From Euler-Lagrange equations, the fidelity is minimized if \mathcal{J} is geodesic. It is worth mentioning the same problem as was with Theorem 8. It is only stated here that *there exist such slow driving, that the fidelity is minimized on geodesics.* Not how slow this driving needs to be.

Imagine at every point of transport that the fidelity is small enough, so for some small parameter $\delta\boldsymbol{\lambda} \in \mathbb{R}^n$ the transport over distance ds in eigenbasis at time $t = 0$ is

$$|o(\boldsymbol{\lambda})\rangle \equiv \begin{pmatrix} Z_0(\boldsymbol{\lambda}) \\ 0 \\ \vdots \\ 0 \end{pmatrix} \xrightarrow{\text{transport } ds} |o(\boldsymbol{\lambda} + \delta\boldsymbol{\lambda})\rangle \equiv \begin{pmatrix} Z_0(\boldsymbol{\lambda} + \delta\boldsymbol{\lambda}) \\ 0 \\ \vdots \\ 0 \end{pmatrix} + \underbrace{\begin{pmatrix} 0 \\ \Delta_1(\boldsymbol{\lambda} + \delta\boldsymbol{\lambda}) \\ \vdots \\ \Delta_n(\boldsymbol{\lambda} + \delta\boldsymbol{\lambda}) \end{pmatrix}}_{\boldsymbol{\Delta}(\boldsymbol{\lambda} + \delta\boldsymbol{\lambda})}.$$

This has interesting implications for slow transports or small distance transports. For slow transport, the element $\boldsymbol{\Delta}$ increases with time and is hardly fulfilled because one needs to neglect the sum of many of these terms. One possible way out of this is to reset the state into the ground-state when the fidelity would get too far from 1. It can be achieved by projecting the state $|\psi(t)\rangle$ to the ground state $|o(t)\rangle$ periodically. Then because

$$\langle \boldsymbol{\Delta}(\boldsymbol{\lambda} + \delta\boldsymbol{\lambda}) | o(\boldsymbol{\lambda} + \delta\boldsymbol{\lambda}) \rangle = 0,$$

the fidelity of such driving is almost one. These small jumps are sometimes called *quenches*, and they can be achieved by introducing thermalization to the system.

If we imagine $\delta\boldsymbol{\lambda}$ to be finite (not infinitely small, as the notation suggests), the *transport* means *doing a sequence of quenches and measuring the system after every quench*. This consequently leads to the unit fidelity transport.

3.3 Adiabatic perturbation theory

Until now, our interest was mainly in *unit fidelity protocols*. But how to calculate the case when the fidelity is “almost one”? This is the aim of *adiabatic perturbation theory*.

Following the article from Rigolin et al. [19], the wavefunction can be approximated by series. Because every element is then decomposed into another series, we bear in mind the *locality of variables*, which clarifies the reason for performing

this procedure. Let's call variable $V(\boldsymbol{\lambda}(t))$ *local* if it depends only on the system characteristics in point $\boldsymbol{\lambda}(t)$. These variables can usually be obtained only from the spectrum $\sigma(\hat{H}(\boldsymbol{\lambda}(t)))$ and are written in shades of blue. In opposite, a *non-local* variable, written in shades of red, depends on the driving path. These are usually expressed as an integral over the driving path \mathcal{J} , but might generally depend on any point which is not on this path.

We are interested in the driving along path \mathcal{J} defined by Eq. 3.1, where t is time and T final time of the driving. Let the initial condition be

$$|\psi(0)\rangle =: |\psi_0\rangle \in \mathcal{PM}_0. \quad (3.38)$$

Solving the Schrödinger equation might seem like a straightforward solution. However, if the fidelity is close to 1, the approximate methods are, in comparison with numerical methods, relatively stable. Second reason is, that they might result in an analytical solution to the problem.

The power series is derived using a small parameter $v := 1/T$

$$|\Psi(t)\rangle = \sum_{p=0}^{\infty} v^p |\Psi^{(p)}(t)\rangle, \quad (3.39)$$

for

$$|\Psi^{(p)}(t)\rangle = \sum_{s=0}^{N-1} e^{-\frac{i}{v}\omega_s(t)} e^{i\gamma_s(t)} b_s^{(p)}(t) |s(t)\rangle. \quad (3.40)$$

Here we have

$$\text{dynamical phase } \omega_s(t) := \frac{1}{\hbar} \int_0^t E_s(\tau) d\tau, \quad (3.41)$$

$$\text{Berry phase } \gamma_s(t) := i \int_0^t \langle s(\tau) | \frac{d}{d\tau} s(\tau) \rangle d\tau \equiv i \int_0^t M_{ss}(\tau) d\tau \quad (3.42)$$

and $|s(t)\rangle$ are solutions to

$$\hat{H}(t) |s(t)\rangle = E_s(t) |s(t)\rangle. \quad (3.43)$$

Variables $\omega_s(t)$ and $\gamma_s(t)$ are defined using integration over the whole protocol, therefore they are *non-local variables*. The problem now lies in determining $b_s^{(p)}(t)$, which is also *non-local*. Because it depends on its relative *geometrical* and *dynamical phase* to other *energy levels*, let's write it as a series

$$b_s^{(p)}(t) = \sum_{m=0}^{N-1} e^{\frac{i}{v}\omega_{sm}(t)} e^{-i\gamma_{sm}(t)} b_{sm}^{(p)}(t), \quad (3.44)$$

where $\omega_{sm} := \omega_m - \omega_s$, $\gamma_{sm} := \gamma_m - \gamma_s$. The reason for *locality* of $b_{sm}^{(p)}(t)$ will be clear soon.

Inserting all to original series 3.39, we get

$$|\Psi(t)\rangle = \sum_{s,m=0}^{N-1} \sum_{p=0}^{\infty} v^p e^{-\frac{i}{v}\omega_m(t)} e^{i\gamma_m(t)} b_{sm}^{(p)}(t) |s(t)\rangle. \quad (3.45)$$

Because the initial state is an eigenstate of the Hamiltonian at time $t = 0$, we get initial condition $b_{sm}^{(0)}(t) = 0$. In addition, one can rewrite equation 3.45 to the iteratively solvable form

$$\frac{i}{\hbar} \Delta_{sm}(t) b_{sm}^{(p+1)}(t) + \dot{b}_{sm}^{(p)}(t) + W_{sm}(t) b_{sm}^{(p)}(t) + \sum_{k=0, k \neq s} M_{sk}(t) b_{km}^{(p)}(t) = 0, \quad (3.46)$$

for $\Delta_{sm}(t) := E_m - E_s$, $W_{sm}(t) := M_{ss}(t) - M_{mm}(t)$, where M_{ms} is defined in Eq. 3.42. We can see that $b_{ms}^{(p)}$, as a solution to Eq. 3.46, only depends on difference between energy levels, eigenstates during the path and their directional derivatives. Not on the path itself. All of these are easily obtained, once the driving path is prescribed.

4. Two level system

A simple two-level system is investigated before moving to a more complicated Hamiltonian model. To understand the general behavior of fidelity on a Hamiltonian spectrum, two analytically solvable drivings — *geodesic* and *linear* — are investigated.

All numerical calculations were performed in software Mathematica. Some results were compared with code in Julia to check the numerical precision of the calculations.

4.1 Hamiltonian

Let's have a Hamiltonian

$$\hat{H}(t) = \begin{pmatrix} \Omega(t) & \Delta(t) \\ \Delta(t) & -\Omega(t) \end{pmatrix} \quad (4.1)$$

for $\Omega : \mathbb{R}^+ \rightarrow \mathbb{R}$, $\Delta : \mathbb{R}^+ \rightarrow \mathbb{R}$ and time t . Its spectrum is

$$E_1(t) = -E_0(t) = \sqrt{\Omega^2(t) + \Delta^2(t)} \quad (4.2)$$

and using the eigenbasis

$$\mathcal{B} := \left\{ |0\rangle \equiv \begin{pmatrix} 1 \\ 0 \end{pmatrix}, |1\rangle \equiv \begin{pmatrix} 0 \\ 1 \end{pmatrix} \right\}, \quad (4.3)$$

the eigenvectors can be written as

$$|0(t)\rangle = N_+ \begin{pmatrix} 1 \\ \frac{E_0(t)+\Omega(t)}{\Delta(t)} \end{pmatrix}, \quad |1(t)\rangle = N_- \begin{pmatrix} 1 \\ \frac{E_1(t)+\Omega(t)}{\Delta(t)} \end{pmatrix} \quad (4.4)$$

for normalization constants $N_{\pm} := \left(\left(\frac{\pm E_0(t)+\Omega(t)}{\Delta(t)} \right)^2 + 1 \right)^{-1/2}$. The instantaneous eigenbases changes in time, but is described using constant basis \mathcal{B} , which forms an eigenbasis at time $t = 0$.

The goal is to find *fidelity* between initial state and state evolved along \mathcal{J} , $F_{\mathcal{J}}(t) := |\langle 0(t) | \psi(t) \rangle|^2$ for different driving protocols

$$\mathcal{J} := \{ \boldsymbol{\lambda}(t) | t \in [0, T], \boldsymbol{\lambda} \in \mathcal{U} \} \subset \mathbb{R}^n. \quad (4.5)$$

For this we need to solve time Schrödinger equation

$$\hat{H}(t) |\psi(t)\rangle = i \frac{d}{dt} |\psi(t)\rangle \quad (4.6)$$

with time varying Hamiltonian $\hat{H}(\boldsymbol{\lambda}(t)) =: \hat{H}(t)$ and $\boldsymbol{\lambda}$ on path \mathcal{J} . For 2-dimentional system with

$$|\psi(t)\rangle =: \begin{pmatrix} a(t) \\ b(t) \end{pmatrix}, \quad (4.7)$$

we get the system of *two coupled differentials equations of the first order with non-constant coefficients*

$$\Omega(t)a(t) + \Delta(t)b(t) = i\dot{a}(t) \quad (4.8)$$

$$\Delta(t)a(t) - \Omega(t)b(t) = i\dot{b}(t) \quad (4.9)$$

with normalization

$$a^2(t) + b^2(t) = 1, \quad \forall t \in [0, T], \quad (4.10)$$

and initial value

$$\begin{pmatrix} a(0) \\ b(0) \end{pmatrix} = |0(0)\rangle. \quad (4.11)$$

4.2 Harmonic oscillator correspondence

Coupled Equations 4.8, 4.9 have no general analytical solution, with an exception to a few easy protocols \mathcal{J} . Before moving to some of these special cases, it is important to understand the general behavior of such coupled system of equations.

N-dimensional Schrödinger equation can be rewritten to *one differential equation of N^{th} order with non-constant coefficients*. In our two-dimensional case, this equation corresponds to a *damped harmonic oscillator without external force*

$$0 = \ddot{a}(t) + \gamma(t)\dot{a}(t) + \omega^2(t)a(t) \quad (4.12)$$

$$\gamma(t) := -\frac{\dot{\Delta}(t)}{\Delta(t)} \quad (4.13)$$

$$\omega^2(t) := i \left(\dot{\Omega}(t) - \frac{\dot{\Delta}(t)}{\Delta(t)} \Omega(t) \right) + \Delta^2(t) + \Omega^2(t). \quad (4.14)$$

Along with normalization condition 4.10 and initial condition

$$\begin{pmatrix} a(0) \\ b(0) \end{pmatrix} = |0(0)\rangle; \quad \dot{a}(0) = -i(\Omega(0)a(0) + \Delta(0)b(0)). \quad (4.15)$$

The condition $\Delta \neq 0$ is used here. Because the energy spectrum has $\Delta \leftrightarrow \Omega$ symmetry, we can change the driving by interchanging Δ and Ω on any intervals, where the parameters 4.13, 4.14 would diverge.

Classical mechanics correspondence

It might be useful to know some analogy to classical mechanics Lagrangian when solving differential equations. It is not used any further, but it can be useful for additional analysis.

From the perspective of classical mechanics, meaning $x(t) := a(t)$ is a position in a phase space (\mathbf{x}, \mathbf{p}) , we can write classical Lagrangian from Eq. 4.12 as

$$\mathcal{L} = \frac{1}{2} \exp \left(\int_0^t \gamma(s) ds \right) (\dot{x}^2 - \omega^2(t)x^2) \quad (4.16)$$

Proof. The correspondence of Lagrangian 4.16 with Eq. 4.12 can be shown by direct evaluation of Euler-Lagrange equations

$$\begin{aligned} \frac{\partial \mathcal{L}}{\partial x} - \frac{d}{dt} \frac{\partial \mathcal{L}}{\partial \dot{x}} &= 0 \\ \frac{1}{2} \exp\left(\int_0^t \gamma(s) ds\right) (-2\omega^2(t)x) - \frac{d}{dt} \left(\exp\left(\int_0^t \gamma(s) ds\right) \dot{x} \right) &= 0 \\ -\omega^2(t)x - \gamma(t)\dot{x} - \ddot{x} &= 0. \end{aligned} \quad (4.17)$$

□

4.3 Energy variance for two-level system

For two level system, the variance of wavefunction at time t

$$\delta E^2(t) := \langle \psi(t) | \hat{H}^2(t) | \psi(t) \rangle - \langle \psi(t) | \hat{H}(t) | \psi(t) \rangle^2 \quad (4.18)$$

can be rewritten inserting identity $\mathbb{1} = |0\rangle\langle 0| + |1\rangle\langle 1|$ around Hamiltonian. Omitting the time dependence of every element we get

$$\begin{aligned} \delta E^2 &= \langle \psi | \mathbb{1} \hat{H}^2 \mathbb{1} | \psi \rangle - \langle \psi | \mathbb{1} \hat{H} \mathbb{1} | \psi \rangle^2 \\ &= \langle \psi | 0 \rangle \langle 0 | \hat{H}^2 | 0 \rangle \langle 0 | \psi \rangle + \langle \psi | 1 \rangle \langle 1 | \hat{H}^2 | 1 \rangle \langle 1 | \psi \rangle \\ &\quad + \langle \psi | 0 \rangle \langle 0 | \hat{H}^2 | 1 \rangle \langle 1 | \psi \rangle + \langle \psi | 1 \rangle \langle 1 | \hat{H}^2 | 0 \rangle \langle 0 | \psi \rangle \\ &\quad - \left(\langle \psi | 0 \rangle \langle 0 | \hat{H} | 0 \rangle \langle 0 | \psi \rangle + \langle \psi | 1 \rangle \langle 1 | \hat{H} | 1 \rangle \langle 1 | \psi \rangle \right. \\ &\quad \left. + \underbrace{\langle \psi | 0 \rangle \langle 0 | \hat{H} | 1 \rangle}_{\propto \langle 0 | 1 \rangle = 0} \langle 1 | \psi \rangle + \underbrace{\langle \psi | 1 \rangle \langle 1 | \hat{H} | 0 \rangle}_{\propto \langle 0 | 1 \rangle = 0} \langle 0 | \psi \rangle \right)^2. \end{aligned} \quad (4.19)$$

Using Fidelity definition $F(t) = |\langle 0(t) | \psi(t) \rangle|^2$ and Schrödinger equation $\hat{H} |k\rangle = E_k |k\rangle$ we get a simplified formula for energy variance

$$\delta E^2(t) = F(t)(1 - F(t))(E_0(t) - E_1(t))^2. \quad (4.20)$$

For three level system we have $\mathbb{1} = |0\rangle\langle 0| + |1\rangle\langle 1| + |2\rangle\langle 2|$ and

$$\delta E^2 = \sum_{k=1}^3 E_k^2 F_k (1 - F_k) - 4 \prod_{k=1}^3 E_k F_k - 2F_0 F_1 E_0 E_1 - 2F_0 F_2 E_0 E_2 - 2F_1 F_2 E_1 E_2, \quad (4.21)$$

for $F_k := \langle k | \psi \rangle$, which has no practical simplification.

4.4 Geodesic driving

First analytically solvable driving emphasized here is the *geodesic driving* on the ground state manifold. It can be defined in 3-dimensional space as

$$d(t) \equiv \begin{pmatrix} \Omega(t) \\ \Xi(t) \\ \Delta(t) \end{pmatrix} := \begin{pmatrix} -s \cos(\omega(T)t) \\ 0 \\ s \sin(\omega(T)t) \end{pmatrix} \quad (4.22)$$

for speed regulating function $\omega(T) := \pi/T$. The reason for 3-dimensional driving is the possibility to use Pauli matrix formalism. Such defined drivings are half-spheres in the parametric space, see Fig. 4.1. Note that the driving velocity is constant in the parametric space and on the manifold.

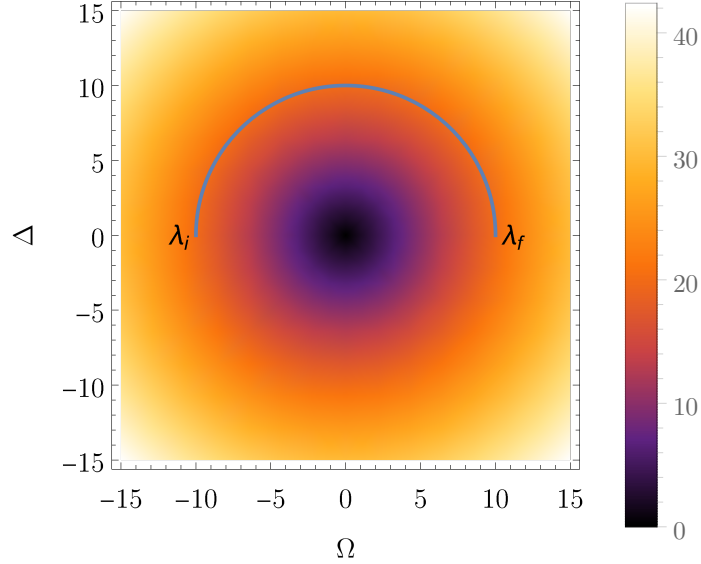


Figure 4.1: Driving along the geodesic. $\lambda_i \equiv (\Omega_i, \Delta_i)$ and $\lambda_f \equiv (\Omega_f, \Delta_f)$ are initial and final parameters respective. Density plot shows the difference between Hamiltonian eigenvalues.

4.4.1 Derivation of the fidelity

Because the Hamiltonian can be rewritten using Pauli matrices

$$\hat{H}(t) = \begin{pmatrix} -s \cos(t\omega) & s \sin(t\omega) \\ s \sin(t\omega) & s \cos(t\omega) \end{pmatrix} = \Delta(t)\sigma_x + \Omega(t)\sigma_z = d(t) \cdot \hat{\boldsymbol{\sigma}}, \quad (4.23)$$

for vector $\hat{\boldsymbol{\sigma}} := (\hat{\sigma}_1, \hat{\sigma}_2, \hat{\sigma}_3)^T$.

One can see that changing from the [original frame](#) with function $|\psi\rangle$ to [moving frame of reference](#), with $|\tilde{\psi}\rangle$ (let's omit the final time dependence $\omega = \omega(T)$ for a while) is described as

$$\psi(t) =: e^{\frac{i\omega}{2}\hat{\sigma}_y t} \tilde{\psi}(t). \quad (4.24)$$

This reflects the rotational symmetry of the system. The change of reference frame transforms Schrödinger equation as

$$\begin{aligned} \hat{H}(t)\psi(t) &= i\psi'(t) \\ \hat{H}(t)e^{\frac{i\omega}{2}\hat{\sigma}_y t}\tilde{\psi}(t) &= ie^{\frac{i\omega}{2}\hat{\sigma}_y t} \left(\frac{i\omega\hat{\sigma}_y}{2} \right) \tilde{\psi}(t) + ie^{\frac{i\omega}{2}\hat{\sigma}_y t} \tilde{\psi}'(t) \\ \underbrace{\left(e^{-\frac{i\omega}{2}\hat{\sigma}_y t} \hat{H}(t) e^{\frac{i\omega}{2}\hat{\sigma}_y t} + \frac{\omega}{2} \hat{\sigma}_y \right)}_{\hat{H}(t)} \tilde{\psi}(t) &= i\tilde{\psi}'(t). \end{aligned} \quad (4.25)$$

One can equivalently solve the Fidelity problem in this new coordinate system.

Hamiltonian in the moving frame is

$$\tilde{H} = \begin{pmatrix} -s & -i\omega(T)/2 \\ i\omega(T)/2 & s \end{pmatrix}, \quad (4.26)$$

which is time independent and depends only on final time. The Schrödinger equation can now be easily solved using evolution operator

$$\hat{U}(t) = e^{-i\tilde{H}t} = \begin{pmatrix} \cos\left(\frac{t}{2}q\right) + \frac{2is\sin\left(\frac{t}{2}q\right)}{q} & -\frac{\omega\sin\left(\frac{t}{2}q\right)}{q} \\ \frac{\omega\sin\left(\frac{t}{2}q\right)}{q} & \cos\left(\frac{t}{2}q\right) - \frac{2is\sin\left(\frac{t}{2}q\right)}{q} \end{pmatrix}, \quad (4.27)$$

for $q := \sqrt{4s^2 + \omega(T)^2}$.

In the original frame we get the evolution of $\psi(0)$ as

$$\psi(t) = e^{\frac{i\omega}{2}\hat{\sigma}_y t} \hat{U}(t) \tilde{\psi}(0) = \underbrace{e^{\frac{i\omega}{2}\hat{\sigma}_y t} \hat{U}}_{\hat{U}(t)} \underbrace{e^{-\frac{i\omega}{2}\hat{\sigma}_y t} e^{\frac{i\omega}{2}\hat{\sigma}_y t} \tilde{\psi}(0)}_{\psi(0)}. \quad (4.28)$$

The evolved wavefunction the reads as

$$|\psi(t)\rangle = \begin{pmatrix} \cos\left(\frac{t}{2}q\right) + \frac{2is}{q} \cos(t\omega) \sin\left(\frac{t}{2}q\right) \\ \frac{\omega - 2is\sin(t\omega)}{q} \sin\left(\frac{t}{2}q\right) \end{pmatrix} \quad (4.29)$$

and the ground state

$$|0(t)\rangle = \mathcal{N} \begin{pmatrix} -\cot\left(\frac{t}{2}\omega\right) \\ 1 \end{pmatrix}, \quad (4.30)$$

for a normalization constant $\mathcal{N} := |\langle 0(t)|0(t)\rangle|^{-1}$. Fidelity during the transport is then¹

$$F = |\langle 0(t)|\psi(t)\rangle|^2. \quad (4.31)$$

An explicit formula for fidelity in time t and geodesic driving with final time T is finally

$$F(t, T) = \frac{\pi^2 \left(\cos\left(t\sqrt{\frac{\pi^2}{T^2} + 4s^2}\right) + 1 \right) + 8s^2 T^2}{2 \sin^4\left(\frac{\pi t}{2T}\right) (4s^2 T^2 + \pi^2) \left(\left| \cot\left(\frac{\pi t}{2T}\right) \right|^2 + 1 \right)^2}. \quad (4.32)$$

The domain can be extended from $t \in (0, T)$ to $[0, T]$ for any $T \in [0, \infty]$, because

$$\lim_{t \rightarrow 0} F = 1, \quad \lim_{T \rightarrow 0} F = 0.$$

It is practical to define *Infidelity* as

$$F^* := 1 - F. \quad (4.33)$$

It has a meaning of *excitation probability during the transport*.

¹If we calculate the fidelity in the [comoving frame](#), we get exactly one. This realization leads to the counter-diabatic driving.

4.4.2 Analysis of the infidelity formula

Infidelity can be calculated by numerical evolution of Schrödinger equation, or from Eq. 4.32. Sometimes both solutions are plotted for comparison between numerical precision.

For some fixed final time, the infidelity is an oscillating curve with values close to 0, see the driving for final time $T = 1$ in Fig. 4.2. The *final infidelity* (fidelity at $t = T$) dependence on final time T can be seen in Fig. 4.3 and 4.4.

From the fidelity formula 4.32 goes that condition $F = 1$ is equivalent to

$$\cos\left(\sqrt{T_s^2 + \pi^2}\right) = 1, \quad (4.34)$$

for $T_s := 2sT$. The solution to this equation is

$$T_s = \sqrt{(2\pi k)^2 - \pi^2} \text{ for } k \in \mathbb{N}, \quad (4.35)$$

see Fig. 4.5. This implies that spikes in Fig. 4.4 have minimal value $1 - F = 0$, and their density is linear in T .

Fidelity as a function of time and final time can be seen in Fig. 4.6. Note that only $t < T$ has physical meaning.

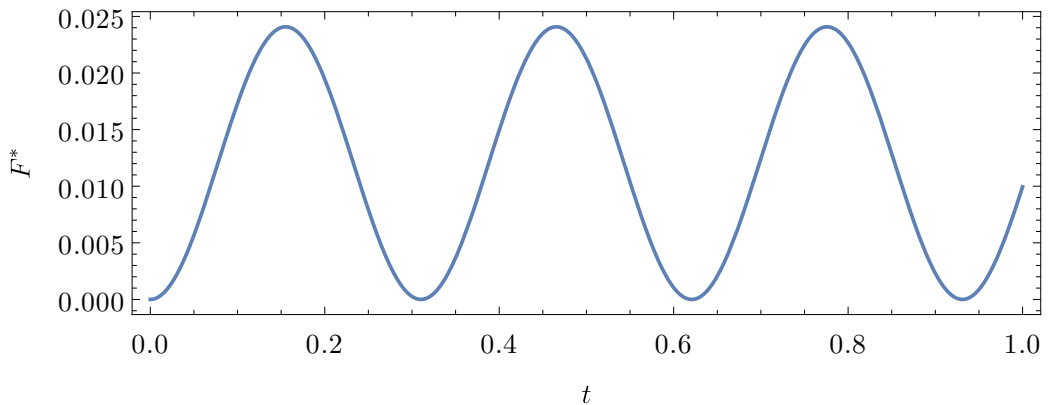


Figure 4.2: Infidelity in time for final time $T = 1$ for geodesical driving.

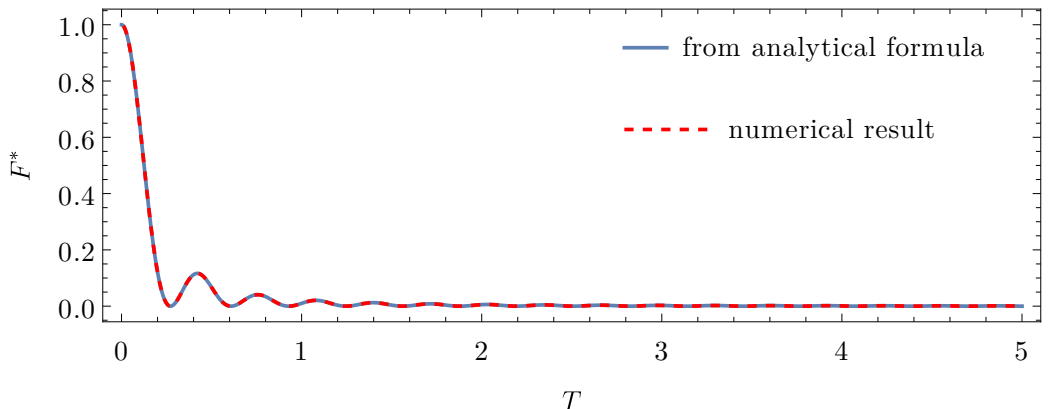


Figure 4.3: Final infidelity dependence on final time T for geodesical driving.

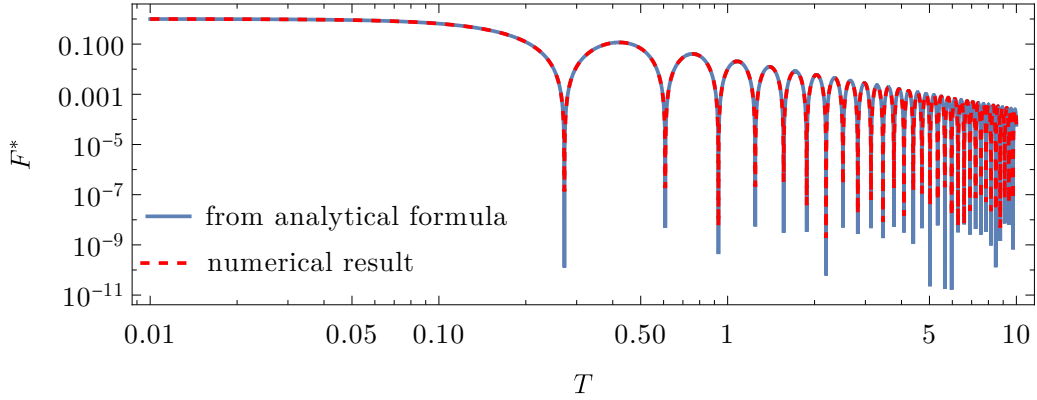


Figure 4.4: Final infidelity dependence on final time T for geodesical driving; in logarithmic scale⁹. The difference in numerical precision of both methods can be seen in the spike's height. As it will be shown later, the spikes should go to zero, thus analytical formula has higher numerical precision.

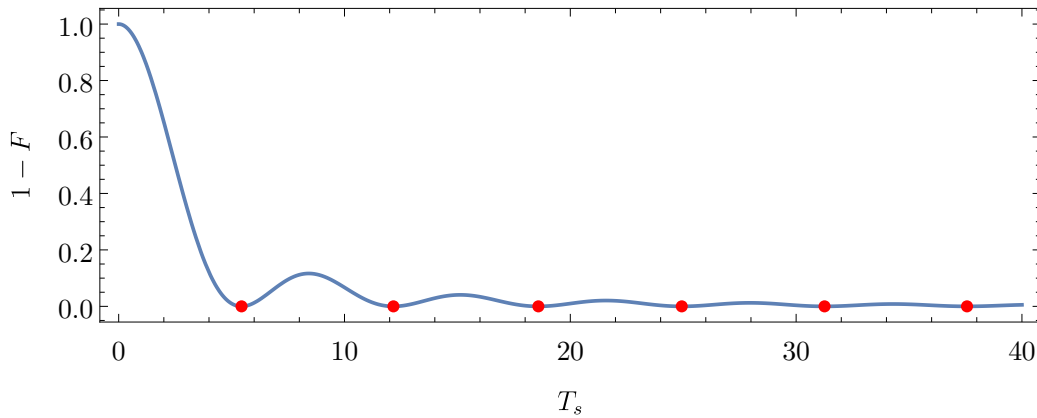


Figure 4.5: Rescaled final infidelity $T_s := 2sT$ dependence on final time. Red points mark the condition $F = 1$.

4.4.3 Energy variance

Another interesting quantity is the energy variance, specially because of Theorem 8. Evaluating the fidelity for geodesical driving gives a function of time t and final time T

$$\begin{aligned} \delta E^2 = & \frac{s^2}{2q^2} \left[\left[16s^4 + 2s^2 \left((\omega^2 - 8s^2) \cos(2t\omega) - 8\omega^2 \cos^2(t\omega) \cos(t\sqrt{q}) \right) \right. \right. \\ & + 14s^2\omega^2 + \omega^4 \Big] - \omega^2 \left((2s^2 + \omega^2) \cos(2t\omega) - 2s^2 \right) \cos(2tq) \\ & \left. \left. + 8s^2\omega q \sin(2t\omega) \sin(tq) + \omega^3 q \sin(2t\omega) \sin(2tq) \right], \right] \end{aligned} \quad (4.36)$$

see the definition of q under Eq. 4.27. The result of energy variance can be seen in Fig. 4.7. Note that only $t < T$ has a physical meaning, therefore the dependence is smooth along the whole geodesical driving protocols.

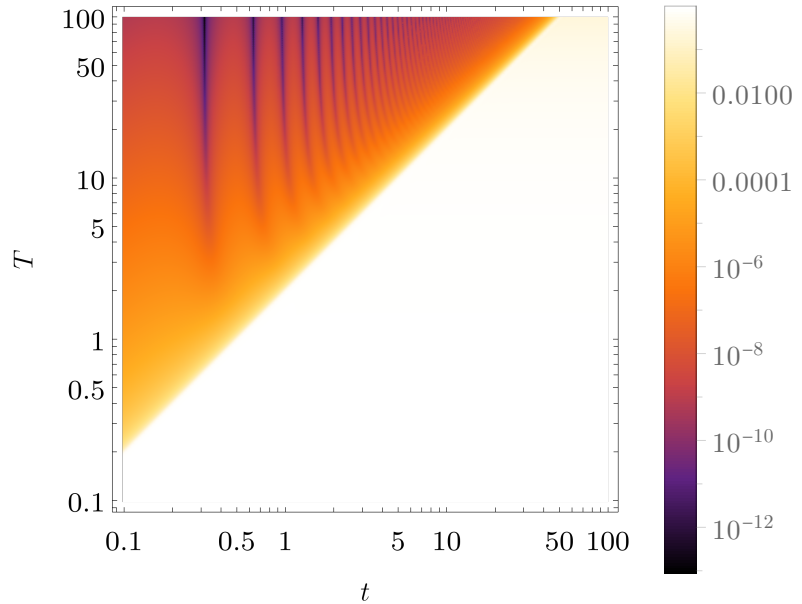


Figure 4.6: Fidelity dependence on time and final time in log-log scale. Only $t < T$ has a physical meaning.

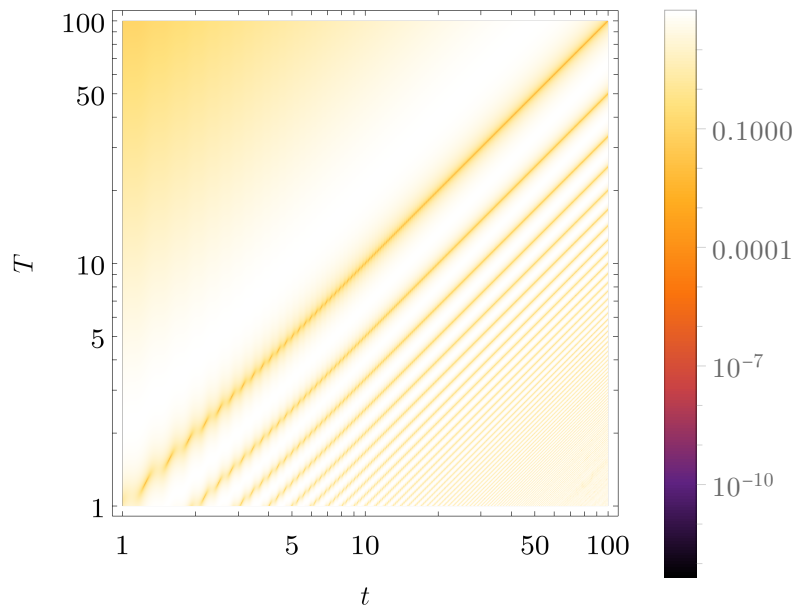


Figure 4.7: Energy variance for geodesical driving protocol, dependent on time t and final time T . Driving occurs only in area $t < T$.

4.5 Linear driving

Another analytically solvable driving is defined using two scaling parameters Ω_{sc} , Δ_{sc} , as

$$\Omega(t) = \Omega_{sc} \left(\frac{2t}{T} - 1 \right), \quad \Delta(t) = \Delta_{sc}, \quad \text{for } \Omega_{sc} = 10, \Delta_{sc} = 1, \quad (4.37)$$

see Fig. 4.8.

From linear driving definition 4.37 and energy dependence 4.2 we have

$$\dot{\Delta}(t) = 0; \quad \Delta(t) \stackrel{\Delta(t) > 0}{=} \sqrt{\frac{E_{dif}^2(t)}{4} - \Omega^2(t)}; \quad E_{dif} := E_1 - E_0. \quad (4.38)$$

Substituting to Harmonic oscillator damping and frequency functions (Eq. 4.13 and 4.14) we get

$$\gamma(t) = 0 \quad (4.39)$$

$$\omega^2(t) = i \frac{2\Omega_{sc}}{T} + \frac{\Omega_{sc}}{4} \left(\frac{2t}{T} - 1 \right)^2 + \frac{\Delta_{sc}^2}{4} = i \frac{2\Omega_{sc}}{T} + \frac{E_{dif}^2(t)}{4}. \quad (4.40)$$

Corresponding differential equation of second order is

$$a''(t) + \omega^2(t)a(t) = 0, \quad (4.41)$$

which is of *Weber type*² with Parabolic Cylinder functions³ as a solution, see Matus et al. [20].

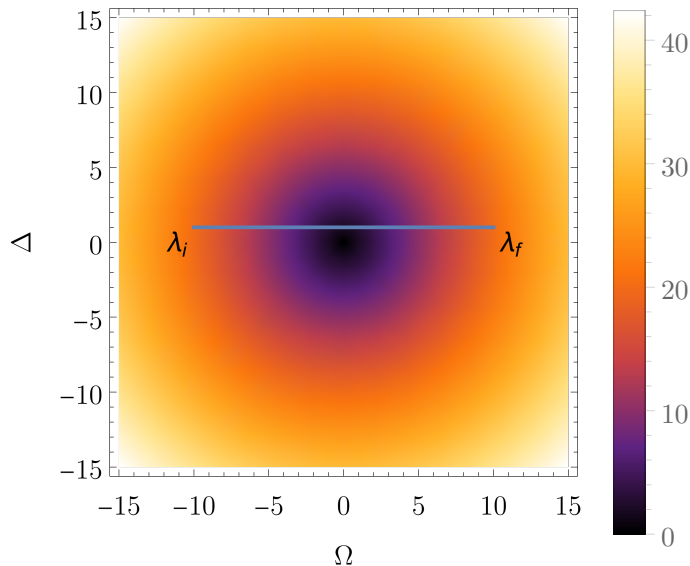


Figure 4.8: Driving along the linear path. $\lambda_i := (-10; 1)$ and $\lambda_f := (10; 1)$ are initial and final parameters respective. Density plot shows the difference between Hamiltonian eigenvalues.

²<https://mathworld.wolfram.com/WeberDifferentialEquations.html>

³<https://mathworld.wolfram.com/ParabolicCylinderFunction.html>

4.5.1 Dependence on time

The fidelity in time can be seen in Fig. 4.9. For $t \approx T/2$, the difference between energy levels is minimal, which leads to fast state excitation. Then the Harmonic oscillator damping gets involved, and oscillations quickly go to zero, never disappearing entirely.

We can see that the final fidelity decreases with a longer final time, which correctly leads to adiabatic driving, where $\lim_{T \rightarrow \infty} F^* = 0$. For short final times we can observe so-called quench, $\lim_{T \rightarrow 0} F^* = 1$. The interesting phenomena in this image are the oscillations around $t = T/2$, for which the frequency increases with a longer final time.

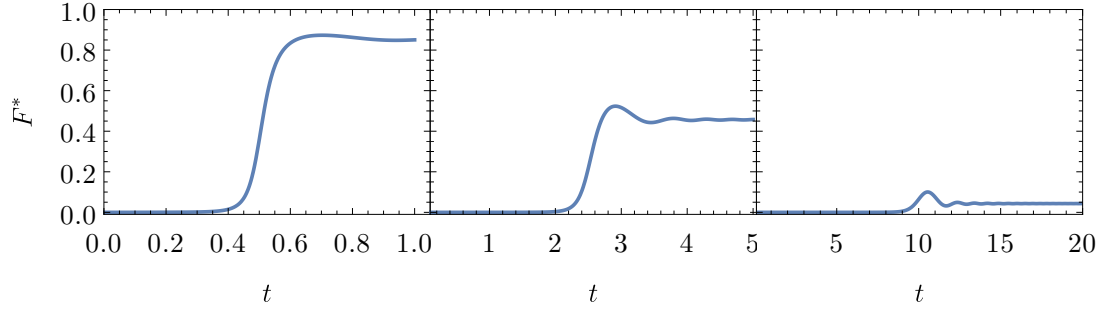


Figure 4.9: Infidelity in time for three final times $T \in \{1, 5, 20\}$ for the linear driving defined in 4.37.

Because in the Harmonic oscillator $\gamma(t) = 0$, the oscillations of $a(t)$ are not damped. What we are observing is infidelity

$$F^*(t) := 1 - |\langle 0(t) | \psi(t) \rangle|^2 = 1 - |\alpha(t)a(t) + \beta(t)b(t)|^2,$$

where the $|\psi(t)\rangle =: (a, b)^T$ represents the evolved state and $|0(t)\rangle =: (\alpha, \beta)^T$ evolved ground state in fixed eigenbasis \mathcal{B} . The ground state is not generally constant. In our case, the ground state described by Eq. 4.4 and is slowly changing its value from the first element α to the second element β , see Fig. 4.10. This means that at the beginning of driving, the projection to the ground state selects $b(t)$. Then it's getting more influenced by $a(t)$ until almost only $a(t)$ influences the fidelity.

Because of varying ground state during transport, the oscillations cannot be analyzed only from $\omega^2(t)$ described by Eq. 4.40. At the end of the driving we have

$$\frac{1}{N_+} |0(t)\rangle^1 = \frac{E_0(t) + \Omega(t)}{\Delta(t)} \gg 1 = \frac{1}{N_+} |0(t)\rangle^2, \quad (4.42)$$

leading to the *fidelity at the end of the driving*

$$F_{end} = \left| N_+ \left(\frac{E_0(t) + \Omega(t)}{\Delta(t)} a(t) + b(t) \right) \right|^2 \approx b^2(t), \quad (4.43)$$

therefore when t is getting close to T the fidelity is oscillating with harmonic oscillator frequency 4.14.

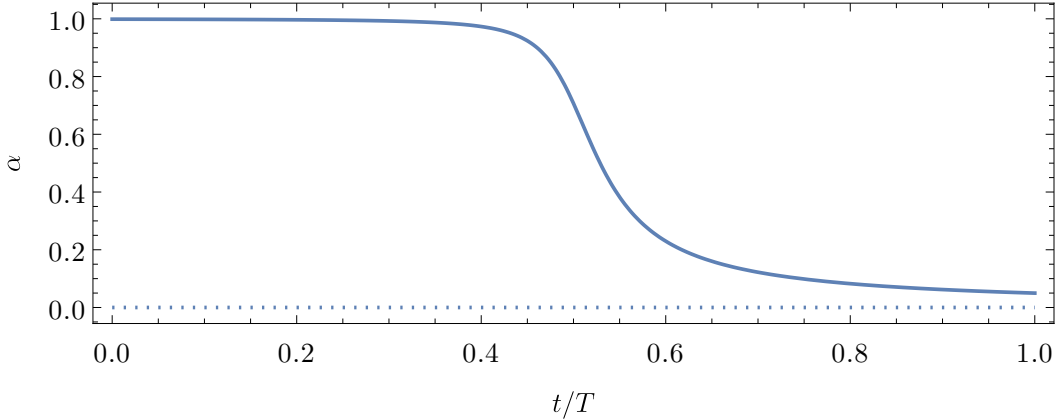


Figure 4.10: Value of first element of the ground state vector $\alpha \equiv |0(t)\rangle^1$ during linear driving.

4.5.2 Final fidelity

Because the oscillations after fast parameter change in the Hamiltonian never disappear entirely, we must observe these oscillations even at the final time. *Final fidelity* (meaning the fidelity at $t = T$) has dependence on T as can be seen in Fig. 4.11. Because after the final time $T \approx 120$, the values are small enough to observe some fine structure of the fidelity along with numerical error artifacts.

First, the numerical precision of this calculation was found to be around 10^{-13} . This means that the oscillations we see in Fig. 4.11 are of physical origin with some additional numerical error. These small oscillations are the remnants of the fast excitation during the close approach of energy levels, see Fig. 4.9. The reason is that the choice $t = T$ sometimes corresponds to the oscillation minima and sometimes to its maxima.

Averaged final fidelity

We can eliminate the effect of oscillations by averaging over time. For that we define the *average final infidelity*

$$\langle F^* \rangle_p(T) := \frac{1}{(1-p)T} \int_{pT}^T F^*(t) dt. \quad (4.44)$$

It turned out that averaging over 1 % ($p = 0.99$) or 10 % ($p = 0.9$) of the driving gave approximately the same results for long enough drivings ($T \gtrsim 10$). The same result can be obtained from the analytical continuation of the fidelity formula to $t \rightarrow \infty$. This analytical continuation of the harmonic oscillator solution leads to the Fidelity value around which the oscillations occur. The result of averaging can be seen in Fig. 4.12.

Using this we can describe the driving using three regimes⁴.

The boundary between exponential and linear regime is not strict and can be seen in Fig. 4.13, as transition between *smooth* and *chaotic* regimes. This happens

⁴The coefficient p is assumed to be small enough not to cover the biggest oscillations after $t = T/2$ and big enough to average over sufficient number of oscillations. Approximately $p \in [0.6T, 0.999T]$.

around $t = T_c$. The fine structure, see Fig. 4.14, is caused by the oscillatory character of the final fidelity. This can be smoothed out using the averaged final fidelity. The approximated dependence for final time was numerically estimated as

$$T_c \underset{\sim}{\propto} \Delta_{sc}^{-2}. \quad (4.45)$$

- *Exponential/fast-driving regime* — $\langle F^* \rangle_p = \exp(-\xi T)$, $\xi \in \mathbb{R}^+$
- *transitional regime* — happens around *critical time* T_c .
- *Polynomial/close-adiabatic regime* — $\langle F^* \rangle_p \propto T^{-\kappa}$ for $\kappa \in \mathbb{R}^+$.

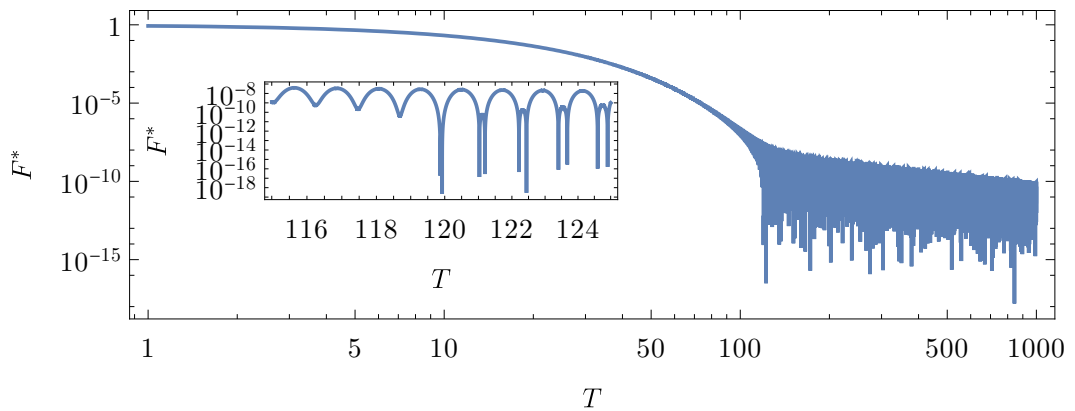


Figure 4.11: Final infidelity as a function of T with zoom on the transitional part.

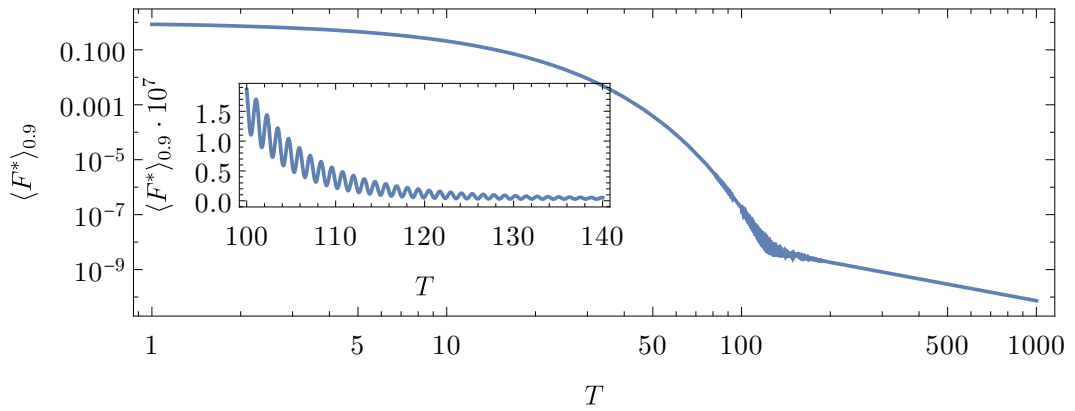


Figure 4.12: Final infidelity as a function of T in log-log scale with linear scaled plot inserted.

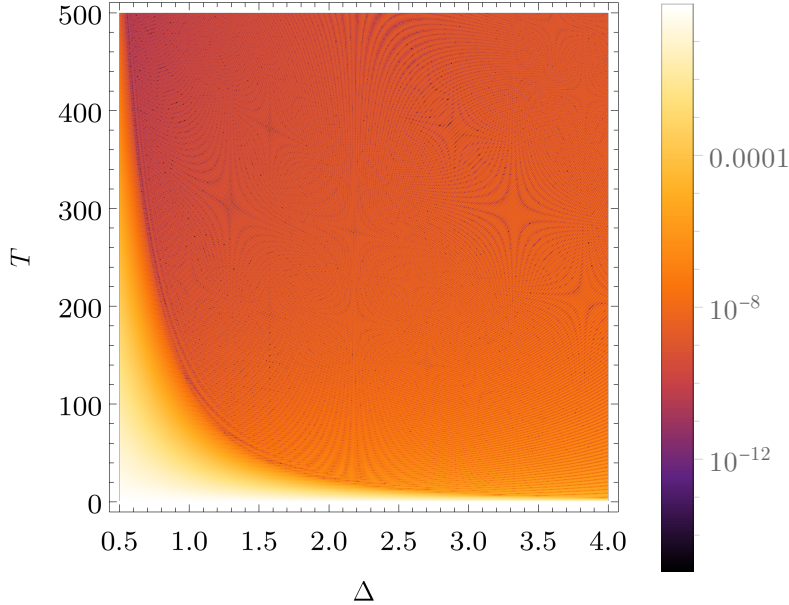


Figure 4.13: Final infidelity as a function of Δ and T and its three regimes. Zoom on the boundary between them can be seen on 4.14.

To understand the infidelity oscillations, compare Fig. 4.15 with 4.16. Here we see two regimes, one for $t < T_c$ and one for $T > T_c$. The important observation is that in the first case, $F^* \neq 0$ for all $t > 0$, and in the second case, it touches zero periodically. The fidelity can be decomposed into a sum of two elements. The small oscillatory part, which the theory of APT can explain, and exponentially decreasing fidelity with final time, is described by the Landau-Zener formula.

Exponential and polynomial part, Landau-Zener and APT

Landau-Zener-Stueckelberg's theory provides the WKB approximation formula for the fidelity during some transport. The complete form can be seen in the book by Nakamura [21]. In this case, only a simplified theorem is needed. First, let's review some definitions.

Definition 16 (Diabatic coupling). *Diabatic coupling functions are off-diagonal elements of two-level Hamiltonian. At avoided crossing, it is half of Hamiltonian eigenvalue difference,*

$$A = \frac{E_2 - E_1}{2}. \quad (4.46)$$

Definition 17 (Diabatic potential). *Difference between Hamiltonian eigenvalues can be linearly approximated as*

$$\Delta E \equiv E_1 - E_0 =: \alpha t \quad (4.47)$$

Diabatic potential difference is the ratio

$$|\Delta F| := \left| \frac{\alpha}{t} \right|. \quad (4.48)$$

Theorem 9 (Landau-Zener-Stueckelberg (LZS) for linear driving). *For*

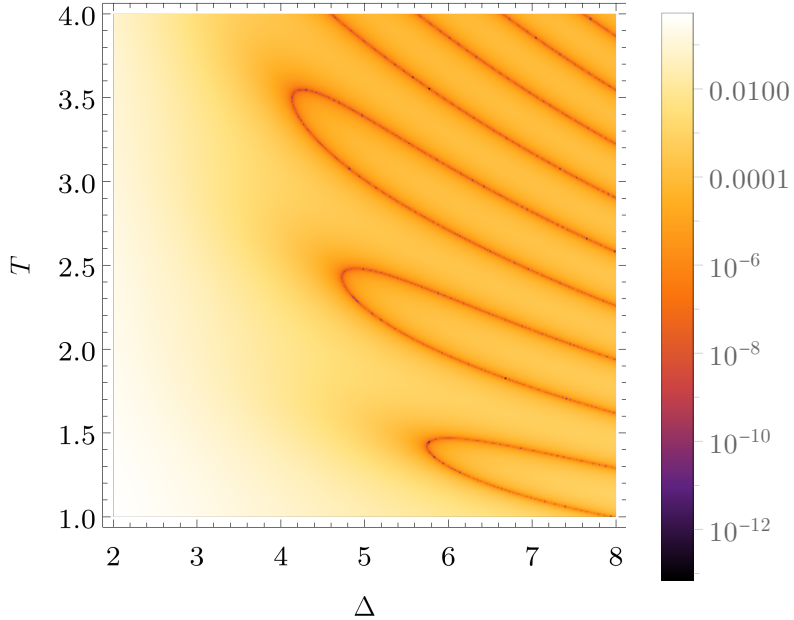


Figure 4.14: Fine structure of the boundary between fast-driving and adiabatic regimes of final infidelity.

- *two level Hamiltonian*
- *with degeneracy in only one point,*
- *on the linear driving path in a parametric space,*

the fidelity can be described for times $t \in (0, T_c)$ as

$$F = \exp\left(-\frac{2\pi A^2}{v|\Delta F|}\right), \quad (4.49)$$

for a diabatic coupling A , and diabatic potential difference $|\Delta F|$.

In our case, the speed $v = 1/T$ is constant, off-diagonal elements are also constant $A = \Delta_{sc}$, and the driving path is symmetric along $\Omega = 0$ axis, leading to $|\Delta F| = 2\Omega_i$.

The polynomial, or chaotic regime, can be explained using APT. It holds that

$$\log(F^*) = \log(T^{-2}) + \log\left(\sum_{i=1}^n |b_n^{(1)}(T)|^2\right), \quad (4.50)$$

for functions $b_n^{(1)}$ from Eq. 3.44. For more details, see Matus et al. [20].

The Lzs approximation can be seen in Fig. 4.17. The Lzs and APT approximations give the leading order in corresponding regimes (omitting the oscillations) and intersect at time T_c . These two parts are not only a good approximation on both intervals, but if added together, they represent the whole fidelity curve with very high precision. Adding these two solutions together might not give a good mathematical meaning. It can be done because the APT gives the infidelity of order 10^{-9} , it creates a negligible error. The advantage is that one gets a suitable approximation for the transitional regime with this process.

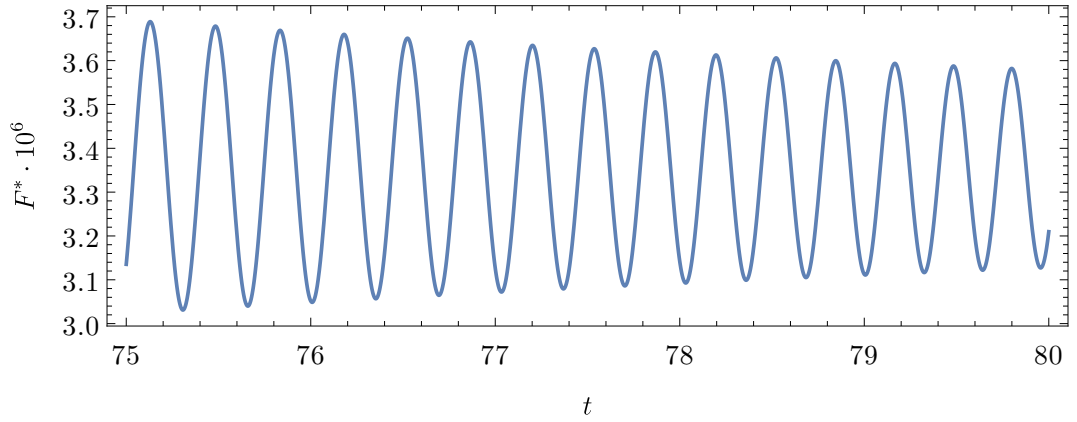


Figure 4.15: Infidelity as a function of time for fast-driving regime, $T = 80 < T_c$.

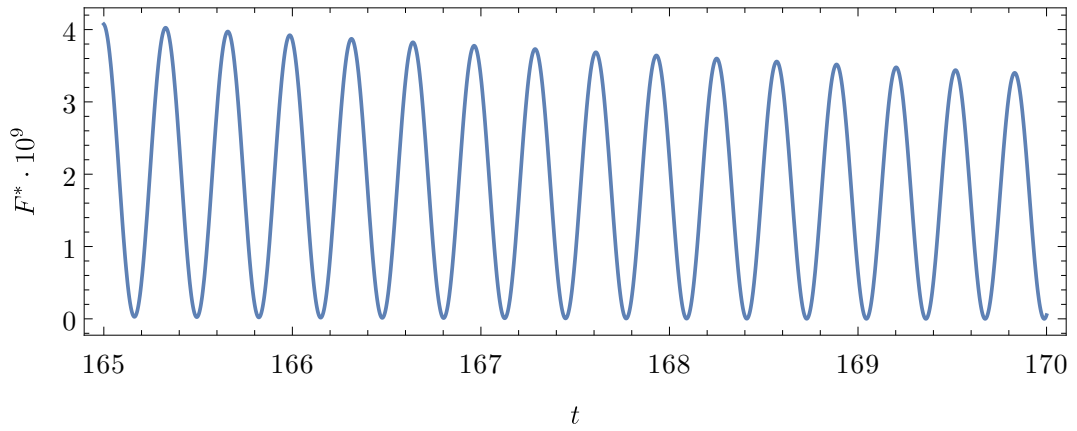


Figure 4.16: Infidelity as a function of time for close-adiabatic regime. $T = 170 > T_c$

4.5.3 Energy variance

Analogically to the geodesical driving, one might be interested in energy variance. In the linear driving case, the analytical formula is more complicated and only numerical result are displayed here. In Fig. 4.18 the energy variance is plotted as a function of time and final time.

4.5.4 Linear driving summary

Now that we understand all results separately let's put it all together. In Fig. 4.19 the most important results can be seen. The difference between the close adiabatic regime and the fast regime at the end of the driving is if $F^* = 0$. The chaotic regime is below $t = T$ line for $T < T_c$ and the chaotic cone is crossing this line around $t = T_c$.

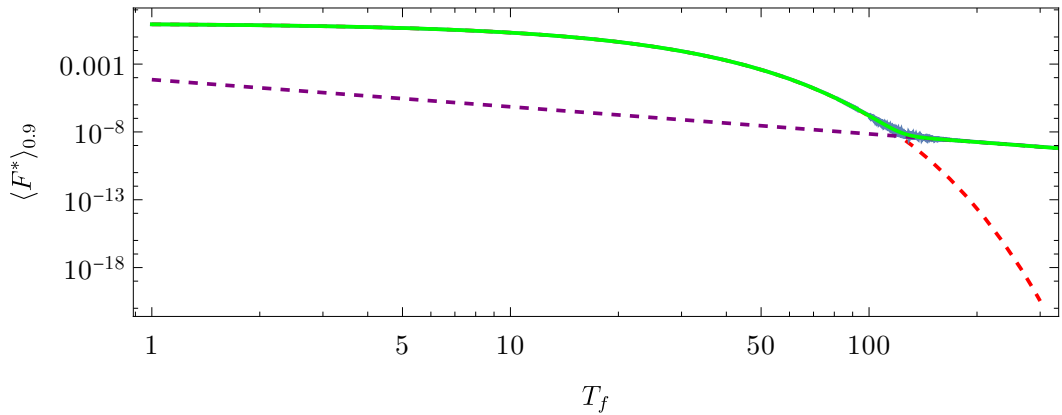


Figure 4.17: Fidelity as a function of driving final time, approximated by the sum (green) of Landau-Zener (red, dashed) and APT (purple, dashed)

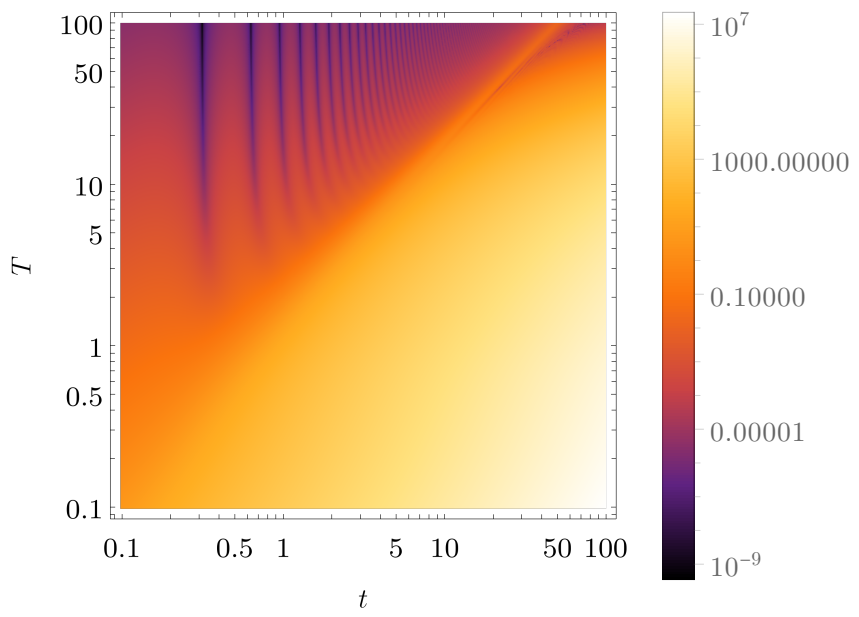


Figure 4.18: Energy variance for $\Delta_{sc} = 0.2$ for linear driving. Note that only $t < T$ has physical meaning.

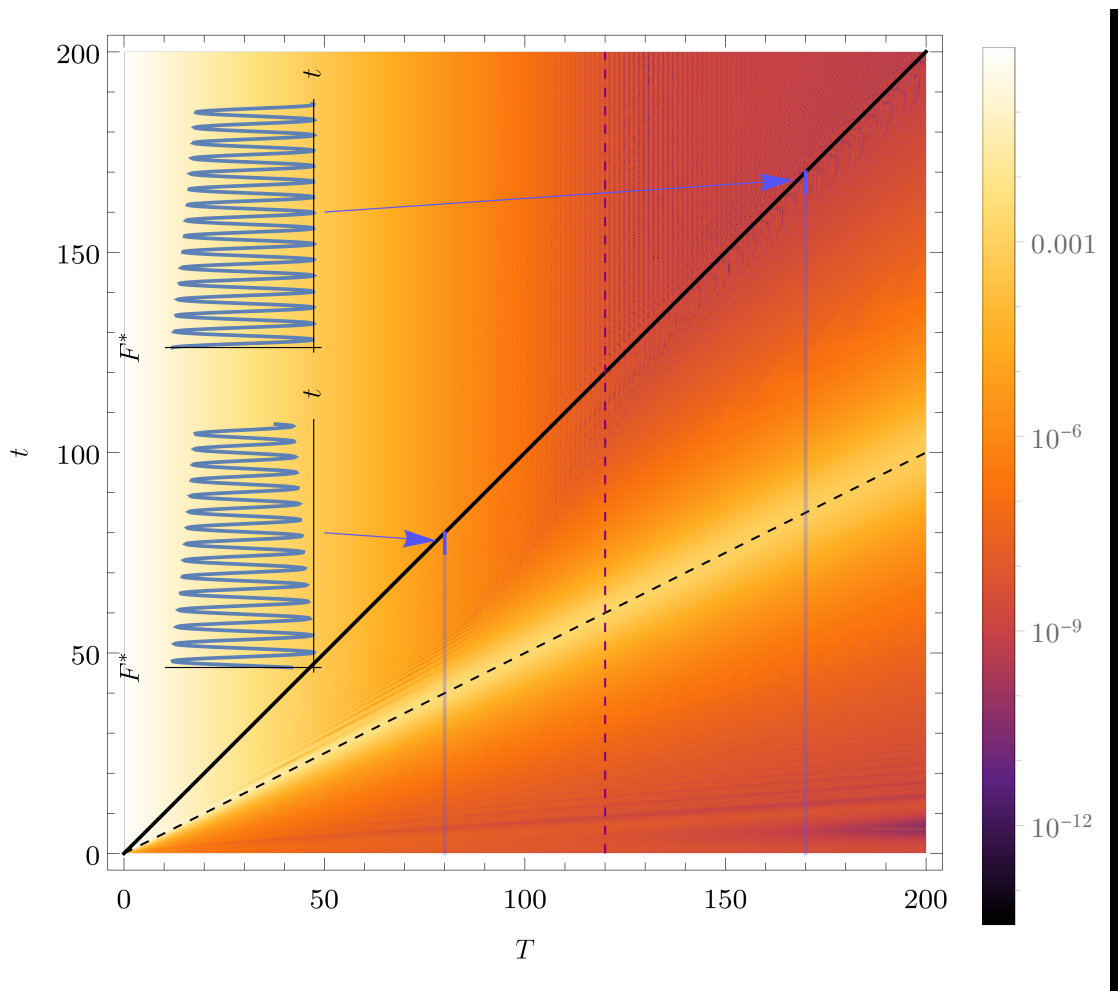


Figure 4.19: Fidelity dependence for linear driving with $\Delta = 1$. Black line marks $t = T$, dashed black line $t = T/2$ and **purple** dashed line is the approximate value of T_c . **Blue** lines marks driving from Fig. 4.15, 4.16, visualizing the final times of the driving.

5. Lipkin-Meshkov-Glick model

The Lipkin-Meshkov-Glick (LMG) model is a simple model manifesting the quantum phase transitions. It was introduced as a toy model for many-body fermion systems, but its applications are much wider. Generally it describes any *fully connected qubit system*. *Fully connected* means the interactions have infinite range. In the *qubit system*, the individual atoms have only two energy eigenstates. This chapter aims to understand the properties of the ground state and its influence on different driving protocols. Understanding the fidelity during the phase transitions is important, because these changes are often present in the quantum annealing.

5.1 Hamiltonian

The LMG model is defined on a parametric space $\lambda \equiv (\lambda; \chi) \in \mathcal{U} := \mathbb{R}^2$ with Hamiltonian

$$\hat{H}(\lambda, \chi) = \hat{J}_3 + \lambda \hat{V}_1 + \chi \hat{V}_2 + \chi^2 \hat{V}_3, \quad (5.1)$$

where

$$\hat{V}_1 := -\frac{1}{2j} \hat{J}_1^2 \quad (5.2)$$

$$\hat{V}_2 := -\frac{1}{2j} [\hat{J}_1(\hat{J}_3 + j\mathbb{1}) + (\hat{J}_3 + j\mathbb{1})\hat{J}_1] \quad (5.3)$$

$$\hat{V}_3 := -\frac{1}{2j} (\hat{J}_3 + j\mathbb{1})^2 \quad (5.4)$$

and *angular momentum operator* $\hat{\mathbf{J}} = (\hat{J}_1, \hat{J}_2, \hat{J}_3)^T$.

Using the Spherical harmonics¹ basis $\{|j, m\rangle\}$ for quantum numbers j as the angular momentum and m its projection to the direction of \hat{J}_3 and defining

$$\hat{J}_{\pm} := \frac{1}{2}(\hat{J}_1 \pm i\hat{J}_2), \quad (5.5)$$

we get matrix elements

$$\langle j'm' | \hat{J}^2 | jm \rangle = j(j+1)\delta_{j'j}\delta_{m'm} \quad (5.6)$$

$$\langle j'm' | \hat{J}_3 | jm \rangle = m\delta_{j'j}\delta_{m'm} \quad (5.7)$$

$$\langle j'm' | \hat{J}_{\pm} | jm \rangle = \sqrt{(j \mp m)(j \pm m + 1)}\delta_{j'j}\delta_{m'm\pm1}, \quad (5.8)$$

where $\delta_{a'b}$ is Kronecker delta. The Hamiltonian in Eq. 5.1 can then be written as

$$\begin{aligned} \hat{H} = & J_3 - \frac{\lambda}{8j}(J_+ + J_-)^2 - \frac{\chi}{4j} [(J_+ + J_-)(J_3 + j\mathbb{1}) + (J_3 + j\mathbb{1})(J_+ + J_-)] \\ & - \frac{\chi^2}{2j} (J_3 + j\mathbb{1})^2, \end{aligned} \quad (5.9)$$

¹<https://mathworld.wolfram.com/SphericalHarmonic.html>

which has pentadiagonal matrix representation. During the whole chapter, $j = N/2$ is used.

First, the low dimensional cases of the Hamiltonian are analyzed, especially $N = 3$, where the analytical formula for energy spectrum can be found. The limit $N \rightarrow \infty$ is then taken, showing the correspondence to the classical system. Finally, some generalization to an arbitrary dimension and an example of transport using quenches is presented.

5.2 Geometry for fixed dimension

Because of a penta-diagonal form of the Hamiltonian, the discussion starts at $N = 3$, followed by $N = 5$ and $N \rightarrow \infty$.

Due to the complexity of our Hamiltonian, it is not possible to prove every statement analytically. Some numerical methods, supported by mathematical theorems, are therefore used.

5.2.1 3-dimensional Hamiltonian

The lowest dimension behaving similarly to higher N is 3. The matrix represented Hamiltonian is

$$\hat{H} = \begin{pmatrix} -\frac{\lambda+6}{4} & -\frac{\chi}{2\sqrt{3}} & -\frac{\lambda}{2\sqrt{3}} & 0 \\ -\frac{\chi}{2\sqrt{3}} & \frac{(-7\lambda-4\chi^2-6)}{12} & -\chi & -\frac{\lambda}{2\sqrt{3}} \\ -\frac{\lambda}{2\sqrt{3}} & -\chi & \frac{(-7\lambda-16\chi^2+6)}{12} & -\frac{5\chi}{2\sqrt{3}} \\ 0 & -\frac{\lambda}{2\sqrt{3}} & -\frac{5\chi}{2\sqrt{3}} & -\frac{\lambda}{4} - 3\chi^2 + \frac{3}{2} \end{pmatrix}. \quad (5.10)$$

The spectrum of this Hamiltonian can be calculated analytically using some complex functions $D, E, F, G : \mathbb{C} \rightarrow \mathbb{C}$, see Appendix B, as

$$E_0 = \frac{1}{12} \left(G - F - \frac{\sqrt{D - E}}{2} \right) \quad (5.11)$$

$$E_1 = \frac{1}{12} \left(G - F + \frac{\sqrt{D - E}}{2} \right) \quad (5.12)$$

$$E_2 = \frac{1}{12} \left(G + F - \frac{\sqrt{D + E}}{2} \right) \quad (5.13)$$

$$E_3 = \frac{1}{12} \left(G + F + \frac{\sqrt{D + E}}{2} \right). \quad (5.14)$$

Eigenvectors can also be expressed analytically, but due to their complexity only analytical results are presented here. On sections $\lambda = 1$ and $\chi = 1$ (see energy spectrum on Figures 5.1 and 5.2 respective), the energies get close to each other somewhere around the center of our coordinate system $(\lambda; \chi)$ and then separate monotonously to never meet again. The spectrum has $\chi \leftrightarrow -\chi$ symmetry. These close approaches of energy levels are important, because of their influence on geometry of energy state manifolds.

From Eq. 5.11, 5.12 can be seen the possible existence of spectrum degeneracies between every two neighboring energy levels². Degeneracy $E_0 = E_1$ holds for $D = E$, which for real values λ, χ has two solutions

$$(\lambda_d, \pm\chi_d) = \left(-\frac{1}{2}; \sqrt{\frac{3}{5}} \right). \quad (5.15)$$

According to Theorem 1, Hamiltonian driven by two real parameters can be degenerated only on 0-dimensional manifolds. This means that degeneracies are separated points in the parametric space.

If the energy spectrum is degenerate and the metric tensor diverges, see individual elements in Fig. 5.3, its determinant also diverges, as shown in Fig. 5.4, along with Christoffel symbols in Fig. 5.5. The metric tensor determinant is positive definite; therefore, the manifold is Riemannian. Further on, it reflects the symmetry $\chi \leftrightarrow -\chi$, except for elements $g_{12}, \Gamma_{121}, \Gamma_{211}$, and Γ_{222} , which switch their sign.

Due to metric tensor degeneracy, the space is not geodesically maximal. To see that the singularity is not only *coordinate one*³ the Ricci scalar can be calculated, see Fig. 5.6. Divergent Ricci scalar implies that singularity is physical. This can be seen from sections in χ -direction drawn in Fig. 5.7, which at coordinate $(\lambda_d; \chi_d)$ diverges. The coordinate independence implies the singularity is *physical*.

Geodesics

The importance of geodesics was described in Chapter 3.2. In addition, they give a tool for observing some system characteristics, such as singularities, or curvature in general. *Initial valued Geodesics* are solutions to

$$\begin{aligned} (\lambda(0); \chi(0)) &=: (\lambda_i; \chi_i) \\ \left. \left(\frac{d\lambda(t)}{dt}; \frac{d\chi(t)}{dt} \right) \right|_{t=0} &=: (\lambda'_i; \chi'_i), \end{aligned}$$

where zero was set as initial time.

One might also choose *boundary valued geodesics* with fixed initial $(\lambda(0); \chi(0))$ and final position $(\lambda(T); \chi(T))$. Because the shape of geodesics in parametric space does not depend on the initial derivative, it does not depend on the speed of driving in the parametric space. Initial valued geodesics are therefore more advantageous to calculate because they have only three free parameters — the initial coordinates $(\lambda_i; \chi_i)$ and ratio λ'_i/χ'_i . Another reason is purely numeric, which is that boundary-valued geodesics are calculated by numerous evolutions of initial valued geodesics. Usually the software evolves many initial valued geodesics and checks if the final boundary condition is satisfied. If not, the initial parameters are tweaked in response until it fits the boundary condition. Calculating the boundary valued geodesics is generally much slower. In this case, the calculation time was 10 to 100 times longer.

²If the functions D, E, F, G were into real numbers, degeneracies would exist between every two neighboring energy levels. Because they are complex, the solution $E_i = E_j$ might not exist. From numerical results, degeneracies exist between every two neighboring energy levels.

³Coordinate singularity is present only in some coordinates. This is different from the so-called *physical singularity*, which is present in every choice of the coordinate system.

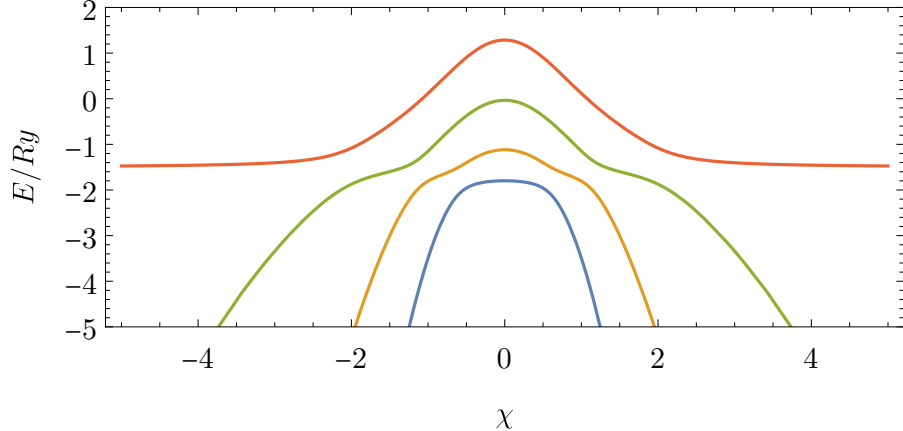


Figure 5.1: Energy spectrum for $N = 3$, section $\lambda = 1$

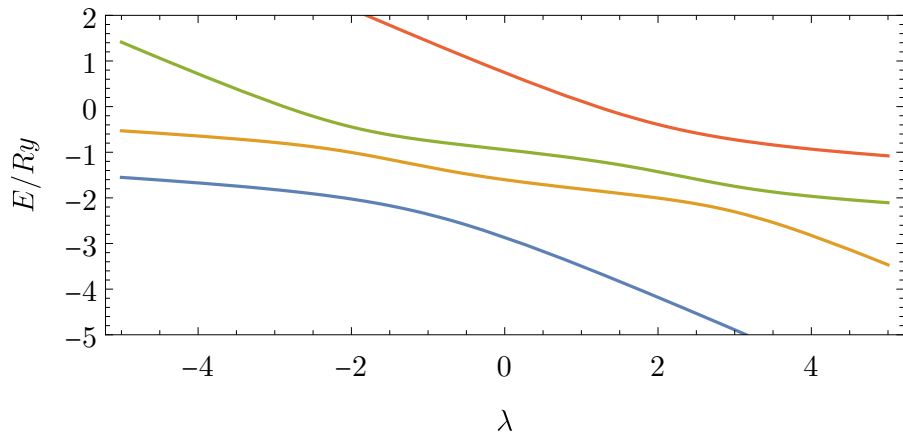


Figure 5.2: Energy spectrum for $N = 3$, section $\chi = 1$.

Results for geodesics starting at $(\lambda_i; \chi_i) = (0; 0)$, $(\lambda', \chi') = (\cos \theta; \sin \theta)$ can be seen in Fig. 5.8. Other values θ result in a close approach of the geodesics to the singularity, making the calculation numerically unstable. The fact that geodesics lean toward singularities is well known from the theory of General Relativity (GR). The main difference here is that our “test particle” seems to be partially repulsed by the singularity. The analogy with GR then fails because of the nonexistence of negative mass and gravitational dipoles. The better analogy is electromagnetism, which has a downside in the fact that geometrical formalism is not used so much in this theory. A comparison of these two intuitive examples can be seen in Fig. 5.9. The geodesic behavior is caused not only by the singularity but also by a large Ricci curvature leaning to the right from it. This means the distance across this *unreachable gap*, marked by *blue line* in Fig. 5.8, is also large. The geodesics then have a strong tendency to avoid its crossing. The presence of singularities means that our ground state manifold is geodesically incomplete, and according to Theorem 3, there exist some geodesically unreachable coordinates. From this goes the term *unreachable gap*.

The fact that geodesics lean toward singularities and parts of parametric space with small energy level difference ΔE implies that for general fidelity driving, the geodesics cannot be advantageous in the case of fidelity. The excitation probability increases with smaller ΔE leading to a fidelity decrease for such drivings.

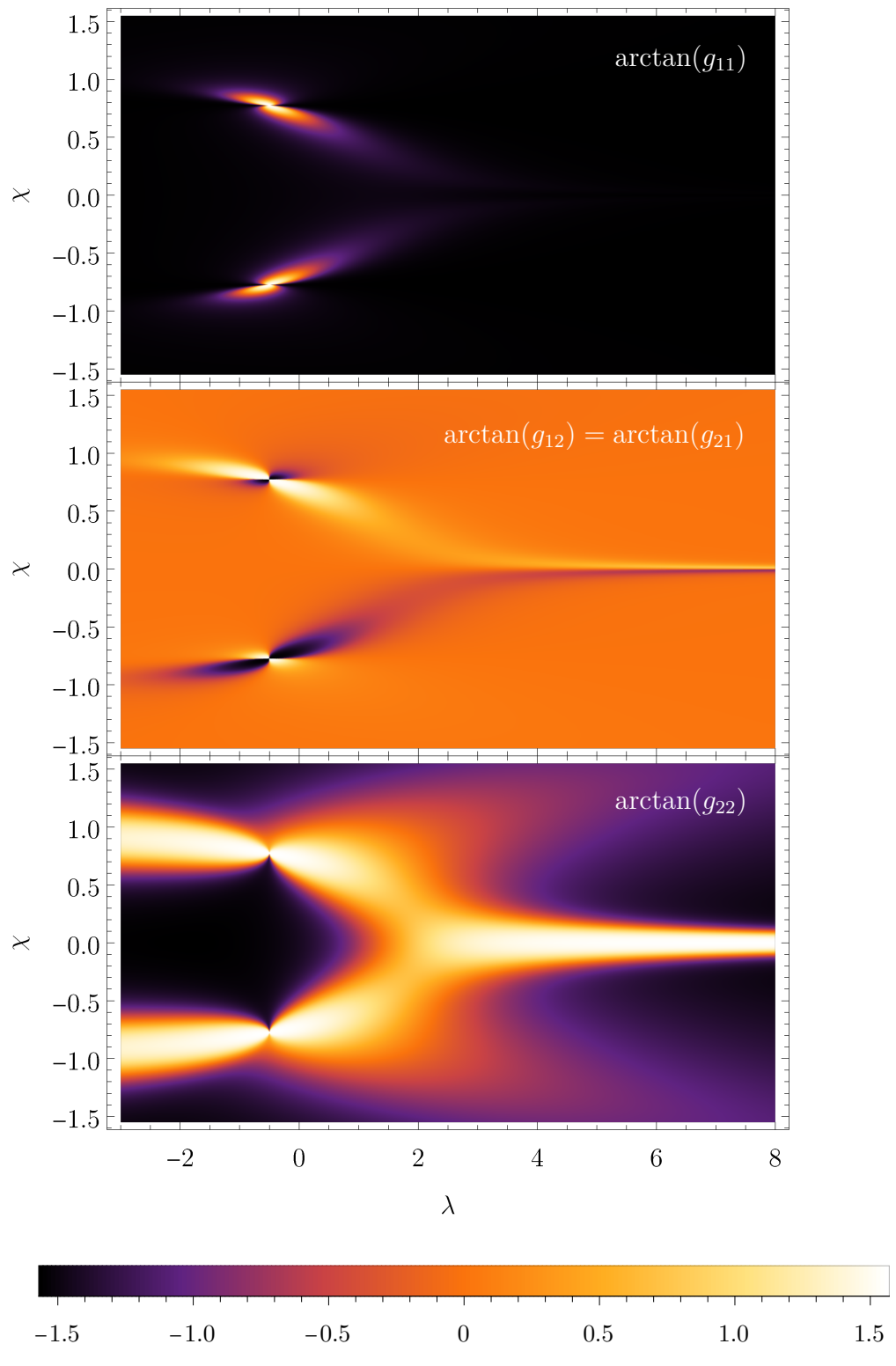


Figure 5.3: Arctangent of the metric tensor elements for $N = 3$ in the parametric space.

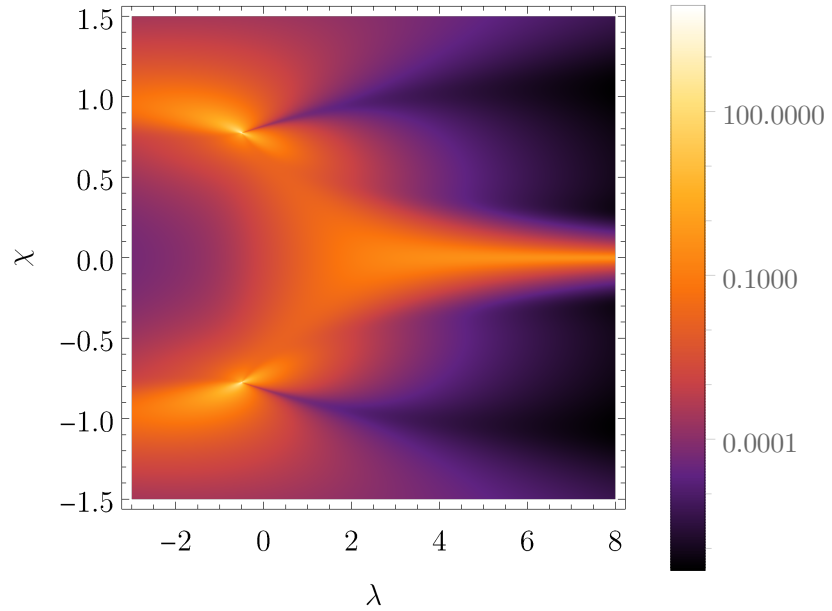


Figure 5.4: Ground state metric tensor determinant in a parametric space for $N = 3$.

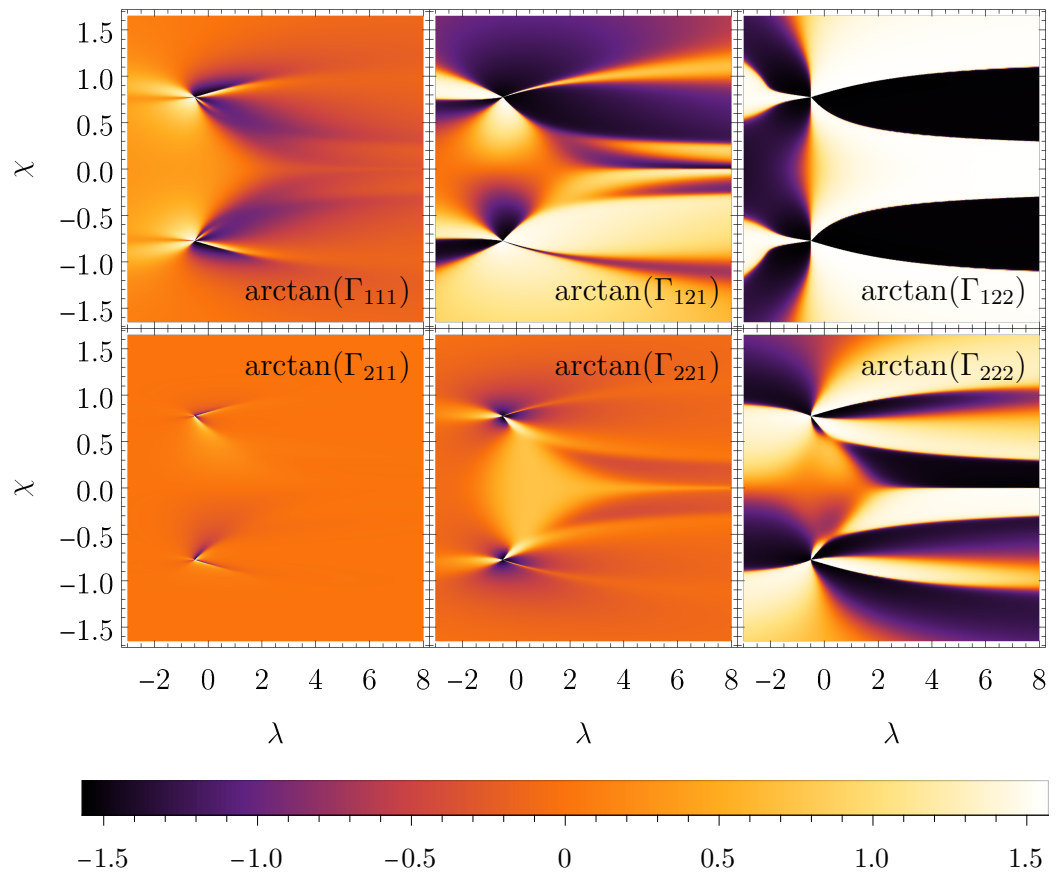


Figure 5.5: Arctangent of the ground state Christoffel symbols for $N = 3$.

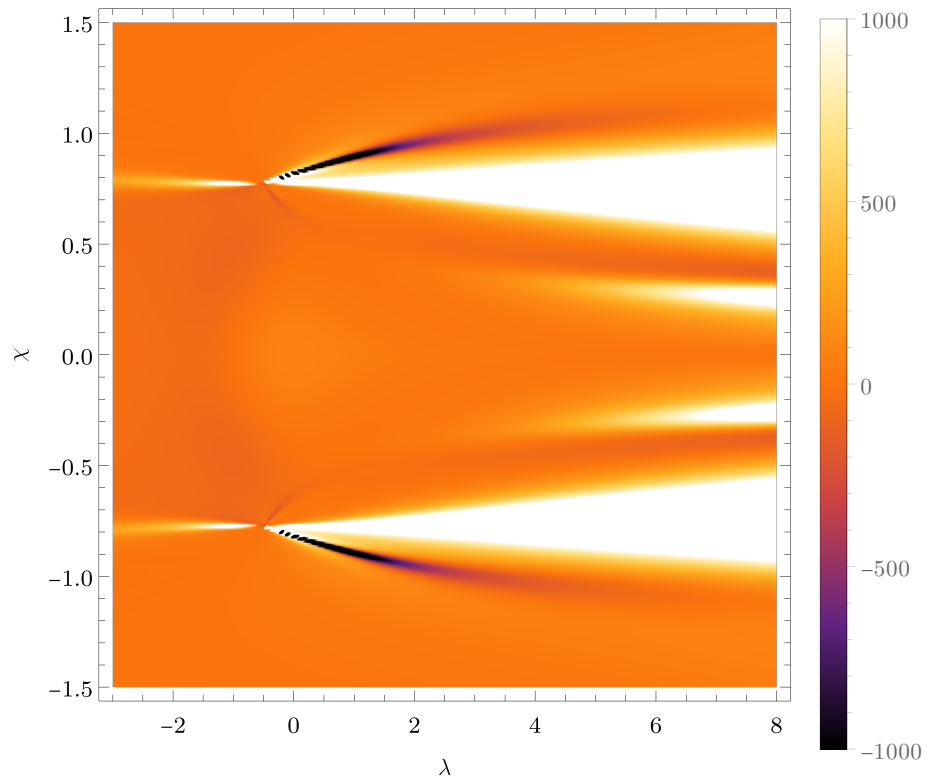


Figure 5.6: Arctangent of Ricci curvature for the case $N = 3$.

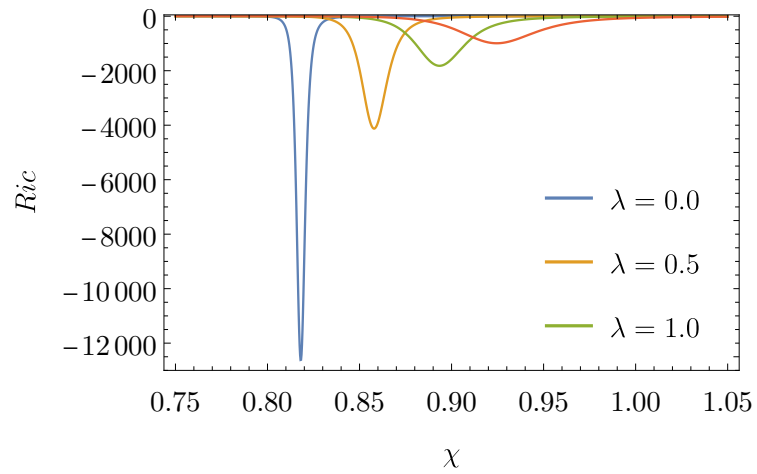


Figure 5.7: Ricci curvature sections for three different λ . $N = 3$.

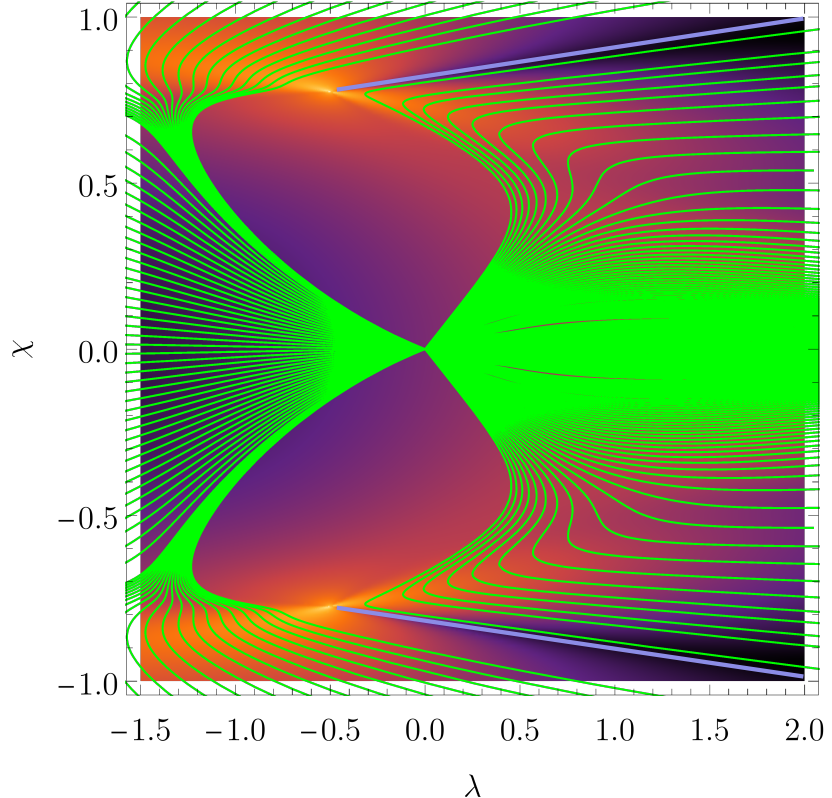


Figure 5.8: Geodesics for $N = 3$ starting from $(\lambda_i; \chi_i) = (0; 0)$ with $(\lambda'_i; \chi'_i) = (\cos \theta; \sin \theta)$, parametrized by angle $\theta \in [-0.63; 0.63]$, $\theta \in [\pi - 0.225; \pi + 0.225]$, with step $\Delta\theta = 0.01$. Blue line marks the unreachable gap, where the Ricci curvature is big.

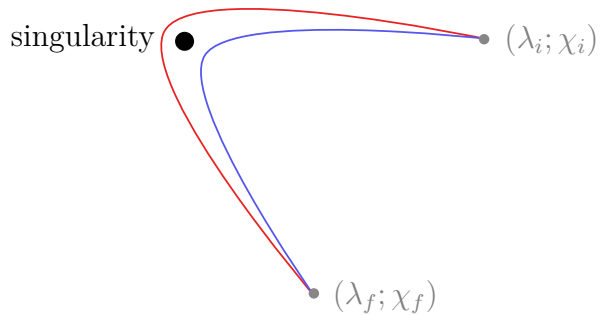


Figure 5.9: Comparing boundary valued geodesics for repulsing (inner line) and attracting (outer line) metric tensor divergence in the spherically symmetrical space.

5.2.2 5-dimensional Hamiltonian

Another special case is $N = 5$. Between every two neighboring energy levels, there are many degeneracies, as can be seen in Fig. 5.10. $E_0 = E_1$ degeneracy lies approximately on the line called *separatrix* (see Chap. 5.2.3) and other singularities are distributed around. The $\chi \leftrightarrow -\chi$ symmetry holds for all of them.

The ground state manifold can be understood from the metric tensor determinant, see Fig. 5.11. Here we see the spectrum degeneracy causes high positive values of metric tensor determinant and the [unreachable gap](#) is characterized by small determinant values.

Geodesics for case $N = 5$ starting at $(\lambda; \chi) = (0; 0)$ have the characteristics already seen in the case $N = 3$. However, when starting at $(1; 0)$, the behavior around the singularity is not the only interesting thing happening. As can be seen in Fig. 5.12, the geodesics tend to deflect themselves from the area with high curvature around the axis $\chi = 0$, which happens even for other initial conditions, just that for $(0; 0)$ it is not so apparent. Small irregularity can be seen in Fig. 5.8 around point $(0.5; 0.1)$ and means that the geodesic equation might have at least two solutions as candidates for the globally shortest path between two points.⁴

⁴One might recall the effect of gravitational lensing here. In the presence of any mass in spacetime, there exist more possible light paths (solutions to the geodesic equation) between two points, differing by the initial condition.

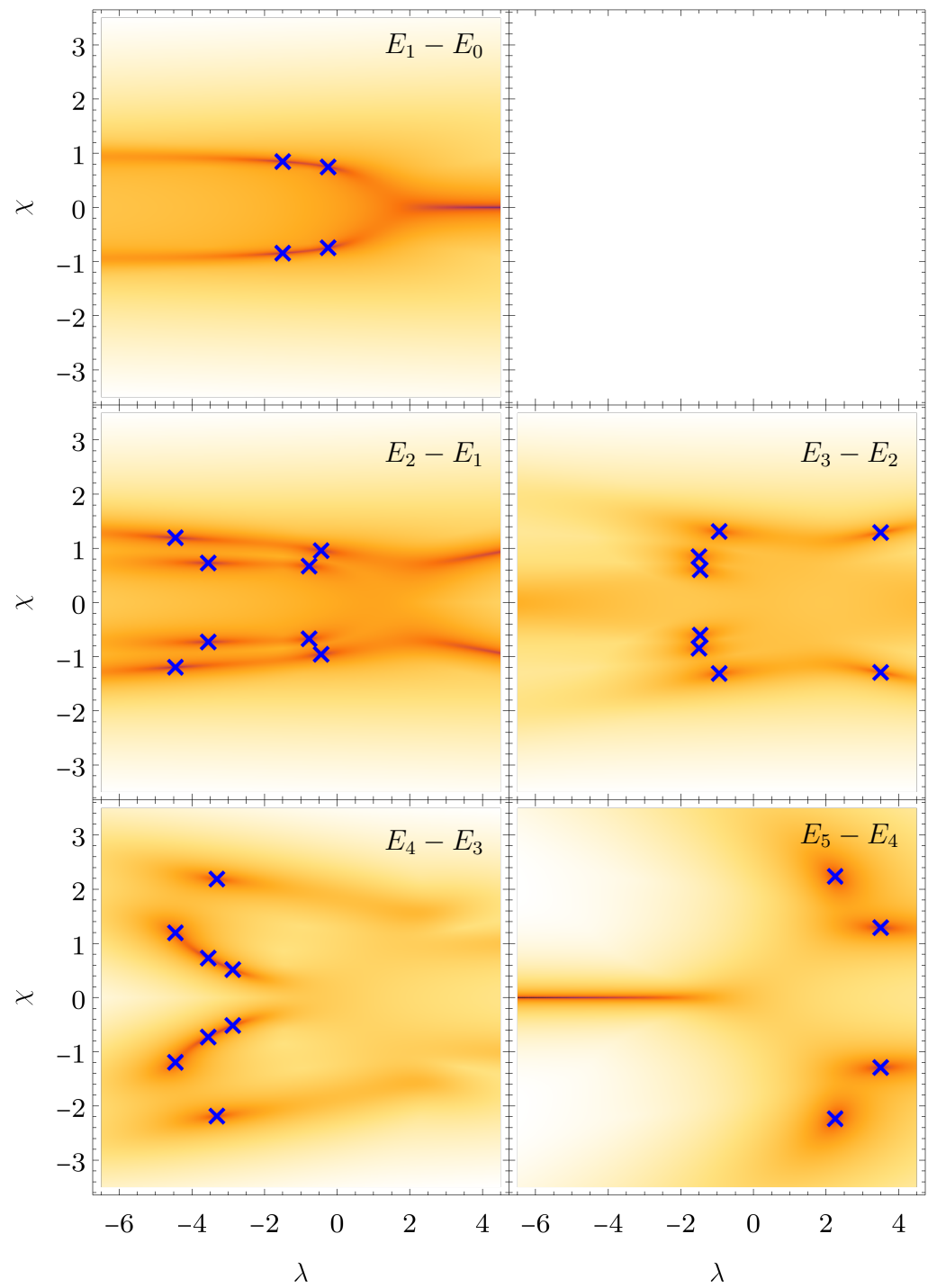


Figure 5.10: Energy differences between neighboring energy levels for $N = 5$. Spectra degeneracies are marked with blue cross.

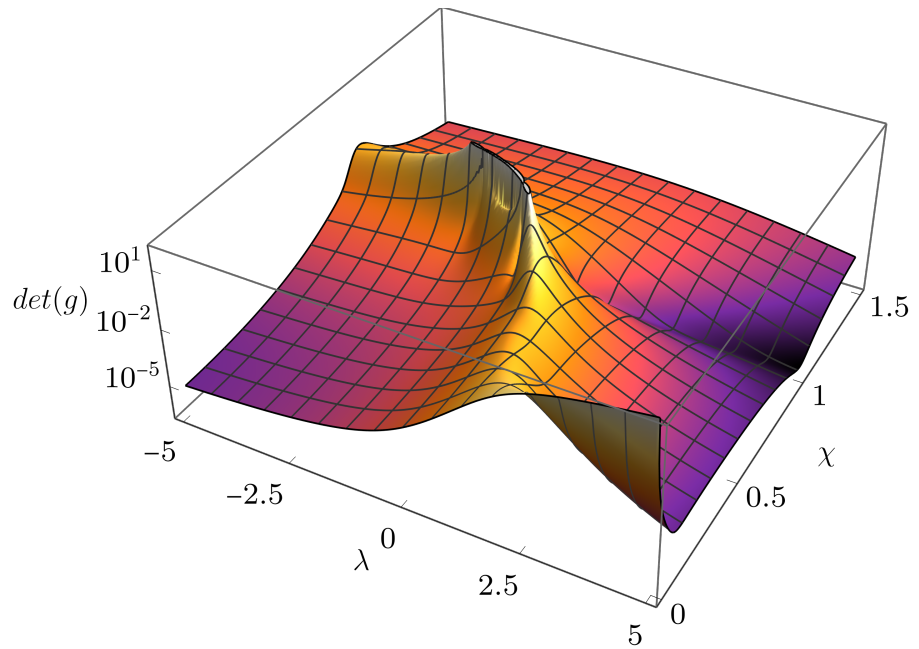


Figure 5.11: Metric tensor determinant for the case $N = 5$.

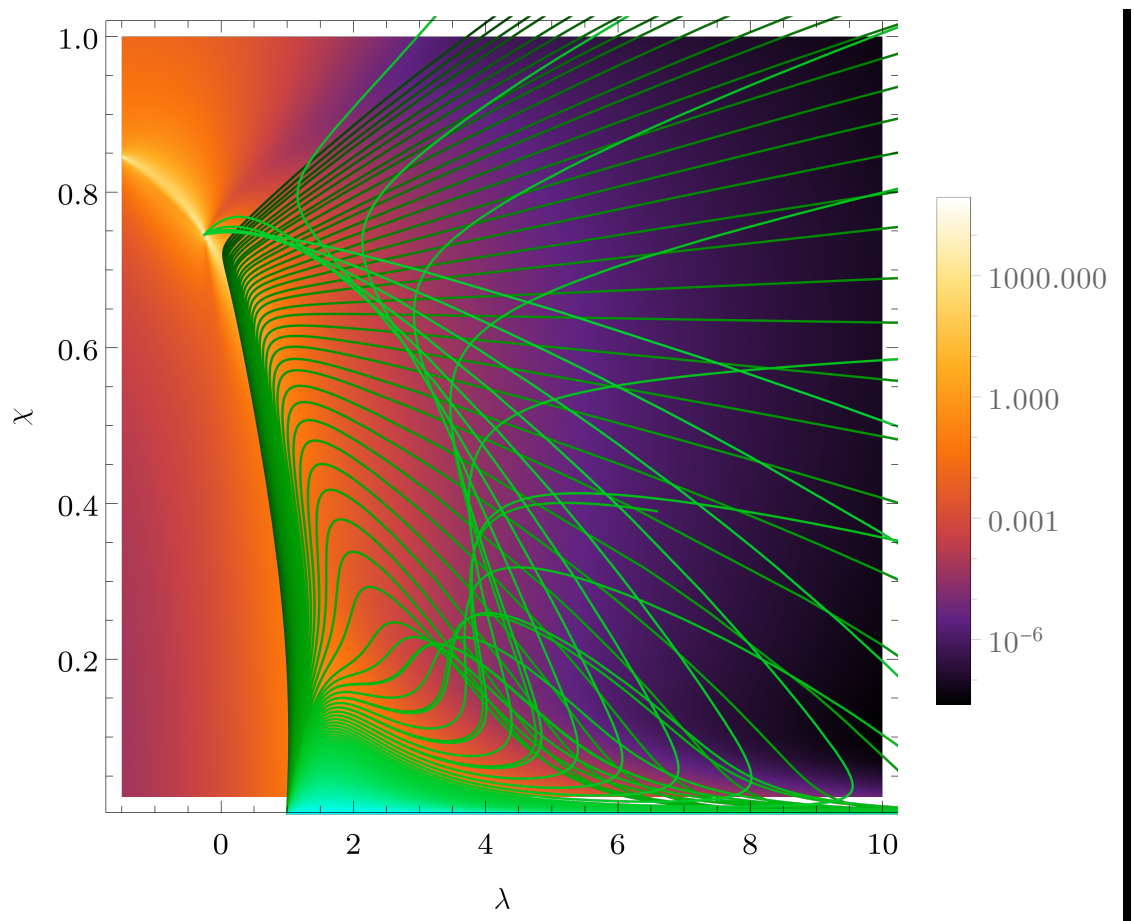


Figure 5.12: Geodesics for the case $N = 5$, starting at $(1; 0)$. *The numerics for geodesics passing close to singularity can be observed to break down.*

5.2.3 Infinite dimension limit

The limit $N \rightarrow \infty$ can be taken from Hamiltonian in Eq. 5.1 using Holstein-Primakoff mapping Holstein and Primakoff [22] for bosonic operators

$$\mathcal{H} := \lim_{j \rightarrow \infty} \frac{\hat{H}}{2j}, \quad (5.16)$$

resulting in classical Hamiltonian

$$\begin{aligned} \mathcal{H}(x, p) = & -\frac{1}{2} + \frac{1-\lambda}{2}x^2 + \frac{\lambda-\chi^2}{4}x^4 - \frac{\chi x^3}{2}\sqrt{2-x^2-p^2} - \frac{\chi^2}{4}p^4 \\ & + \frac{p^2}{4} \left[2 + (\lambda-2\chi^2)x^2 - 2\chi x\sqrt{2-x^2-p^2} \right]. \end{aligned} \quad (5.17)$$

For more, see Matus et al. [20].

The minima of function $\mathcal{H}(x, p)$ form a line, called *separatrix*. In this case it can be expressed as

$$\chi^2 = \frac{\lambda-1}{\lambda-2}. \quad (5.18)$$

The separatrix represents phase transition in the limit $N \rightarrow \infty$. In the case of the LMG model, the transition is of first-order everywhere, except in $(\lambda; \chi) = (1; 0)$, where it has order two. The separatrix is shown in Fig. 5.13 compared to minimum of $E_1 - E_0$ function line, so-called *minimal line*. With increasing N , it converges to separatrix. The driving over the first order transition are generally more advantageous than when the transition is of the second order. The reason is in the energy difference $E_1 - E_0$ dependence on system dimension N . For details, see Schuetzhold and Schaller [23].

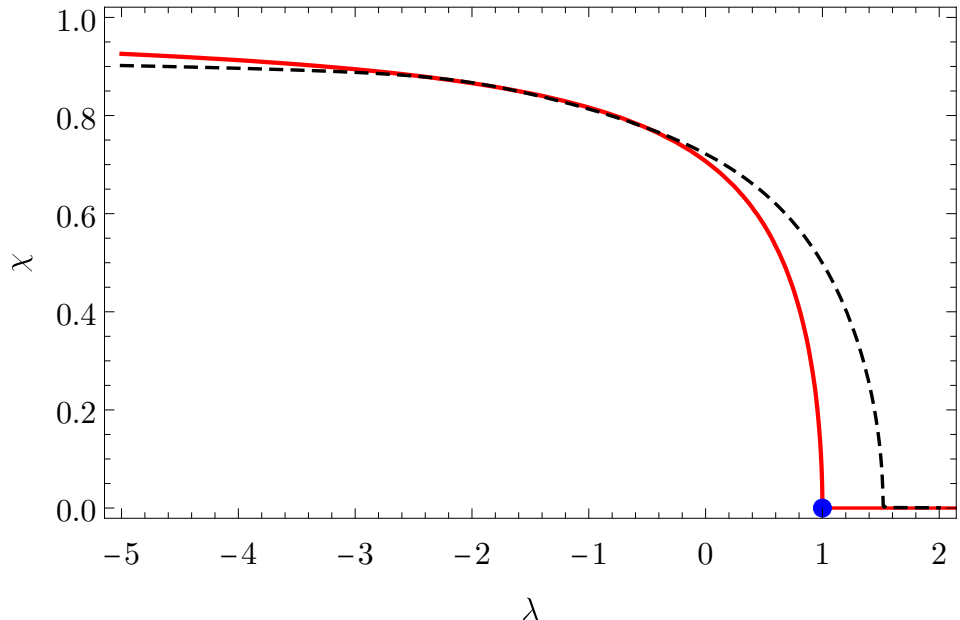


Figure 5.13: First order phase transition, the separatrix (red line), second order transition (blue point) compared to minimal line in $N=3$ case (black, dashed).

5.3 General spectrum behavior

For higher dimensions we see the same characteristic behavior in the energy spectrum sections, see the example in Fig. 5.14, 5.15 for $N = 10$ case. It is not yet clear if there is a degeneracy between every two neighboring energy levels. From numerical observation on $N < 10$ goes that there are $N - 2$ crossings for N odd and $N - 3$ for N even. Here the analytical proof needs to be found.

Special attention is given to the spectrum degeneracies between zeroth and first energy level because these influence the metric tensor and ground-state manifold geodesics the most. Their exact calculation is numerically expensive, and only the first few cases, namely, $N \in \{3, 4, 5, 6, 7\}$, were calculated, see Tab. 5.1.

N	$(\lambda_l; \pm \chi_l)$	$(\lambda_2; \pm \chi_2)$	$(\lambda_r; \pm \chi_r)$
3	$(-\frac{1}{2}; \sqrt{\frac{3}{5}})$		
4	$(-3; \sqrt{\frac{4}{5}})$		$(-\frac{1}{3}; \sqrt{\frac{4}{7}})$
5	$(-\frac{3}{2}; \sqrt{\frac{5}{7}})$		$(-\frac{1}{4}; \sqrt{\frac{5}{9}})$
6	$(-5; \sqrt{\frac{6}{7}})$	$(-1; \sqrt{\frac{2}{3}})$	$(-\frac{1}{5}; \sqrt{\frac{6}{11}})$
7	$(-\frac{5}{2}; \sqrt{\frac{7}{9}})$	$(-\frac{3}{4}; \sqrt{\frac{7}{11}})$	$(-\frac{1}{6}; \sqrt{\frac{7}{13}})$

Table 5.1: Singularities between the zeroth and first energy levels for dimensions 3–7. Subscript $l(r)$ means the most *left(right)-wise* positioned coordinates in the (λ, χ) -plot.

From singularity behavior in low dimensions, one might see the pattern for (λ_l, χ_l) and (λ_r, χ_r) , i.e., those with minimal, resp maximal λ coordinate

$$(\lambda_l; \pm \chi_l) = \begin{cases} \left(1 - \frac{N}{2}; \sqrt{\frac{N}{N+2}}\right) & , N \geq 3, N \text{ is odd} \\ \left(1 - N; \sqrt{\frac{N}{N+1}}\right) & , N \geq 3, N \text{ is even} \end{cases} \quad (5.19)$$

$$(\lambda_r; \pm \chi_r) = \left(\frac{1}{1-N}; \sqrt{\frac{N}{2N-1}} \right) , N \geq 3. \quad (5.20)$$

These were numerically proven to be singularities for cases up to $N = 1000$.

Dimensions 3 to 10 are shown in Fig. 5.16. In addition, the degeneracies between zeroth and first energy levels belong to the separatrix described by Eq. 5.18. Due to this, the position of singularities is constrained to the *second order phase transition line* between points $(\lambda_l, \pm \chi_l)$ and $(\lambda_r, \pm \chi_r)$.

In the limit $N \rightarrow \infty$ they converge to

$$\lim_{N \rightarrow \infty} (\lambda_l; \pm \chi_l) = (-\infty, 1)$$

$$\lim_{N \rightarrow \infty} (\lambda_r; \pm \chi_r) = \left(0, \frac{1}{\sqrt{2}}\right).$$

It is still unclear if in the limit $N \rightarrow \infty$ the singularities cover the part of separatrix with $\lambda < 0$.

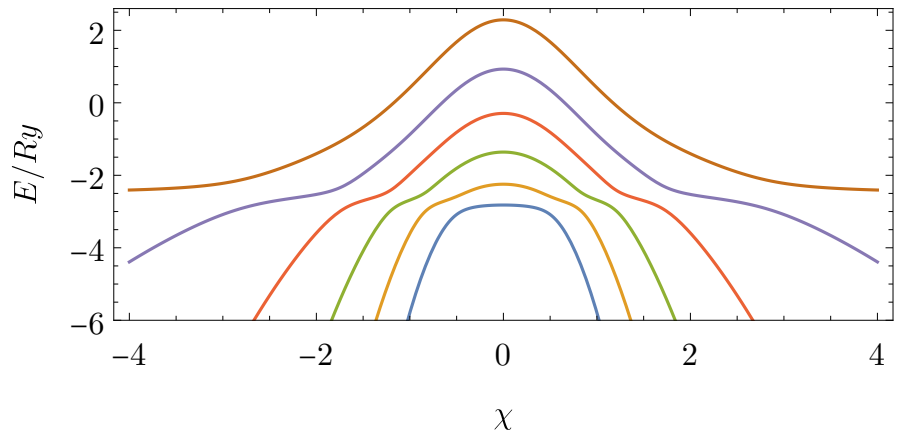


Figure 5.14: Energy spectrum as function of χ . $\lambda = 1$ and $N = 10$.

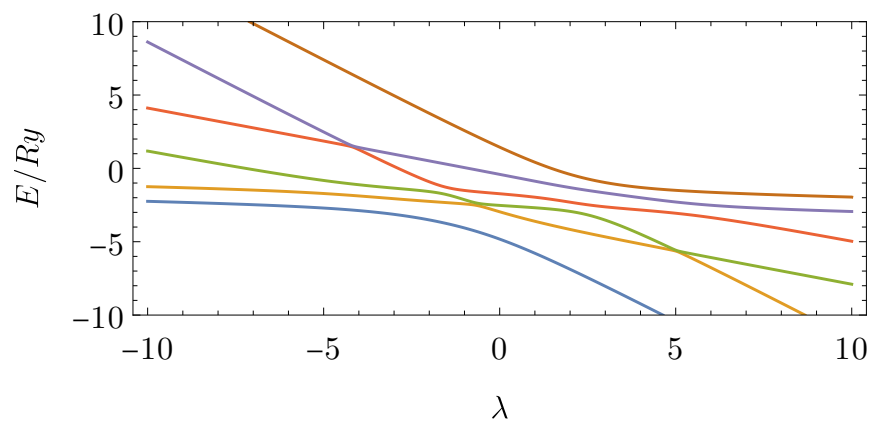


Figure 5.15: Energy spectrum as function of λ . $\chi = 1$ and $N = 10$.

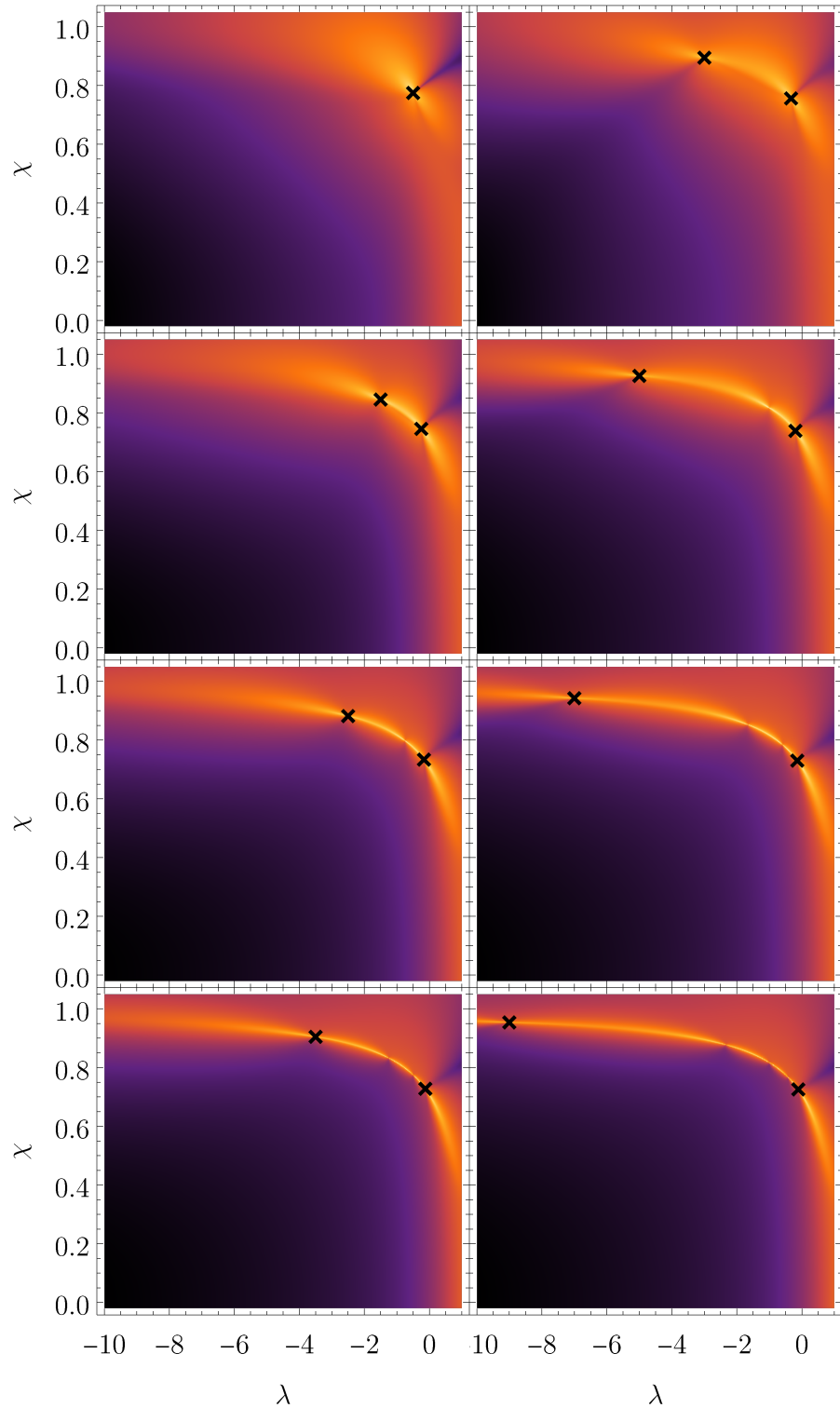


Figure 5.16: Spectrum degeneracies between E_0 and E_1 . Hamiltonian dimensions are 1,3,5,7 in the first column and 2,4,6,8 in the second column. Black crosses mark most left-wise and right-wise singularity and the background corresponds to the metric tensor determinant. Other singularities are also well visible in the determinant as defects on the *high determinant value line*.

5.4 Transport using quenches

In Chapter 3.2, the transport using quenches was introduced. This transport also resembles some ground-state manifold characteristics. Performing quench from $(\lambda_i; \chi_i) = (0; 0)$ to $(\lambda; \chi)$, the fidelity is small if the final coordinates are below separatrix. When it is behind the [minimal line](#), the fidelity decreases dramatically, as can be seen in Fig. 5.17.

Transport using quenches can be observed in Fig. 5.18. The quenches are performed around paths with $\int_a^b ds = \text{const}$ between every two neighboring points on ground-state manifold geodesic. If the system is measured periodically, the quenches jump smaller distances when the coordinates in parametric space are closer to the degeneracy. Decreasing time step Δt has no effect on the relative fidelity of quenches during the evolution but affects their absolute fidelity. As one would expect that for $\Delta t \rightarrow 0$, transport becomes adiabatic, and the fidelity at any time will become 1. See that the shape of the curves looks similar in plots in the columns, but their magnitude decreases.

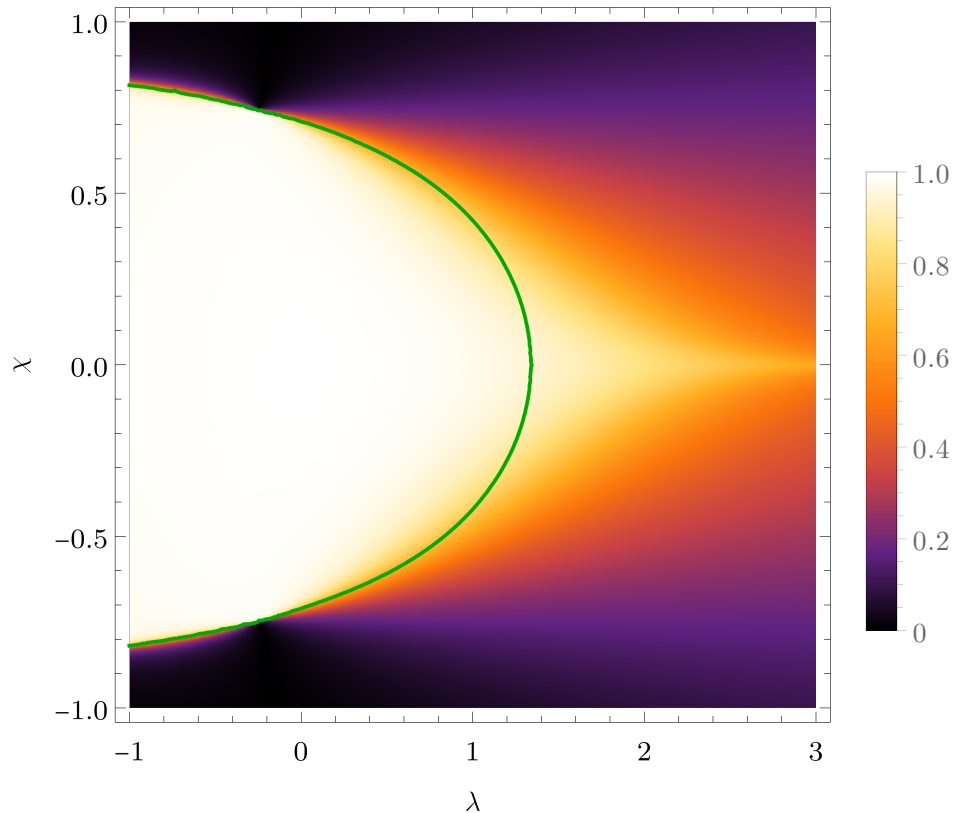


Figure 5.17: Fidelity of quench from $(\lambda_i; \chi_i) = (0; 0)$ to the coordinate $(\lambda; \chi)$. Minimal line (green) is plotted for comparison.

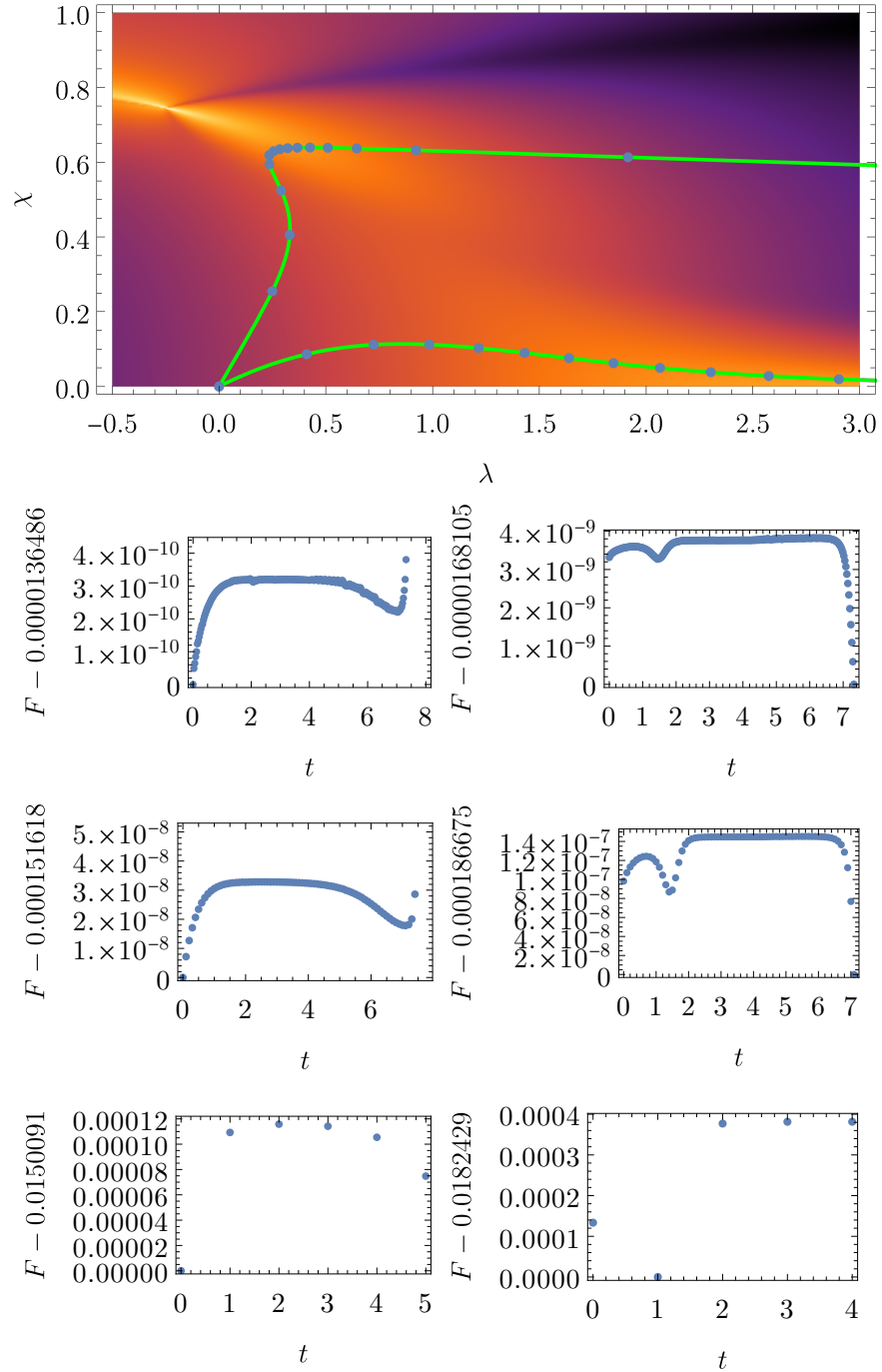


Figure 5.18: Fidelity for sequential quenches along geodesics (see green lines on top). Left (right) column corresponds to lower (upper) geodesic. Time steps from top are $\Delta t \in \{0.03, 0.1, 0.5\}$. Time difference between points in the plot on top is $\Delta t = 0.5$.

Conclusion

This thesis presents the theory of quantum state driving theory of finite Hamiltonian systems. The well known claims were reformulated into more rigorous theorems and definitions style of writing. This mathematical approach has potential to reduce the barrier for any mathematically based scientist without training in quantum mechanics when trying to approach this theory. The playground in the form of fiber space was constructed, and the geometry of energy states reformulated on it. Some theorems were proposed based on previous knowledge from the area of physics concerning quantum state driving, and clear definitions of generally used terms were presented.

The correspondence to a damped harmonic oscillator in the fidelity behavior was shown on a simple two-level system. In the case of geodesic driving, the fidelity oscillates with constant frequency and periodically becomes one. For linear driving, the fidelity has essentially two regimes — fast transport regime, described by the semiclassical Landau-Zener formula, and close adiabatic regime, described by APT. In both models, the fidelity is excited when the difference between energy levels gets small. These excitations lead to damped oscillations.

In the LMG model, the ground state manifold is analyzed. The Riemannian manifold characteristics were calculated along with their implications. These are ground state manifold geodesics and coordinates of diabolic points in parametric space, dependent on the Hamiltonian dimension. In three dimensions, this was done analytically, proving the existence of diabolic points. For higher dimensions, numerical methods were used. The transport using quenches was numerically demonstrated, showing the transformation to adiabatic transport by shortening the quenches.

Many questions still lay unsolved, and some were newly opened. For example: “What are the possibilities for quantum quench transport?”. “What is the correspondence of energy variance and driving fidelity?”. Further on, from the LMG model, the proposed analytical formula for diabolic points coordinates remains to be proven analytically, along with the number of these points.

This thesis provides a significant amount of numerical analysis on two quantum models, which will hopefully serve for future discoveries in this area of physics. The state manifold analyses might lead the search for better fidelity protocols, or maybe the geodesics will be found to be somewhat “most stable protocols” for counter-diabatic driving. Either way, the possibilities are yet open and not known.

Bibliography

- [1] D. Loss and D. P. DiVincenzo. Quantum computation with quantum dots. *Phys. Rev. A*, 57:120–126, Jan 1998. doi: 10.1103/PhysRevA.57.120.
- [2] Y. Makhlin, G. Schön, and A. Shnirman. Josephson junction based quantum computing. *AAECC 10*, page 375–382, 2000. doi: 10.1007/978-3-030-20726-7_17.
- [3] P. Krtouš. Geometrické metody ve fyzice, studijní text k přednáškám geometrické metody fyziky i a ii, 2013.
- [4] W. Tu Loring. *Differential Geometry*. Springer International Publishing, 2017. doi: 10.1007/978-3-319-55084-8.
- [5] M. Fecko. *Differential Geometry and Lie Groups for Physicists*. Cambridge University Press, 2006. doi: 10.1017/CBO9780511755590.
- [6] L. D. Landau and L. M. Lifshitz. *Quantum Mechanics Non-Relativistic Theory, Third Edition: Volume 3*. Butterworth-Heinemann, 3 edition, 1981. ISBN 0750635398.
- [7] P. Petersen. *Riemannian Geometry*. Springer Verlag, 1998. ISBN 978-0-387-29403-2.
- [8] C. Gorodski. An introduction to riemannian geometry, 2012. URL <https://www.ime.usp.br/~gorodski/teaching/mat5771-2016/gorodski-riem-geom-2012.pdf>. Preliminary version.
- [9] D. Gutiérrez-Ruiz, D. Gonzalez, J. Chávez-Carlos, J. G. Hirsch, and J. D. Vergara. Quantum geometric tensor and quantum phase transitions in the lipkin-meshkov-glick model. *Phys. Rev. B*, 103, May 2021. doi: 10.1103/PhysRevB.103.174104.
- [10] M. Kolodrubetz, P. Mehta, and A. Polkovnikov. Geometry and non-adiabatic response in quantum and classical systems. *Physics Reports*, 697:1–87, 2017. ISSN 0370-1573.
- [11] M. V. Berry. Quantal phase factors accompanying adiabatic changes. *Proc. R. Soc. Lond. A*, 392(1802):45–57, 1984. doi: 10.1098/rspa.1984.0023.
- [12] M. V. Berry. The quantum phase, five years after. *A Shapere, F Wilczek. (World Scientific) 7-28*, 1989. Geometric phases in physics, 7–28, Adv. Ser. Math. Phys., 5,.
- [13] M. V. Berry. Transitionless quantum driving. *Journal of Physics A: Mathematical and Theoretical*, 42(36), 2009. doi: 10.1088/1751-8113/42/36/365303.
- [14] A. Uhlmann. The “transition probability” in the state space of a $*$ -algebra. *Reports on Mathematical Physics*, 9(2):273–279, 1976. ISSN 0034-4877. doi: [https://doi.org/10.1016/0034-4877\(76\)90060-4](https://doi.org/10.1016/0034-4877(76)90060-4).

- [15] J. R. R. Tolkien. *The Lord of the Rings*. Folio Society, 1977. ISBN 978-0458907502.
- [16] R. Cheng. Quantum Geometric Tensor (Fubini-Study Metric) in Simple Quantum System: A pedagogical Introduction. *arXiv:1012.1337 [math-ph, physics:quant-ph]*, 2013. URL <http://arxiv.org/abs/1012.1337>.
- [17] J. J. Sakurai and Jim Napolitano. *Modern Quantum Mechanics*. Cambridge University Press, 3 edition, 2020. doi: 10.1017/9781108587280.
- [18] M. Bukov, D. Sels, and A. Polkovnikov. Geometric Speed Limit of Accessible Many-Body State Preparation. *Physical Review X*, 9(1):011034, 2019. ISSN 2160-3308.
- [19] G. Rigolin, G. Ortiz, and V. H. Ponce. Beyond the quantum adiabatic approximation: Adiabatic perturbation theory. *Physical Review A* 78, no. 5 (November 18, 2008): 052508, 2008. doi: 10.1103/PhysRevA.78.052508.
- [20] F. Matus, P. Cejnar, P. Stránský, and J. Střeleček. unpublished. *MFF UK*, 2022.
- [21] H. Nakamura. *Nonadiabatic transition: concepts, basic theories and applications*. World Scientific, Hackensack, New Jersey, second edition edition, 2012. ISBN 978-981-4329-77-4.
- [22] T. Holstein and H. Primakoff. Field dependence of the intrinsic domain magnetization of a ferromagnet. *Phys. Rev.*, 58:1098–1113, Dec 1940. doi: 10.1103/PhysRev.58.1098.
- [23] R. Schuetzhold and G. Schaller. Adiabatic quantum algorithms as quantum phase transitions: First versus second order. *Phys. Rev. A*, 74(6), 12 2006. ISSN 1050-2947. doi: 10.1103/PHYSREVA.74.060304.
- [24] A. Ashtekar and T. A. Schilling. Geometrical Formulation of Quantum Mechanics. *arXiv:gr-qc/9706069*, 1997. URL <http://arxiv.org/abs/gr-qc/9706069>. arXiv: gr-qc/9706069.
- [25] A. Ashtekar and T. A. Schilling. Geometry of quantum mechanics. In *AIP Conference Proceedings*, volume 342, pages 471–478, Cancun (Mexico), 1995. AIP. ISSN: 0094243X.
- [26] M. Molitor. Exponential families, Kahler geometry and quantum mechanics. *Journal of Geometry and Physics*, 70:54–80, 2013. ISSN 03930440. doi: 10.1016/j.geomphys.2013.03.015. arXiv: 1203.2056.

List of Figures

1	Visualization of the state adiabatic transport compared to transport with excitation in a system with time varying energy eigenstates.	5
2.1	Base manifold $\mathcal{U} \subset \mathbb{R}^n$ is visualized as a line. For every point $\lambda \in \mathcal{U}$ one Hilbert space $\mathcal{H}(\lambda)$ (blue disk) is constructed as a fiber. The union of all these fibers creates the full Hilbert space \mathcal{H}_{full} (hollow cylinder) and from every Hilbert space there exist projection π onto the base manifold.	14
2.2	For every λ we have the projective Hilbert space $\mathcal{PH}(\lambda)$ containing physical states $ \psi(\lambda)\rangle$ corresponding to density matrix $\rho \equiv \psi(\lambda)\rangle\langle\psi(\lambda) $. Every state can be multiplied by phase factor $e^{i\varphi}$, extending it to Hilbert space $\mathcal{H}(\lambda)$.	14
2.3	From the full Hilbert space \mathcal{H}_{full} (the biggest hollow cylinder) we identified eigenstates and unified them into state manifolds \mathcal{M}_s . These are drawn as inner cylinders of \mathcal{H}_{full} , especially see the ground state manifold \mathcal{M}_0 as the inner cylinder. The phase φ introduces gauge symmetry $e^{i\varphi}$. If it is fixed, we get projective state manifolds \mathcal{PM}_s , especially see \mathcal{PM}_0 . Projective state manifolds are isomorphic to the base manifold \mathcal{U} .	16
2.4	The cylinders from Fig. 2.3 are now displayed as two-dimensional sheets. The transport of states is performed on state manifolds \mathcal{M}_s along the path $\mathcal{J}(t)$, defined in parametric space. The information about gauge phase φ is represented by color (see the changing color on the paths in \mathcal{M}_s).	17
4.1	Driving along the geodesic. $\lambda_i \equiv (\Omega_i, \Delta_i)$ and $\lambda_f \equiv (\Omega_f, \Delta_f)$ are initial and final parameters respective. Density plot shows the difference between Hamiltonian eigenvalues.	36
4.2	Infidelity in time for final time $T = 1$ for geodesical driving.	38
4.3	Final infidelity dependence on final time T for geodesical driving.	38
4.4	Final infidelity dependence on final time T for geodesical driving; in logarithmic scale ⁹ . The difference in numerical precision of both methods can be seen in the spike's height. As it will be shown later, the spikes should go to zero, thus analytical formula has higher numerical precision.	39
4.5	Rescaled final infidelity $T_s := 2sT$ dependence on final time. Red points mark the condition $F = 1$.	39
4.6	Fidelity dependence on time and final time in log-log scale. Only $t < T$ has a physical meaning.	40
4.7	Energy variance for geodesical driving protocol, dependent on time t and final time T . Driving occurs only in area $t < T$.	40
4.8	Driving along the linear path. $\lambda_i := (-10; 1)$ and $\lambda_f := (10; 1)$ are initial and final parameters respective. Density plot shows the difference between Hamiltonian eigenvalues.	41
4.9	Infidelity in time for three final times $T \in \{1, 5, 20\}$ for the linear driving defined in 4.37.	42

4.10	Value of first element of the ground state vector $\alpha \equiv 0(t)\rangle^1$ during linear driving.	43
4.11	Final infidelity as a function of T with zoom on the transitional part.	44
4.12	Final infidelity as a function of T in log-log scale wit linear scaled plot inserted.	44
4.13	Final infidelity as a function of Δ and T and its three regimes. Zoom on the boundary between them can be seen on 4.14.	45
4.14	Fine structure of the boundary between fast-driving and adiabatic regimes of final infidelity.	46
4.15	Infidelity as a function of time for fast-driving regime, $T = 80 < T_c$	47
4.16	Infidelity as a function of time for close-adiabatic regime. $T = 170 > T_c$	47
4.17	Fidelity as a function of driving final time, approximated by the sum (green) of Landau-Zener (red, dashed) and APT (purple, dashed)	48
4.18	Energy variance for $\Delta_{sc} = 0.2$ for linear driving. Note that only $t < T$ has physical meaning.	48
4.19	Fidelity dependence for linear driving with $\Delta = 1$. Black line marks $t = T$, dashed black line $t = T/2$ and purple dashed line is the approximate value of T_c . Blue lines marks driving from Fig. 4.15, 4.16, visualizing the final times of the driving.	49
5.1	Energy spectrum for $N = 3$, section $\lambda = 1$	53
5.2	Energy spectrum for $N = 3$, section $\chi = 1$	53
5.3	Arctangent of the metric tensor elements for $N = 3$ in the parametric space.	54
5.4	Ground state metric tensor determinant in a parametric space for $N = 3$	55
5.5	Arctangent of the ground state Christoffel symbols for $N = 3$	55
5.6	Arctangent of Ricci curvature for the case $N = 3$	56
5.7	Ricci curvature sections for three different λ . $N = 3$	56
5.8	Geodesics for $N = 3$ starting from $(\lambda_i; \chi_i) = (0; 0)$ with $(\lambda'_i; \chi'_i) = (\cos \theta; \sin \theta)$, parametrized by angle $\theta \in [-0.63; 0.63]$, $\theta \in [\pi - 0.225; \pi + 0.225]$, with step $\Delta\theta = 0.01$. Blue line marks the unreachable gap, where the Ricci curvature is big.	57
5.9	Comparing boundary valued geodesics for repulsing (inner line) and attracting (outer line) metric tensor divergence in the spherically symmetrical space.	57
5.10	Energy differences between neighboring energy levels for $N = 5$. Spectra degeneracies are marked with blue cross.	59
5.11	Metric tensor determinant for the case $N = 5$	60
5.12	Geodesics for the case $N = 5$, starting at $(1; 0)$. The numerics for geodesics passing close to singularity can be observed to break down.	60
5.13	First order phase transition, the separatrix (red line), second order transition (blue point) compared to minimal line in $N=3$ case (black, dashed).	61
5.14	Energy spectrum as function of χ . $\lambda = 1$ and $N = 10$	63

5.15	Energy spectrum as function of λ . $\chi = 1$ and $N = 10$.	63
5.16	Spectrum degeneracies between E_0 and E_1 . Hamiltonian dimensions are 1,3,5,7 in the first column and 2,4,6,8 in the second column. Black crosses mark most left-wise and right-wise singularity and the background corresponds to the metric tensor determinant. Other singularities are also well visible in the determinant as defects on the <i>high determinant value line</i> .	64
5.17	Fidelity of quench from $(\lambda_i; \chi_i) = (0; 0)$ to the coordinate $(\lambda; \chi)$. Minimal line (green) is plotted for comparison.	65
5.18	Fidelity for sequential quenches along geodesics (see green lines on top). Left (right) column corresponds to lower (upper) geodesic. Time steps from top are $\Delta t \in \{0.03, 0.1, 0.5\}$. Time difference between points in the plot on top is $\Delta t = 0.5$.	66

A. Geometrization of quantum mechanics

Differential geometry is believed to be the modern language of physics, and there is a strong urge to reformulate theories in this language. As introduction to the problem, see Ashtekar and Schilling [24], [25], or more mathematical work by Molitor [26].

The whole thesis uses a classical formulation of quantum mechanics with some parts described using differential geometry. Here, the complete reformulation of quantum mechanics and the bridge between this theory and the already formulated are introduced. Reformulating the whole theory of quantum driving into the language of differential geometry might give some new insights, but it is beyond the scope of this thesis.

A.1 From the projective Hilbert space to state manifolds

Consider the Hilbert space \mathcal{H} to be a space of *bare states* and \mathcal{S} to be the space of *normalized bare states*. Physical observables are related to the *space of rays*, defined as $\mathcal{PH} := \mathcal{H}/U(1)$, for the factorization by elements of one-dimensional unitary group $U(1)$. This group consists of unitary transformations $e^{i\varphi}$ for $\varphi \in \mathbb{R}$, defining gauge symmetry between quantum states. \mathcal{PH} is then considered to be the *space of pure states*. We will consider the states to be normalized, leading to the *space of normalized pure physical states*.

It can be shown that \mathcal{PH} is of Kähler structure, meaning it has two non-degenerate sesquilinear¹ 2-forms embedded along with complex unit operator J , defining structure

$$(J, G, \Omega),$$

such that

$$J^2 = \mathbb{1}. \quad (\text{A.1})$$

Any bracket of $|\psi_1\rangle, |\psi_2\rangle \in \mathcal{PH}$ can be decomposed into real and imaginary part[24]

$$\langle \psi_1 | \psi_2 \rangle \equiv Q(\psi_1, \psi_2) = \frac{1}{2}G(\psi_1, \psi_2) - \frac{i}{2}\Omega(\psi_1, \psi_2). \quad (\text{A.2})$$

From bra-ket, sesquilinearity goes that G is symmetric and Ω antisymmetric form thus they can be uniquely written into one 2-form called *Fubini-Study metric* with property

$$G = \text{Re}Q; \quad \Omega = \text{Im}Q. \quad (\text{A.3})$$

Because $|\langle \psi_1 | \psi_2 \rangle| \in [0, 1]$ we say, that the *metric is measuring the geodesic distance on the Bloch sphere*. Here if we define

$$|\langle \psi_1 | \psi_2 \rangle| = \cos^2 \frac{\theta}{2}, \quad (\text{A.4})$$

¹Complex conjugated is the first input of the 2-form.

we get $d\theta = 2ds = 2\sqrt{|g_{\mu\nu}d\lambda^\mu d\lambda^\nu|}$, see the paper from Cheng [16].

To write the metric in a standard form, we need to realize how our space looks like. For finite $(N + 1)$ -dimensional Hilbert space, one dimension is lost in the gauge transformation, leaving us with N -dimensional \mathcal{PH} . Another dimension is lost due to normalization, which is usually done by mapping to an n -dimensional complex sphere

$$CP^N = \left\{ \mathbf{Z} = (Z_0, Z_1, \dots, Z_N) \in \mathbb{C}^{N+1}/\{0\} \right\} / \{\mathbf{Z} \sim c\mathbf{Z} \text{ for } c \in \mathbb{C}\}.$$

Natural property of such complex spaces is splitting of its tangent space to holonomic and anholonomic part²

$$\mathcal{T}_0^1 \mathcal{M} = \text{Span} \left\{ \frac{\partial}{\partial Z_i} \right\}; \quad \mathcal{T}_1^0 \mathcal{M} = \text{Span} \left\{ \frac{\partial}{\partial Z_{\bar{i}}} \right\}.$$

For suitable distance dZ , this can be used to define distance on state manifolds.

Distance on \mathbb{C}^{n+1} is usually defined using Hermitian metric³

$$ds^2 = d\bar{Z} \otimes dZ. \quad (\text{A.5})$$

A.2 Restriction to eigenstate manifolds

In quantum mechanics, one can examine a Hamiltonian $\hat{H}(\lambda)$, for some parameter $\lambda \in \mathcal{U} \subset \mathbb{R}^n$. At every point λ we get projective Hilbert space $\mathcal{PH}(\lambda)$. This creates a fiber structure space, in which there are some sections with interesting physical applications. Some of these sections are *eigenstate manifolds*, defined by setting only one non-zero coefficient Z_k in eigenbasis $|\psi\rangle = \sum_{k=0}^n Z_k |k\rangle$. From normalization goes automatically $Z_k = 1$. The distance on these manifolds is, as derived in Eq. 2.27,

$$\begin{aligned} ds^2 &= 1 - \langle k + \delta k | k \rangle \langle k | k + \delta k \rangle = 1 - \langle k + \delta k | \left(\mathbb{I} - \sum_{j \neq k} |j\rangle \langle j| \right) |k + \delta k \rangle \\ &= \sum_{j \neq k} \langle k + \delta k | j \rangle \langle j | k + \delta k \rangle. \end{aligned} \quad (\text{A.6})$$

Using the Schrödinger equation $\hat{H}|k\rangle = E_k|k\rangle$, distributivity of derivative and projection to some state $|j\rangle$, we get

$$\begin{aligned} \hat{H}|k\rangle &= E_k|k\rangle \\ (\delta \hat{H})|k\rangle + \hat{H}|k + \delta k\rangle &= (\delta E_k)|k\rangle + E_k|k + \delta k\rangle \\ \langle j | (\delta \hat{H} - \delta E_k) |k\rangle &= \langle j | (E_k - \hat{H}) |k + \delta k\rangle = \langle j | (E_k - E_j) |k + \delta k\rangle. \end{aligned} \quad (\text{A.7})$$

We can set $\delta E_k = 0$, leading for $j \neq k$ to

$$\frac{\langle j | \delta \hat{H} | k \rangle}{(E_k - E_j)^2} = \langle j | k + \delta k \rangle. \quad (\text{A.8})$$

²The line over index means complex conjugation.

³Hermitian metric is by definition sesquilinear, as one would expect in quantum mechanics later on.

Plugging to Equation A.6 and considering $\hat{H} = \hat{H}(\boldsymbol{\lambda})$, we get metric on a ground state manifold

$$ds^2 = \operatorname{Re} \sum_{j \neq k} \frac{\langle 0 | \partial_\mu \hat{H} | j \rangle \langle j | \partial_\nu \hat{H} | 0 \rangle}{(\textcolor{teal}{E}_k - \textcolor{blue}{E}_j)^2} d\boldsymbol{\lambda}^\mu d\boldsymbol{\lambda}^\nu. \quad (\text{A.9})$$

Definition of the k -state manifold is then

$$g_{\mu\nu}^{(k)} = \operatorname{Re} \sum_{j \neq k} \frac{\langle k | \frac{\partial \hat{H}(\boldsymbol{\lambda})}{\partial \lambda^\mu} | j \rangle \langle j | \frac{\partial \hat{H}(\boldsymbol{\lambda})}{\partial \lambda^\nu} | k \rangle}{(E_k - E_j)^2}. \quad (\text{A.10})$$

The Fubini-Study metric on the eigenstate manifold is sometimes called *Geometric tensor*.

B. Eigenvalues for Lipkin-Meshkov Glick model

Eigenvalues for $N = 3$ case of the Lipkin-Meshkov Glick model are

$$E_0 = \frac{1}{12} \left(G - F - \frac{\sqrt{D - E}}{2} \right) \quad (\text{B.1})$$

$$E_1 = \frac{1}{12} \left(G - F + \frac{\sqrt{D - E}}{2} \right) \quad (\text{B.2})$$

$$E_2 = \frac{1}{12} \left(G + F - \frac{\sqrt{D + E}}{2} \right) \quad (\text{B.3})$$

$$E_3 = \frac{1}{12} \left(G + F + \frac{\sqrt{D + E}}{2} \right), \quad (\text{B.4})$$

for

$$\begin{aligned} A = & 16\sqrt[3]{2} \left(64\lambda^6 - 192\lambda^5\chi^2 + 24\lambda^4 (52\chi^4 - 93\chi^2 + 36) \right. \\ & - 8\lambda^3 (29\chi^4 + 414\chi^2 - 513)\chi^2 \\ & + 6\lambda^2 (1225\chi^8 - 10053\chi^6 + 17595\chi^4 - 10557\chi^2 + 1377) \\ & + \left((64\lambda^6 + 864\lambda^4 + 8262\lambda^2 + 3(818\lambda - 27285)\chi^{10} \right. \\ & + 6(\lambda(1225\lambda - 3198) + 27108)\chi^8 \\ & - (2\lambda(\lambda(116\lambda + 30159) - 89073) + 326727)\chi^6 \\ & + 6(\lambda(\lambda(8\lambda(26\lambda - 69) + 17595) - 42660) + 51516)\chi^4 \\ & - 3(2\lambda(\lambda(4\lambda(\lambda(8\lambda + 93) - 171) + 10557) - 16119) + 36207)\chi^2 \quad (\text{B.5}) \\ & \left. + 24013\chi^{12} + 25515 \right)^2 \\ & - \left((16\lambda^4 + 144\lambda^2 + 2(74\lambda - 1185)\chi^6 + 3(4\lambda(16\lambda - 77) + 1329)\chi^4 \right. \\ & - 2(2\lambda(\lambda(8\lambda + 93) - 207) + 1161)\chi^2 + 889\chi^8 + 1053 \left. \right)^{1/2} \\ & + 6\lambda(409\chi^8 - 3198\chi^6 + 29691\chi^4 - 42660\chi^2 + 16119)\chi^2 + 24013\chi^{12} \\ & - 81855\chi^{10} + 162648\chi^8 - 326727\chi^6 + 309096\chi^4 \\ & \left. - 108621\chi^2 + 25515 \right)^{1/3} \end{aligned}$$

$$\begin{aligned} B = & \frac{256\sqrt[3]{2}}{3A} \left(16\lambda^4 + 144\lambda^2 + 2(74\lambda - 1185)\chi^6 + 3(4\lambda(16\lambda - 77) \right. \\ & \left. + 1329)\chi^4 - 2(2\lambda(\lambda(8\lambda + 93) - 207) + 1161)\chi^2 + 889\chi^8 + 1053 \right) \quad (\text{B.6}) \end{aligned}$$

$$C = 4\sqrt{\frac{A}{3\sqrt[3]{2}} + B + \frac{16}{3}(4\lambda^2 - (4\lambda + 33)\chi^2 + 49\chi^4 + 45)} \quad (\text{B.7})$$

$$D = -\frac{A}{3\sqrt[3]{2}} - B - \frac{8}{3} \left(59\lambda^2 + 436\lambda\chi^2 + 392\chi^4 + 132\chi^2 - 180 \right) \\ + 8 \left(5\lambda + 14\chi^2 \right)^2 \quad (B.8)$$

$$E = \frac{9216}{C} \left((\lambda - 1)\chi^4 - 4(\lambda - 1)\chi^2 + \lambda - 2\chi^6 \right) \\ F = \frac{1}{2} \sqrt{\frac{A}{3\sqrt[3]{2}} + B + \frac{16}{3} (4\lambda^2 - (4\lambda + 33)\chi^2 + 49\chi^4 + 45)} \quad (B.9) \\ G = -5\lambda - 14\chi^2$$